Advanced Multi-Antenna Systems for Next Generation Wideband Access: Capacity Analysis and Channel Estimation

by

Bamelak Tadele

A Thesis submitted to The Faculty of Graduate Studies of

The University of Manitoba

in partial fulfillment of the requirements for the degree of

Master of Science

Department of Electrical and Computer Engineering

University of Manitoba

Winnipeg

August 2023

When you look at yourself from a universal standpoint, something inside always reminds or informs you that there are bigger and better things to worry about.

ALBERT EINSTEIN

Abstract

With the ever-increasing need for wireless broadband services next generation wireless systems are being designed to meet three main requirements. These are massive Machine Type Communication, Ultra-Reliable Low-Latency Communication, and enhanced Mobile Broadband. In this thesis, we explore all three areas and show that multi-antenna systems are the framework to meet these demands. We first investigate the age-limited capacity of the Gaussian many channel with total N users, out of which a random subset are active, and a multi-antenna base station. In the setting in which both the number of users, N, and the number of antennas at the BS, M, are allowed to grow large at a fixed ratio $\zeta = M/N$, we derive the achievability bound under maximal ratio combining. Further extensions of the analysis to the zero-forcing receiver as well as imperfect CSI are provided. Using the age of information (AoI) metric as our measure of timeliness we investigate the trade-offs between the AoI and spectral efficiency in the context massive connectivity with large-scale antenna arrays. We find that while the spectral efficiency can be made large, the penalty is an increase in the minimum AoI obtainable. The proposed achievability bound is further compared against recent unsourced random access schemes. One underlying assumption in the previous analysis is the construction of uncoupled arrays. This assumption starts to break down in massive MIMO and therefore in the second part of this thesis, we focus on a physically-consistent single-user MIMO system and model the mutual coupling using multiport networks. Based on this model, in single-carrier frequency-flat channels we show that neglecting the mutual coupling effects leads to inaccurate characterization of the channel and noise correlations. In multi-carrier frequency-selective channels we show that the coupling also increases the number of resolvable channel taps. We therefore develop

a linear minimum mean-square error (LMMSE) estimator that calibrates the coupling and optimally estimates the MIMO channel. It is shown that appropriately accounting for mutual coupling through the developed physically consistent model leads to remarkable performance improvements. We demonstrate these gains in a rich-scattering environment using the broadband connected array of slot antennas.

Table of Contents

List of Figures viii

List of Tables ix

List of Abbreviations x

1 Introduction 1

1.1 Overview . . . 1

1.1.1 Massive MTC and Unsourced Random Access . . . 2

1.1.2 URLLC and Age of Information . . . 3

1.1.3 Enhanced Mobile Broadband and Multiport Communication . . . 4

1.2 Contribution . . . 7

1.2.1 Age of Information in Massive Access Massive MIMO Systems . . . 7

1.2.2 Channel Estimation with Tightly-Coupled Arrays . . . 8

1.3 Scholastic Outputs and Achievements . . . 11

1.4 Thesis Organization and Notations . . . 11

2 Age of Information in Massive Access Massive MIMO Systems 14

2.1 System Model, Assumptions, and Methodology of Analysis . . . 14

2.1.1 System Model and Definition of AoI . . . 14

2.1.2 Methodology of Analysis . . . 17

2.2 Derivation of Packet Error Probability 18
2.2.1 Derivation of Exact PEP 18
2.2.2 Asymptotic Approximation of PEP 20
2.3 Trade-Off Between AoI and Spectral Efficiency 23
2.4 Analysis with Imperfect CSI 27
2.4.1 Maximal-Ratio Combining 27
2.4.2 Zero-Forcing 29
2.5 Numerical Results and Discussion 33
2.5.1 Trade-Off Between AoI and Spectral Efficiency 33
2.5.2 Performance under Imperfect CSI 34
2.5.3 Application to Unsourced Random Access (URA) 35

3 Channel Estimation with Tightly-Coupled Arrays 39
3.1 System Model 39
3.1.1 Impedance Description 40
3.1.2 Scattering Description 42
3.2 Single-Carrier System 42
3.2.1 Classical Channel Estimation 44
3.2.2 Antenna Aware Channel Estimation 45
3.3 Multicarrier Systems 46
3.3.1 Classical OFDM Channel Estimation 48
3.3.2 Antenna Aware OFDM Channel Estimation 52
3.4 Simulation Results 53
3.4.1 Connected Array of Slot Antennas 54
3.4.2 Single-Carrier System 56
3.4.3 OFDM System 60
3.4.4 Scattering/Impedance Channel Equivalence 64

4 Conclusion and Future Directions **67**

4.1 Concluding Remarks 67

4.2 Future Directions 68

4.2.1 User-Scheduled Access Scheme 68

4.2.2 Improving the Channel Estimation Algorithm 68

4.2.3 Physically-Consistent Modelling of Multi-User Systems 69

Appendices **70**

A Derivation of the AoI **70**

B Proofs of the Various Approximations **72**

C Finding the Spectral Efficiency from the Packet Error Probability **80**

Bibliography **91**

List of Figures

2.1 Slotted system with $N = 3$ total users and unit slot length. 16

2.2 AoI vs Spectral Efficiency at $p_e = 10^{-5}$ and $\zeta = 0.3$. In the simulation, for $N = 100$ we set the number of slots to be 10^5. 34

2.3 Achievable rate against Channel Estimation Error, here we use $\zeta = 1.2$, and $\tau = 0.95$. 35

2.4 Performance of two recent URA schemes against the newly established achievability bound in (2.31) with $p_e = 10^{-2}$. 37

3.1 Generic Multi-port Communication System 40

3.2 Connected array of slot antennas with 16 antenna elements 55

3.3 Empirical SNR against carrier frequency for the array with and without the backed-plane. Total Symbol Power is 1 [W] with a bandwidth of 5 [MHz] for each frequency point. 55

3.4 NMSE against pilot power at carrier frequency of 1 [GHz] with a bandwidth of 5 [MHz]. 56

3.5 NMSE against carrier frequency where total power used in estimation for each frequency is 1 [W] with a bandwidth of 5 [MHz]. 57

3.6 Achievable rate at $f_c = 1$ [GHz]. 59

3.7 Rate against frequency. 59

3.8 NMSE against pilot power in OFDM Estimation using total bandwidth of 708 [MHz] 61
3.9 NMSE against number of taps at high SNR with and without the BP . . 62
3.10 Achievable rate plot and power allocation plot using the backed-plane array with 64 subcarriers over the frequency band $1 - 1.5$ [GHz] with 2 channel taps. 64
3.11 Array of two dipole antennas 65
3.12 Open circuit/Terminated antenna gains as well as effective channels . . . 66

A.1 Decomposition of a sample function of the AoI. 70

List of Tables

1.1 Summary of Scholastic Outputs 10

List of Abbreviations

AoI	Age of information
BS	Base station
CSI	Channel state information
DFT	Discrete-fourier transform
eMBB	Enhanced mobile broadband
IoT	Internet of things
LMMSE	Linear mean square error
LNA	Low noise amplifiers
MIMO	Multiple-input multiple-output
mMTC	massive Machine Type Communication
MRC	Maximal ratio combining
MTD	Machine type devices
NMSE	Normalized mean square error
OFDM	Orthogonal frequency-division multiplexing
PEP	Packet error probability
SNR	Signal-to-noise ratio
URA	Unsourced random access
URLLC	Ultra-reliable low-latency communication
ZF	Zero-forcing

Chapter 1

Introduction

1.1 Overview

An essential ingredient of next generation wireless communication networks is the Internet of Things (IoT), which will enable unprecedented services and applications. In order to deal with the diversified IoT applications, next generation wireless programs have been classified into three main categories; 1) massive machine-type communication (mMTC), 2) ultra-reliable and low-latency communication (URLLC), and 3) enhanced mobile broadband (eMBB) [1,2]. A promising technology to meet these highly stringent demands is to use advanced multi-antenna systems. Multiple-Input Multiple-Output (MIMO) wireless systems, which use antenna arrays at the transmitter and receiver, leverage the spatial dimension of the channel to (not necessarily simultaneously) increase the data rate, enhance reliability, improve energy efficiency, and reduce interference [3]. These effects are further amplified in massive MIMO [4] where the number of elements in the arrays are in the order of tens or hundreds. Furthermore, the operational bandwidth of the system can be increased by carefully designing the elements of the array [5]. We detail how these advanced antenna systems are used to meet the

wireless requirements for IoT.

1.1.1 Massive MTC and Unsourced Random Access

Machine-type communication (MTC) has two distinct features [6] that make them drastically different from human-type communications (HTC) around which previous cellular systems have mainly evolved: *i*) machine-type devices (MTDs) require sporadic access to the network and *ii*) MTDs usually transmit small data payloads using short-packet signaling. The sporadic access leads to the overall mMTC traffic being generated by an unknown and random subset of active MTDs (at any given transmission instant or frame). This calls for the development of scalable random access protocols that are able to accommodate a massive number of MTDs. Short-packet transmissions, however, make the traditional grant-based access (with the associated scheduling overhead) fall short in terms of spectrum efficiency and latency, which are two key performance metrics in next-generation wireless networks. Hence, a number of grant-free random access schemes have been recently investigated within the specific context of massive connectivity (see [7, 8] and references therein). From the information-theoretic point of view, the problem of massive random access is not recent and dates back to the seminal work of Gallager in [9]. However, with an increasing number of possible applications the problem has reappeared in a new context [10, 11]. As opposed to classical treatments of the Gaussian multiple access channel in which the number of users stays fixed, in the new Gaussian many channel formalism the number of users is allowed to grow with the block-length [10] in a typical massive connectivity setup. Note that when a randomly varying subset of users (with different codebooks) are active over each transmission period, one is bound to sacrifice some of the spectral efficiency for user-identification [10, 12, 13]. However, when all the devices employ the same codebook (aka, unsourced access), the user-identification problem can be separated from the decoding problem as highlighted

in [11]. In fact, by letting all the devices employ the same codebook, the system spectral efficiency depends on the number of active users only and not on total number of users, thereby making different multi-user decoders comparable against each other and to the random coding bound. In particular, it was shown in [11] that increasing the number of active users at a fixed per-user payload renders known solutions such as ALOHA far from the random coding achievability bound. The paradigm in [11] where all users share the same codebook with no need for user identification was later dubbed unsourced random access and now has a number of viable algorithmic solutions. However, most of the existing information-theoretic works on massive connectivity focus on the case of a single receive antenna at the BS. Yet, the idea of using a large-scale antenna array at the BS (i.e. massive MIMO) which was first pioneered in [14], has now become one of the main directions towards which the next-generation of cellular systems are projected to evolve. Some of the best-known algorithms for MIMO URA are the covariance-based scheme in [15], the clustering-based scheme in [16], and tensor-based scheme in [17]. Other more recent methods based on beam-space decoding and Bilinear reconstruction have been developed in [18] and [19, 20], respectively.

1.1.2 URLLC and Age of Information

Ultra-Reliable Low-Latency Communication supports low-latency transmissions (e.g. 4ms) with very high reliability (e.g. with an error probability of 10^{-5}) [21]. This occurs in many critical real-time applications wherein the data must be accurate and its usefulness is directly related to its freshness such as in reliable cloud connectivity, critical connections for industrial automation, and reliable wireless coordination among vehicles [22–24]. While the error probability is a good measure of reliability, due to infrequent access to the network, conventional performance metrics, such as delay fall short in

characterizing the over-all freshness of the data [25]. In this respect, the AoI concept [26] was introduced to adequately characterize the freshness of the information at the receiver side. While many of the existing works on AoI focus primarily on grant-based access with AoI-constrained scheduling policies [27, 28], some have looked at uncoordinated transmission schemes. Recently, a few information-theoretic works have investigated the trade-off between the AoI and achievable data rates [29, 30]. The performance of AoI has been investigated in Multiple-Input Multiple-Output (MIMO) systems [31–34]. In [31], the user scheduling problem has been investigated to minimize AoI in a multiuser MIMO status update system where multiple single-antenna devices send their information over a common wireless uplink channel to a multiple-antenna access point. In [33], a novel MIMO broadcast setting is studied to minimize the sum average AoI through precoding and transmission scheduling. In [32], the authors analyzed and optimized the performance of AoI in a grant-free random-access system with massive MIMO.

1.1.3 Enhanced Mobile Broadband and Multiport Communication

Enhanced Mobile Broadband supports very high peak data rates and, unlike mMTC and URLLC, is characterized by stable device activation patterns and large data payloads [35]. Some of the key technologies that are expected to enable the performance levels of eMBB are massive MIMO and the use of larger bandwidths [36, 37]. Actually, future-generation wireless systems are expected to be super-wideband (i.e., with several octaves of operational bandwidth spanning both sub-6GHz and mmWave bands). The reason for the super-wideband requirement is that future antenna systems are expected to be multi-functional (i.e., used for both sensing and communication), multi-band, multi-standard, and multi-operator as opposed to the current technology [38]. To that

end, future generation wireless systems will require a drastic shift in the design of antenna arrays.

Many of the theoretical promises brought by the MIMO technology are based on modeling antenna arrays with wide inter-element spacing (half-wavelength) wherein the electromagnetic effects of mutual coupling can be reasonably ignored. However in massive MIMO systems, a large number of antennas are to be packed in a compact space. This causes them to endure losses in fading diversity due to the excessive amount of mutual coupling between the antenna elements within the array. While tightly-coupled arrays have less spatial degrees of freedom, they enjoy larger bandwidth due to their ability to support both slowly and rapidly varying spatial current distributions, effectively creating an electrically connected structure [5, 39]. For these reasons, the tightly-coupled connected array of slot antennas appears as one promising antenna structure to use for broadband applications. Due to the fact that it is physically connected, the slot antenna array is effectively a single aperture fed at multiple locations, which leads to tight coupling and an overall increase in the operational bandwidth of the antenna system [5]. Having a single antenna aperture fed at multiple locations is also more convenient from the perspective of analysis/design as well as implementation. As the number of antenna elements in the connected structure increases, enlarging the overall array aperture, the bandwidth keeps expanding with no theoretical low-frequency cut-off [5]. The practical fabrication of such arrays is simplified by the use of PCB technology. To that end, the analysis/design of the overall broadband MIMO system needs to employ channel models (both propagation and antenna) which are both tractable and consistent with the underlying physics.

Although antennas are fundamental devices for wireless transmissions, the analysis and design of MIMO systems have historically evolved around the basic precept of sepa-

rating the mathematical abstractions of communication theory[1] [40] and the physical design considerations from antenna and electromagnetic theories [41, 42]. For instance, the wireless community assesses the performance of MIMO systems in terms of achievable rate and spectral efficiency criteria while the figure of merit for antenna design is the scattering parameters. Research effort has been recently made to bridge such assessment gap between communication and antenna communities, e.g., *wave theory of information* [43], *electromagnetic information theory* [44, 45], *holographic MIMO* [46], and *circuit theory for communication* [47]. Multiport communication theory, first introduced in [48] and popularized by [47], offers a consistent approach to incorporate the physics of radio-communication into the model of the channel matrix and the noise statistics. In this model, we have three interfaces between the transmitter and the receiver. The first and third interfaces consist of the multiport networks that aim to optimize (through different criteria) the link between the transmit/receive signals and their respective antennas. The middle interface is a multiport network that incorporates the physics of propagation as well as the coupling of the antennas in use. Together the communication channel is given by the relationship between the generator signal (voltage/current) and the load signal. This multiport model has led to new insights in beamforming [47], was used to incorporate the impact of the antenna size on the achievable data rate [39, 49] and was adopted to study the performance of near-field communication systems [50]. Further, by merging multiport communication theory with information theory, the achievable rate criterion was used for the design of the matching networks in SISO systems [49, 51] as well as the analysis of coupling in wideband SIMO systems [52].

[1]Particularly the celebrated Shannon capacity formula for band-limited additive white Gaussian noise (AWGN) channels.

1.2 Contribution

The list of contributions is split into two parts. In the first part we investigate a mMTC network and analyze major wireless metrics of the system. In the second part we go into a more in depth analyses of the physics of propagation and develop a physically consistent channel estimation algorithm.

1.2.1 Age of Information in Massive Access Massive MIMO Systems

The major contributions of this part are summarized as follows.

- We derive a closed-form expression of the outage probability in the finite-user, finite-antenna regime and through use of the central-limit theorem (CLT) we express this outage probability in the asymptotic case where both the number of users and the number of antennas are allowed to grow large at a fixed ratio.

- Under the assumption of perfect CSI at the receiver, we derive an achievability bound using a maximal ratio combining (MRC) receiver. We demonstrate how this achievable bound scales with the number of users in the finite regime (e.g. in Theorem 1 in Section IV) and further elaborate on its behaviour in the limit (e.g. through Theorems 2 and 3 in Section 2.3).

- We show that fully uncoordinated non-orthogonal access can achieve minimum AoI as long as all the devices are active in each transmission period. Furthermore, our analysis reveals that with a large-scale antenna array at the BS both high spectral efficiency and low AoI can be achieved.

- We further extend the analysis to the case of imperfect CSI as well as the zero-forcing receiver. We derive the asymptotic as well as limiting spectral efficiency

of both the MRC as well as the zero-forcing receiver when the estimation error is added to the noise contribution.

- Finally, using our bound, we gauge the performance of recent massive MIMO unsourced random access (URA) schemes.

The work that is most closely related to the results presented in Chapter 2 is reported in [13], where the authors considered a massive connectivity with massive MIMO system for uplink data communication. In their paper, they used the state evolution framework to obtain the limiting MSE of the approximate message passing (AMP) channel estimation/activity detection algorithm. They further calculated the achievable rate (interference limited capacity) with the MRC as well as the LMMSE receiver. The limitation of their approach is that it treats only the asymptotic convergence as both the number of antennas and users are infinite while the ratio of the number of antennas to the number of users stays finite. On the other hand, the outage probability formulation together with the approximation analysis presented in this work allows for the asymptotic spectral efficiency characterization of large, yet finite, systems. The non-asymptotic point of view, Theorem 1 in the manuscript, provides the spectral efficiency as well as a precise, $\mathcal{O}(N^{-1.5})$, correction term.

1.2.2 Channel Estimation with Tightly-Coupled Arrays

The mutual coupling effects in antenna systems were previously investigated within the context of carrier frequency offset estimation [53] and the angle of arrival acquisition [54]. Its impact on channel estimation was also explored in [55] where the authors incorporated the mutual coupling in a correlated channel model and have shown the performance degradation due to coupling. In Chapter 3, we provide a more elaborate model that uncovers the effects of mutual coupling both in the channel and noise statistics. As the network parameters of the antennas can be known a priori, we devise

a scheme where one can leverage the mutual coupling to improve channel estimation compared to standard methods. The main contributions embodied in this part are:

- a novel scattering description of the communication channel which requires only the scattering parameters of the arrays as well as the terminated far-field embedded antenna patterns. With the use of only terminated embedded antenna patterns, which can be easily measured as opposed to open/short circuit patterns, the novel description significantly simplifies the antenna design.

- a novel algorithmic solution to the MIMO channel estimation problem in single- and multi-carrier settings, which leverages the knowledge of the antenna scattering parameters to compensate for the effects of mutual coupling and array frequency response.

- in single-carrier systems under frequency-flat channels, we show an improvement of at least 10 [dB] in normalized mean-squared estimation error with respect to standard LMMSE channel estimation. This substantial gain stems from incorporating the array mutual coupling in the channel estimation procedure. We also derive the achievable rate with the new channel estimation procedure and show that almost half of the achievable rate is lost if the mutual coupling is not taken into account.

- in a multi-carrier setting, the proposed algorithm also aims to equalize the frequency selectivity of the antenna array. The gap between the standard LMMSE procedure and the novel antenna-aware procedure widens in presence of antenna array frequency selectivity. This is mainly due to the requirement to estimate a larger number of taps which increases the model complexity. Equivalently the remarkable enhancement in channel estimation performance translates into appreciable achievable rate gains.

- in a multi-carrier setting, we also develop a joint space/frequency power allocation scheme and show that with the newly developed channel estimation procedure the power allocation is close to a perfect CSI scenario.

Table 1.1: Summary of Scholastic Outputs

	Publications	**Appearance**
1.	**B. Tadele**, V. Shyianov, F. Bellili, A. Mezghani and E. Hossain, "Age-Limited Capacity of Massive MIMO," *IEEE Transactions on Communications*, doi: 10.1109/TCOMM.2022.3207820.	Chapter 2
2.	**B. Tadele**, V. Shyianov, F. Bellili, and A. Mezghani, "Channel Estimation for Multicarrier Systems with Tightly-Coupled Broadband Arrays," submitted to *IEEE Journal on Selected Areas in Communication*.	Chapter 3
3.	**B. Tadele**, V. Shyianov, F. Bellili, A. Mezghani and E. Hossain, "Age of Information-Limited Capacity of Uncoordinated Massive Access Using Massive MIMO," *IEEE Wireless Communications and Networking Conference (WCNC)*, doi: 10.1109/WCNC51071.2022.9771933.	Chapter 2
4.	**B. Tadele**, V. Shyianov, F. Bellili, and A. Mezghani,"Channel Estimation with Tightly-Coupled Antenna Arrays," *IEEE International Conference on Acoustics, Speech and Signal Processing (ICASSP)*, doi: 10.1109/ICASSP49357.2023.10096991.	Chapter 3

1.3 Scholastic Outputs and Achievements

This thesis includes material previously published/submitted in peer-reviewed journals and conferences as summarized in Table 1.1. I wish to acknowledge Dr. Amine Mezghani and Dr. Faouzi Bellili for their help and constructive suggestions during the planning and development of this research work.

1.4 Thesis Organization and Notations

We structure the rest of this thesis as follows.

- In Chapter 2 we analyze the AoI and spectral efficiency in massive connectivity massive MIMO systems. Section 2.1 introduces the system model and in Section 2.2, we derive the exact packet probability of error and also find its more insightful asymptotic approximation. In Section 2.3, we state the main results of this chapter on the trade-off between achievable spectral efficiency and the AoI. In Section 2.4, we extend the analysis to the case of imperfect CSI for the MRC and ZF receivers. These results are further corroborated by computer simulations in Section 2.5.

- In Chapter 3 we develop a channel estimation algorithm that accounts for the mutual coupling in the antenna arrays. In Section 3.1, we introduce the model of the broadband MIMO wireless channel based on the impedance [47] as well as scattering descriptions. In Section 3.2, we introduce a single-carrier base-band equivalent channel model as well as develop an antenna-aware channel estimation procedure which we compare to the standard LMMSE channel estimation algorithm. In Section 3.3, we present a base-band equivalent OFDM system and extend the antenna-aware estimation procedure to this framework. Finally, our simulation results are presented in Section 3.4. In this section we 1) describe the slot antenna

including its broadband properties, 2) define the metrics of NMSE and achievable rate and demonstrate performance advantages of the developed antenna-aware estimation procedure, and 3) describe the advantages of using the developed scattering description of the wireless channel and demonstrate the equivalence with the impedance description.

- In Chapter 4, we draw out some concluding remarks and provide future directions to investigate. Additionally, we prove our various claims in the Appendices.

Notations: The following notation is used throughout this thesis. Lower- and upper-case bold fonts (e.g., $\mathbf{x}$ and $\mathbf{X}$) are used to denote vectors and matrices, respectively, and vectors are in column-wise orientation by default. The (m,n)th entry of $\mathbf{X}$ is denoted as $X_{m,n}$, and the nth element of $\mathbf{x}$ is denoted as x_n. We use $\boldsymbol{\mathcal{H}}$ for a channel in the continuous frequency domain, H for the discrete frequency domain, and $\mathbf{H}$ for the discrete time domain. Moreover, $\{.\}^{\mathsf{T}}$ and $\{.\}^{\mathsf{H}}$ stand for the transpose and Hermitian (transpose conjugate) operators, respectively. The operator vec($\mathbf{X}$) stacks the columns of a matrix $\mathbf{X}$ one below the other and tr($\mathbf{X}$) takes its trace. Given a set of matrices $\{\mathbf{X}_1, \mathbf{X}_2, \ldots, \mathbf{X}_N\}$ the operator blockdiag$(\mathbf{X}_1, \mathbf{X}_2, \ldots, \mathbf{X}_N)$ creates a new block diagonal matrix with the matrices $\mathbf{X}_1$, $\mathbf{X}_2$ and $\mathbf{X}_N$ on its diagonal blocks and zeros elsewhere. The Kronecker product is denoted by $\otimes$ and $\triangleq$ is used for definitions. The symbols $|.|$ and $\|.\|_2$ stand for the modulus and Euclidean norm, respectively. The shorthand notation $\mathbf{y} \sim \mathcal{CN}(\mathbf{m}, \mathbf{R})$ means that the random vector $\mathbf{y}$ follows a complex circular Gaussian distribution with mean $\mathbf{m}$ and auto-covariance matrix $\mathbf{R}$. Likewise, $S \sim \Gamma(k, \theta)$ means that the random variable S follows a Gamma distribution with shape parameter k and scale parameter θ. The statistical expectation is denoted as either $\mathbb{E}\{.\}$ or $\mathbb{E}[\cdot]$. $\mathbf{I}_M$ denotes the $M \times M$ identity matrix and where there is no confusion the subscript will be dropped. Given any complex number, $\Re\{\cdot\}$, returns its real part and we use j to denote the imaginary unit (i.e., $j^2 = -1$). Finally, c denotes the speed of light in

vacuum (i.e., $c \approx 3 \times 10^8\,[\mathrm{m/s}]$), T is the temperature in Kelvin, λ is the wavelength, and $k_\mathrm{b} = 1.38 \times 10^{-23}\,[\mathrm{m^2\,kg\,s^{-2}\,K^{-1}}]$ is the Boltzmann constant.

Chapter 2

Age of Information in Massive Access Massive MIMO Systems

2.1 System Model, Assumptions, and Methodology of Analysis

2.1.1 System Model and Definition of AoI

Consider a single-cell network consisting of N single-antenna devices transmitting their status packets over an unreliable multiple-access channel to a BS with M receive antenna elements. To aid synchronization, time is partitioned into slots of equal length T, which is the maximum amount of time for transmission and reception of a single information packet. We assume sporadic device activity where at the start of every time slot user i transmits is current status with probability τ_i. We define $\{\varepsilon_i\}_{i=1}^{N}$ as the binary activity random variables which indicate whether user i transmits its packet or remains idle in

a given slot:

$$\varepsilon_i = \begin{cases} 1 & \text{if user } i \text{ transmits his packet,} \\ 0 & \text{if user } i \text{ remains idle.} \end{cases} \tag{2.1}$$

Moreover, we assume $\{\varepsilon_i\}_{i=1}^{N}$ are independent in each time slot with marginal distributions $\Pr(\varepsilon_i = 1) = \tau_i$. To maintain timely status updates, in every slot a new packet is generated by each user. In this static macro-cell environment, where the coherence time is on the order of hundreds of milliseconds and delay spread is on the order of microseconds [3], the channel remains fairly constant and thus we assume a quasi-static Rayleigh fading model[1] for the duration of the slot in which $\mathbf{h}_i \sim \mathcal{CN}(\mathbf{0}, \mathbf{I}_M)$ denotes the $M \times 1$ channel vector between the i'th user and the BS. The received signal at the BS at discrete time n can then be written as:

$$\mathbf{y}_n \;=\; \sum_{i=1}^{N} \mathbf{h}_i \varepsilon_i x_{i,n} \;+\; \mathbf{w}_n, \tag{2.2}$$

where $x_{i,n} \sim \mathcal{CN}(0, P_i)$ is the transmitted symbol, while $\mathbf{w}_n \sim \mathcal{CN}(\mathbf{0}_M, \sigma_{\mathbf{w}}^2 \mathbf{I}_M)$ is the additive white Gaussian noise (AWGN) which is assumed spatially uncorrelated across all receive antennas. In the presence of K_a active users in a given transmission slot, the above formulation is a K_a-user single-input multiple-output (SIMO) fading Gaussian multiple access channel (GMAC).

Using $p_{e,i}$ to denote the slot-wise packet error probability (PEP) of the ith user, the probability that the ith user updates the BS with its current status is then given by:

$$\gamma_i \;=\; \tau_i(1 - p_{e,i}). \tag{2.3}$$

An example of the slotted system with $N = 3$ users with $T = 1$ is depicted in Fig. 2.1. Under perfect CSI at the receiver we use maximal-ratio combining (MRC) and assume

[1]The assumption of uncorrelated channels between the different antenna elements requires sufficiently large inter-element spacing while the assumption of uncorrelated channel vectors between users is only valid at large separation.

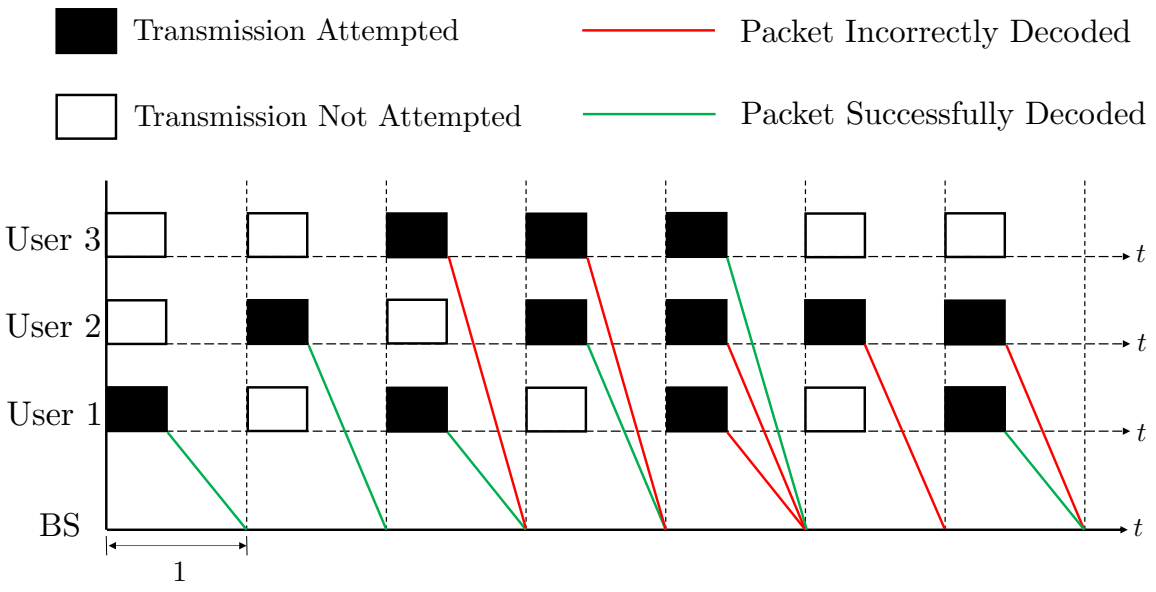

Figure 2.1: Slotted system with $N = 3$ total users and unit slot length.

that the blocklength is sufficiently large such that the capacity limit is approached within a packet, as justified in [56]. Consequently, $p_{e,i}$ can be closely approximated by the following outage probability:

$$1 - p_{e,i} = \Pr\left\{\rho_i < \log_2\left(1 + \frac{\|\mathbf{h}_i\|_2^4 P_i}{\|\mathbf{h}_i\|_2^2 \sigma_{\mathbf{w}}^2 + \sum_{\substack{j=1 \\ j\neq i}}^{N} |\mathbf{h}_i{}^{\mathsf{H}} \mathbf{h}_j|^2 \varepsilon_j P_j}\right)\right\}, \tag{2.4}$$

in which ρ_i [bits/channel-use] is the spectral efficiency of the ith user. Recall that the ultimate goal of each node is to keep the BS updated with its most recent state. If the BS has node i's state that was current at time t_0, the age of that user's state is defined by the random process $\delta_i(t) \triangleq t - t_0$. When node i attempts transmission and gets correctly decoded at the BS we call it an arrival. We denote ith node's jth arrival epoch by $t_{i,j}$. Between two arrival epochs, the age grows as a stair-case function of

time and is reset to T when an arrival occurs, since this is the amount of time that it took for a packet to be transmitted. We denote by $Z_{i,j}$ the inter-arrival time between the jth update and the $(j+1)$th update (i.e. $Z_{i,j} \triangleq t_{i,j+1} - t_{i,j}$). Assuming that the total number of users remains constant in each time slot, user i has a certain success probability, γ_i, that it will update the BS with its state. After normalizing the slotted period to $T = 1$, it then follows that each $Z_{i,j}$ is a geometric random variable with parameter γ_i.

Similar to [57], we define the AoI, Δ_i, of each node i as:

$$\Delta_i \triangleq \lim_{t' \to \infty} \frac{1}{t'} \int_0^{t'} \delta_i(t) dt. \tag{2.5}$$

For completeness, we show in **Appendix A** that the limit in (2.5) exists and that it converges with probability one (WP1) to

$$\Delta_i = \frac{\mathbb{E}[Z_i^2]}{2\mathbb{E}[Z_i]} + \frac{1}{2}, \tag{2.6}$$

as was done in more general terms in [58]. Since the Z_i's are geometric random variables, it follows that $\mathbb{E}[Z_i] = \frac{1}{\gamma_i}$ and $\mathbb{E}[Z_i^2] = \frac{2}{\gamma_i^2} - \frac{1}{\gamma_i}$, thereby leading to[2]:

$$\Delta_i = \gamma_i^{-1}. \tag{2.7}$$

In the presence of N total users, we consider the network-wide average AoI, given by:

$$\Delta = \frac{1}{N} \sum_{i=1}^{N} \Delta_i. \tag{2.8}$$

2.1.2 Methodology of Analysis

Since the AoI solely depends on the parameter τ_i and the outage probability $p_{e,i}$, the main objective will be to find the outage probability. In the following, we will first do

[2]Notice that since the error probability of the ith user $p_{e,i}$ is averaged over the number of active users, the arrival process is still Bernoulli

this in closed-form and thereafter, through use of the central limit theorem, we will find an approximation in the asymptotic regime. This later allows us to find an explicit relationship between the spectral efficiency, τ, the ratio M/N, and the probability of error. To this end, we will illustrate exactly how the spectral efficiency scales in the finite-user, finite-antenna case (e.g., through **Theorem 1** in Section 2.3). Thereafter, we will take the limit as the number of users and the number of antennas grow large and we will find a phase-transition where the AoI is minimized in one regime and grows unbounded in the other (as will be stated in **Theorem 2** and **Theorem 3** in Section 2.3).

2.2 Derivation of Packet Error Probability

2.2.1 Derivation of Exact PEP

Recall from (2.3) that in order for user i to successfully update the BS with its status in a given slot a) it must attempt a transmission in that slot and b) the transmitted packet must be decoded correctly. For ease of analysis, we consider a symmetric system wherein the N users have the same transmit power (i.e. $P_i = P\ \forall i$) and the same attempt probability (i.e. $\tau_i = \tau\ \forall i$). Dividing the second term inside the logarithm in (2.4) by $\|\mathbf{h}_i\|_2^2$ and rearranging the terms we obtain:

$$1 - p_{e,i} = \Pr\left\{ (2^{\rho} - 1)\left(\sigma_{\mathbf{w}}^2 + \sum_{\substack{j=1 \\ j \neq i}}^{N} |P\varepsilon_j \widetilde{\mathbf{h}}_i^{\mathsf{H}} \mathbf{h}_j|^2 \right) \leq \|\mathbf{h}_i\|_2^2 P \right\} \tag{2.9}$$

where $\widetilde{\mathbf{h}}_i = \frac{\mathbf{h}_i}{\|\mathbf{h}_i\|_2}$. For notational compactness we define:

$$\alpha_{\rho} = \frac{1}{2^{\rho} - 1}, \tag{2.10}$$

and we denote the inverse signal-to-noise ratio (SNR) as $\beta \triangleq \frac{\sigma_{\mathbf{w}}^2}{P}$. Using these notations and further simplifying (2.9), we obtain:

$$1 - p_{e,i} \;=\; \Pr\left\{ \alpha_\rho \|\mathbf{h}_i\|_2^2 \;-\; \sum_{\substack{j=1 \\ j\neq i}}^{N} |\widetilde{\mathbf{h}}_i^{\mathsf{H}} \mathbf{h}_j|^2 \varepsilon_j \;\geq\; \beta \right\}. \tag{2.11}$$

As was shown in [59], $\widetilde{\mathbf{h}}_i^{\mathsf{H}} \mathbf{h}_j \sim \mathcal{CN}(0,1)\ \forall\ i,j$ and they are mutually independent and also independent of $\|\mathbf{h}_i\|_2^2$. In order to deal with the random sum in (2.11), we condition on the event of having k other users being active with the ith user. Since the ε_j's are independent and identically distributed (i.i.d) Bernoulli random variables (RVs), the probability that k users are active out of the remaining $N-1$ users (i.e. after excluding user i) is the same as having k successes in $N-1$ Bernoulli trials. Thus, the number of active users follows a Binomial distribution with parameters $N-1$ and τ. In order to calculate $p_{e,i}$ for each ith user it is convenient to marginalize over the number of other active users, thereby leading to:

$$p_{e,i} \;=\; 1 \;-\; \sum_{k=0}^{N-1} \binom{N-1}{k} \tau^k (1-\tau)^{N-1-k} p_{i|k}, \tag{2.12}$$

where $p_{i|k}$ is defined as the conditional probability of successful decoding, conditioned on k other users being also active. More specifically, we have:

$$p_{i|k} \;=\; \Pr\left\{ \alpha_\rho \|\mathbf{h}_i\|_2^2 \;-\; \sum_{j=1}^{k} |\widetilde{\mathbf{h}}_i^{\mathsf{H}} \mathbf{h}_j|^2 \;\geq\; \beta \right\}, \tag{2.13}$$

where $\|\mathbf{h}_i\|_2^2$ follows a gamma distribution with shape parameter M and scale parameter 1 (i.e., $||\mathbf{h}_i||_2^2 \sim \Gamma(M,1)$). Similarly, the second term in (2.13) is a sum of k complex normal RVs squared and hence follows a $\Gamma(k,1)$ distribution. By defining $H \triangleq \alpha_\rho \|\mathbf{h}_i\|_2^2$ and $X_k \triangleq \sum_{j=1}^{k} |\widetilde{\mathbf{h}}_i^{\mathsf{H}} \mathbf{h}_j|^2$, we see that $p_{i|k}$ in (2.13) is the complementary distribution function of the RV $Z \triangleq H - X_k$, as a function of the inverse SNR. In the case there are no other active users (i.e. $k=0$), $p_{i|k}$ is given by the complementary distribution of a

gamma RV[3]. For $k > 0$, however, one can find the probability density function (pdf) of Z through convolution, thereby leading to:

$$f_Z(z) = \begin{cases} \kappa \int_{-\infty}^{z} (-x)^{k-1}(z-x)^{M-1} e^{2\rho x} dx & \text{if } z < 0 \\ \kappa \int_{-\infty}^{0} (-x)^{k-1}(z-x)^{M-1} e^{2\rho x} dx \text{ if } z \geq 0, \end{cases} \tag{2.14}$$

where $\kappa = \frac{e^{\frac{-z}{\alpha_\rho}}}{(k-1)!(M-1)!\alpha_\rho^M}$. Since we are primarily interested in the probability that Z is greater than[4] $\beta > 0$, we are only concerned with $f_Z(z)$ for non-negative values of z. By further manipulating the integral (2.14), it can be shown that the pdf for $z \geq 0$ can be written as:

$$f_Z(z) = \frac{z^{\left(\frac{M+k-2}{2}\right)}}{(M-1)!\alpha_\rho^M 2^{\frac{\rho}{2}(M+k)}} \exp\left(-\frac{z}{2}(2^\rho - 2)\right) \widetilde{W}_{\frac{M-k}{2}, \frac{1-M-k}{2}}(2^\rho z) \tag{2.15}$$

where $\widetilde{W}(.)$ denotes the Whittaker function. Averaging $p_{i|k}$ over the number of active users and incorporating everything together we can finally write $p_{e,i}$ as follows:

$$\begin{aligned} p_{e,i} &= 1 - (1-\tau)^{N-1}\big(1 - \Pr\{H \leq \beta\}\big) \\ &\quad - \sum_{k=1}^{N-1} \binom{N-1}{k} \tau^k (1-\tau)^{N-1-k} \int_\beta^\infty f_Z(z) dz. \end{aligned} \tag{2.16}$$

2.2.2 Asymptotic Approximation of PEP

While (2.16) is an exact expression for PEP, it does not provide insights into the scaling law of error probability as the total number of users and the number of BS antenna branches both increase at a fixed ratio. In this Section, we derive an asymptotic approximation of PEP which becomes increasingly exact in the large system limit. More

[3]A gamma RV, with scale parameter θ, multiplied by a real number α_ρ, is another gamma RV with scale parameter $\alpha_\rho\theta$.

[4]Recall here that β is the inverse SNR which is a positive quantity.

specifically, we will let the number of users N and the number of antennas M grow large, while keeping their ratio, $\zeta \triangleq \frac{M}{N}$, constant.

The analysis technique utilized in what follows capitalizes on the Berry-Esseen theorem. Proofs of the various claims introduced in this Section are detailed in **Appendix B**. Using symmetry arguments, it can be seen that $p_{e,i}$ does not depend on i and after omitting that index it follows from (2.12) that:

$$1 - p_e = \sum_{k=0}^{N-1} \Pr\left\{\varepsilon_1 + \ldots + \varepsilon_{N-1} = k\right\} G_{M,k}(\beta), \tag{2.17}$$

where $G_{M,k}(\beta) = \Pr\left\{\sum_{m=1}^{2M} S_m + \sum_{l=1}^{2k} V_l \geq \beta\right\}$ in which $S_m \sim \Gamma(\frac{1}{2}, \alpha_\rho)$ and $V_l \sim \Gamma(\frac{1}{2}, 1)$. Using Berry-Essen central limit theorem (BE-CLT), the inverse cumulative distribution function (CDF) of the sum of gamma RVs in (2.17) converges uniformly to the standard normal inverse CDF (see Lemma 1 in **Appendix B**), i.e.

$$\Pr\left\{\sum_{m=1}^{2M} S_m + \sum_{l=1}^{2k} V_l \geq \beta\right\} \;=\; Q(w(k)) \;+\; \mathcal{O}\left(\frac{1}{\sqrt{M+k}}\right), \tag{2.18}$$

where $w(k) = \frac{\beta - \alpha_\rho M + k}{\sqrt{\alpha_\rho^2 M + k}}$ and $Q(.)$ is the standard Q-function, (i.e., the tail of the normal distribution):

$$Q(x) \;=\; \frac{1}{\sqrt{2\pi}} \int_x^{+\infty} e^{\frac{-t^2}{2}} dt. \tag{2.19}$$

Now incorporating the result in (2.18) into (2.17) and then using the CLT on $\Pr\{\varepsilon_1 + \ldots + \varepsilon_{N-1} = k\}$, (2.17) can be re-written as (see Lemma 2 in **Appendix B**):

$$p_e \;=\; 1 \;-\; \frac{1}{\sqrt{2\pi}} \int_{-\infty}^{\infty} Q(w(s)) e^{-\frac{s^2}{2}} ds \;+\; \mathcal{O}\left(\frac{1}{\sqrt{N}}\right), \tag{2.20}$$

where

$$w(s) \;=\; \frac{\beta - \alpha_\rho M + s\sqrt{(N-1)\tau(1-\tau)} + (N-1)\tau}{\sqrt{\alpha_\rho^2 M + s\sqrt{(N-1)\tau(1-\tau)} + (N-1)\tau}}. \tag{2.21}$$

For large N, we approximate $N-1$ by N (see Lemma 3 in **Appendix B**) thereby leading to:

$$w(s) \;=\; \frac{\beta - \alpha_\rho M + s\sqrt{N\tau(1-\tau)} + N\tau}{\sqrt{\alpha_\rho^2 M + s\sqrt{N\tau(1-\tau)} + N\tau}} \;+\; \mathcal{O}\left(\frac{1}{\sqrt{N}}\right). \tag{2.22}$$

Then by substituting $\zeta = \frac{M}{N}$ and multiplying both the numerator and denominator by $\frac{1}{\sqrt{N}}$ we obtain:

$$w(s) \;=\; \frac{\frac{\beta}{\sqrt{N}} - \alpha_\rho \zeta\sqrt{N} + s\sqrt{\tau(1-\tau)} + \sqrt{N}\tau}{\sqrt{\alpha_\rho^2\zeta + \frac{s}{\sqrt{N}}\sqrt{\tau(1-\tau)} + \tau}} + \mathcal{O}\left(\frac{1}{\sqrt{N}}\right). \tag{2.23}$$

We further neglect the terms which vanish for large N in (2.23), thereby leading to (see Lemma 4 in **Appendix B**),

$$w(s) = \frac{\sqrt{N}(\tau - \alpha_\rho\zeta) + s\sqrt{\tau(1-\tau)}}{\sqrt{\alpha_\rho^2\zeta + \tau}} + \mathcal{O}\left(\frac{1}{\sqrt{N}}\right). \tag{2.24}$$

We can also neglect the second term in the numerator of (2.24) that involves the integration variable s. In fact, although s grows large inside the integral, the exponential makes the integrand function vanish for large-magnitude values of s. Small values of s, however, can also be neglected for large values of N (i.e., in the asymptotic regime). Finally, our approximation for $w(s)$ makes it independent of s (see Lemma 5 in **Appendix B**):

$$w \;=\; \frac{\sqrt{N}(\tau - \alpha_\rho\zeta)}{\sqrt{\alpha_\rho^2\zeta + \tau}} + \mathcal{O}(1). \tag{2.25}$$

Consequently, one can take $Q(w(s))$ outside of the integral in (2.20) (see Lemma 6 in **Appendix B**):

$$p_e \;=\; 1 - Q(w)\int_{-\infty}^{\infty} \frac{1}{\sqrt{2\pi}} e^{-\frac{s^2}{2}} ds + \mathcal{O}\left(\frac{1}{\sqrt{N}}\right), \tag{2.26}$$

which simplifies to:

$$p_e \;=\; 1 - Q(w) + \mathcal{O}\left(\frac{1}{\sqrt{N}}\right). \tag{2.27}$$

2.3 Trade-Off Between AoI and Spectral Efficiency

In this Section, we characterize the trade-off between the achievable spectral efficiency and the AoI in multiuser systems with a large-scale antenna array at the BS. It is shown that as the number of users, N, and the number of antennas, M, increase while keeping their ratio constant (i.e. $\zeta = \frac{M}{N}$) the maximum achievable spectral efficiency approaches a well-characterized limit for any fixed AoI. The trade-off is manifested by making an observation that spectral efficiencies above the established limit can only be achieved by increasing the overall system AoI. To that end, we rewrite (2.8) more explicitly as a function of the system parameters (see Lemma 7 in **Appendix B**):

$$\Delta(\zeta, N, \rho, \tau) \;=\; \frac{1}{\tau\left(1 - Q\left(\frac{\sqrt{N}(\alpha_\rho \zeta - \tau)}{\sqrt{\alpha_\rho^2 \zeta + \tau}}\right)\right)} + \mathcal{O}\left(\frac{1}{\sqrt{N}}\right), \tag{2.28}$$

from which it follows, in the limit, that the minimum AoI for a given attempt probability τ is given by[5]:

$$\Delta_{\min}(\tau) \;=\; \frac{1}{\tau}. \tag{2.29}$$

We start by defining, for a given N, τ, and $\epsilon > 0$, the set:

$$\Psi_\epsilon \;\triangleq\; \{\rho \in \Re^+ \mid p_e < \epsilon\}, \tag{2.30}$$

as the set of all achievable spectral efficiencies for which the probability of error is less than ϵ. Note also that the condition $p_e < \epsilon$ implies that $\Delta(\zeta, N, \rho, \tau) < \frac{1}{\tau(1-\epsilon)} + \mathcal{O}\big(\frac{1}{\sqrt{N}}\big)$. We illustrate fundamental trade-offs in finite user case in the following theorem.

[5]One can also numerically optimize (2.28), ignoring the error term, and find the τ that minimizes (2.28). Ignoring the error term will have minimal affect in this optimization as seen in the real-time simulation in Fig. 2.2.

Theorem 1. *For any $0 < \tau < 1$, $\zeta > 0$, and $\epsilon > 0$, there exist $N_0 \in \mathbb{N}$ such that for any $N > N_0$, the set Ψ_ϵ is non-empty with a supremum*

$$\rho_N^* \triangleq \sup_{\rho} \Psi_\epsilon = \log_2\left(1 + \frac{\zeta - \frac{Q^{-1}(\epsilon)^2}{N}}{\tau + \sqrt{\tau^2 + \tau\left(1 - \frac{Q^{-1}(\epsilon)^2}{N\zeta}\right)\left(\frac{Q^{-1}(\epsilon)^2}{N} - \tau\right)}}\right) + \mathcal{O}\left(\frac{1}{N^{1.5}}\right). \tag{2.31}$$

Proof. As shown in **Appendix C**, the condition that $p_e < \epsilon$ leads to $\alpha_\rho > \alpha_\rho^+(\epsilon_1)$ where:

$$\alpha_\rho^+(\epsilon_1) = \frac{\tau + \sqrt{\tau^2 - \tau(1 - \frac{Q^{-1}(\epsilon_1)^2}{N\zeta})(\tau - \frac{Q^{-1}(\epsilon_1)^2}{N})}}{\zeta - \frac{Q^{-1}(\epsilon_1)^2}{N}}, \tag{2.32}$$

and $\epsilon_1 = \epsilon + \mathcal{O}\big(1/\sqrt{N}\big)$. Due to the differentiability of Q^{-1}, the error term can be taken out of Q^{-1} in (2.32) thereby leading to:

$$\alpha_\rho^+(\epsilon_1) = \frac{\tau + \sqrt{\tau^2 - \tau\left(1 - \frac{Q^{-1}(\epsilon)^2}{N\zeta} + \mathcal{O}\big(\frac{1}{N^{1.5}}\big)\right)\left(\tau - \frac{Q^{-1}(\epsilon)^2}{N} + \mathcal{O}\big(\frac{1}{N^{1.5}}\big)\right)}}{\zeta - \frac{Q^{-1}(\epsilon)^2}{N} + \mathcal{O}\big(\frac{1}{N^{1.5}}\big)}. \tag{2.33}$$

Recalling the definition of α_ρ, we see that $\alpha_\rho > \alpha_\rho^+(\epsilon_1)$ is equivalent to:

$$\rho < \log_2\left(1 + \frac{1}{\alpha_\rho^+(\epsilon_1)}\right). \tag{2.34}$$

Again, due to the differentiability of the logarithm and due to ϵ being greater than $\epsilon_0(N, \zeta)$ the error term can be taken out of the logarithm and we have:

$$\rho < \log_2\left(1 + \frac{1}{\alpha_\rho^+(\epsilon)}\right) + \mathcal{O}\left(\frac{1}{N^{1.5}}\right). \tag{2.35}$$

Therefore, Ψ_ϵ can be re-written as:

$$\Psi_\epsilon = \left\{\rho \in \Re^+ \;\middle|\; \rho < \log_2\left(1 + \frac{1}{\alpha_\rho^+(\epsilon)}\right) + \mathcal{O}\left(\frac{1}{N^{1.5}}\right)\right\}. \tag{2.36}$$

Note that the upper bound on ρ is always positive as we assume $\epsilon > \epsilon_0(N, \zeta)$ and hence Ψ_ϵ is non-empty and its is supremum is given by (2.31). □

A special case of **Theorem 1** wherein the error probability vanishes in the limit is described in the following two theorems.

Theorem 2. *(Achievability) For any $0 < \tau < 1$ and $\zeta > 0$, we define the age-limited capacity as*

$$C_{\tau,\zeta} \;=\; \log_2\left(1+\frac{\zeta}{\tau}\right), \tag{2.37}$$

such that for any spectral efficiency, $\rho < C_{\tau,\zeta}$, the error probability, $p_e \to 0$, and the AoI, $\Delta(\zeta, N, \rho, \tau) \to \Delta_{min}(\tau)$, as $N \to \infty$.

Proof. Note that the second term in (2.28) goes to zero in the limit as $N \to \infty$ and so the AoI is determined by the first term. Given the parameters τ and ζ, we see that the AoI in (2.28) is monotonically increasing with p_e. Therefore, as $p_e \to 0$ the AoI $\Delta(\zeta, N, \rho, N) \to \Delta_{\min}(\tau)$. Now, fix $\delta > 0$ and $\rho = C_{\tau,\zeta} - \delta$. The probability of error is determined by the Q-function or equivalently its argument. Hence, for a given N and a given value of

$$\varphi(\rho) \;\triangleq\; \frac{\alpha_\rho \zeta - \tau}{\sqrt{\alpha_\rho^2 \zeta + \tau}}, \tag{2.38}$$

the probability of error is well specified. Plugging ρ in (2.38), it follows that:

$$\varphi(C_{\tau,\zeta} - \delta) \;=\; \frac{(\zeta+\tau)(1-2^{-\delta})}{\sqrt{\zeta + \tau(2^{(C_{\tau,\zeta}-\delta)}-1)^2}}, \tag{2.39}$$

which is always positive. Therefore, as $N \to \infty$ the argument inside the Q-function approaches $+\infty$; hence $p_e \to 0$ and $\Delta(\zeta, N, \rho, \tau) \to \Delta_{\min}(\tau)$. □

Theorem 3. *Given τ, ζ and any spectral efficiency $\rho > C_{\tau,\zeta}$, the error probability, $p_e \to 1$, and the AoI $\Delta(\zeta, N, \rho, \tau) \to \infty$ as, $N \to \infty$.*

Proof. We prove this in a similar way as we did for **Theorem 2**. In fact, we choose an arbitrary $\delta > 0$ and set $\rho = C_{\tau,\zeta} + \delta$. Plugging the latter in (2.38) and simplifying we obtain:

$$\varphi(C_{\tau,\zeta} + \delta) \;=\; -\; \frac{(\zeta+\tau)(2^{\delta}-1)}{\sqrt{\zeta + \tau(2^{(C_{\tau,\zeta}+\delta)}-1)^2}}. \tag{2.40}$$

Now, the argument inside the Q-function is negative for all values of N and approaches $-\infty$ as $N \to \infty$, from which it follows that $p_e \to 1$ and $\Delta(\zeta, N, \rho, \tau) \to \infty$. □

Corollary 3.1. *For any $\epsilon > 0$, the age-limited capacity defined in (2.37) is given by*

$$C_{\tau,\zeta} \;=\; \lim_{N \longrightarrow \infty} \rho_N^*. \tag{2.41}$$

Proof. We see that as $N \to \infty$ the threshold, $\epsilon_0(N, \zeta)$ goes to zero as it decays with N. Therefore, for any $\epsilon > 0$, ρ_N^* is well defined. As the function $\log_2 x$ is continuous at $x = 1 + \frac{\zeta}{\tau}$, one can take the limit inside its argument in ρ_N^*, from which the corollary follows. □

Remark 1. *It is interesting to observe the similarity between the age-limited capacity and the capacity of the AWGN channel. In the age-limited capacity, the ratio $\frac{\zeta}{\tau}$ plays the role of the SNR in the AWGN Capacity. In working with asymptotic scenarios where we have both a large number of users and a large number of antennas, the noise variance becomes negligible. In this asymptotic interference-limited scenario the decoding error probability is dominated by τ. It is insightful in this case to view τ as the noise variance. Similarly, the ratio, ζ, of the number of antennas to the number of users plays the role of the transmit power.*

Remark 2. *Note also, that the age-limited capacity, $C_{\tau,\zeta} = \log_2\left(1 + \frac{\zeta}{\tau}\right)$, is parameterized by τ and ζ and can be increased by decreasing the value of τ. Now, for any spectral efficiency below $C_{\tau,\zeta}$ our analysis reveals that the age-limited capacity can be approached as $N \to \infty$ in which case the minimum achievable AoI is given by (2.29). Thus, while the aggregate spectral efficiency can be made large by decreasing τ, the price is an undesired increase in the AoI. This should be expected on intuitive grounds since as τ becomes small, the users that are lucky to transmit in a given slot can be easily separated in the spatial domain by making use of a large-scale antenna array at the BS.*

2.4 Analysis with Imperfect CSI

We incorporate imperfect CSI into our analysis by using a channel estimator and writing the error in channel estimation as $\boldsymbol{\mathcal{E}} \triangleq \widehat{\mathbf{H}} - \mathbf{H}$, where $\widehat{\mathbf{H}}$ is the channel estimate. We assume that $\widehat{\mathbf{H}}$ and $\boldsymbol{\mathcal{E}}$ are independent and $\boldsymbol{\mathcal{E}}_i \sim \mathcal{CN}(\mathbf{0}_M, \sigma_p^2 \mathbf{I}_M)$, $\widehat{\mathbf{h}}_i \sim \mathcal{CN}(\mathbf{0}_M, (1 - \sigma_p^2)\mathbf{I}_M)$ where $\boldsymbol{\mathcal{E}}_i$ and $\widehat{\mathbf{h}}_i$ are the i^{th} columns of $\boldsymbol{\mathcal{E}}$ and $\widehat{\mathbf{H}}$ respectively and σ_p^2 is the mean-squared error (MSE) in channel estimation. We further assume that the columns of $\boldsymbol{\mathcal{E}}$ and $\widehat{\mathbf{H}}$ are independent. In the analysis we append the estimation error into the noise and interference terms. The MSE, σ_p^2, of the MMSE estimator could be obtained from the state evolution of the AMP algorithm [13].

2.4.1 Maximal-Ratio Combining

In the case of MRC our system model becomes:

$$\mathbf{y}_n \;=\; \sum_{i=1}^{N} \widehat{\mathbf{h}}_i \varepsilon_i x_{i,n} \;-\; \sum_{i=1}^{N} \boldsymbol{\mathcal{E}}_i \varepsilon_i x_{i,n} \;+\; \mathbf{w}_n. \tag{2.42}$$

From this view, we can write the outage probability as:

$$p_{e,i} \;=\; 1 - \Pr\{\rho_i \;<\; C_{\text{MRC}}\}, \tag{2.43}$$

where

$$C_{\text{MRC}} \triangleq$$
$$\log_2 \left(1 + \frac{\|\widehat{\mathbf{h}}_i\|_2^4 P_i}{\|\widehat{\mathbf{h}}_i\|_2^2 \sigma_{\mathbf{w}}^2 \;+\; \sum_{\substack{j=1 \\ j \neq i}}^{N} |\widehat{\mathbf{h}}_i^{\mathsf{H}} \widehat{\mathbf{h}}_j|^2 \varepsilon_j P_j \;+\; \sum_{j=1}^{N} |\widehat{\mathbf{h}}_i^{\mathsf{H}} \boldsymbol{\mathcal{E}}_j|^2 \varepsilon_j P_j} \right).$$

Conditioning on k out of the total N users being active and considering a symmetric system as before, i.e., $P_i{=}P$ $\forall i$, and simplifying we write the conditional outage

probability, $p_{e|k}$, as:

$$1 - p_{e|k} = \Pr\left\{ \alpha_\rho \|\widehat{\mathbf{h}}_i\|_2^2 - \sum_{j=1}^{k} |\widetilde{\mathbf{h}}_i^{\mathsf{H}} \widehat{\mathbf{h}}_j|^2 - \sum_{j=1}^{k+1} |\widetilde{\mathbf{h}}_i^{\mathsf{H}} \boldsymbol{\mathcal{E}}_j|^2 \geq \beta \right\}, \tag{2.44}$$

where $\widetilde{\mathbf{h}}_i = \frac{\widehat{\mathbf{h}}_i}{\|\widehat{\mathbf{h}}_i\|_2}$. To make this convenient for use of the CLT we write (2.44) as:

$$1 - p_{e|k} \;=\; \Pr\left\{ \sum_{m=1}^{2M} S_m \;+\; \sum_{l=1}^{2k} V_l \;+\; \sum_{n=1}^{2(k+1)} T_n \;\geq\; \beta \right\}, \tag{2.45}$$

where $S_m \sim \Gamma(\frac{1}{2}, \alpha_\rho(1-\sigma_p^2))$, $V_l \sim \Gamma(\frac{1}{2}, (1-\sigma_p^2))$, and $T_n \sim \Gamma(\frac{1}{2}, \sigma_p^2)$. We now apply the CLT and use the same techniques utilized previously to get the asymptotic results. We will disregard the error terms in this analysis to avoid redundancy. Applying the CLT the conditional outage probability can be written as:

$$p_{e|k} \approx 1 - Q(w(k)), \tag{2.46}$$

where

$$w(k) = \frac{\beta - \alpha_\rho(1-\sigma_p^2)M + (1-\sigma_p^2)k + (k+1)\sigma_p^2}{\sqrt{\alpha_\rho^2(1-\sigma_p^2)^2 M + (1-\sigma_p^2)k + (k+1)\sigma_p^4}}.$$

Similar to the perfect CSI case, we make a normal approximation to the binomial distribution, $k = s\sqrt{(N-1)\tau(1-\tau)} + (N-1)\tau$, we approximate $N-1$ by N, and substitute $\zeta N = M$:

$$w(s) = \frac{(\beta + \sigma_p^2) - \alpha_\rho(1-\sigma_p^2)\zeta N + s\sqrt{N\tau(1-\tau)} + N\tau}{\sqrt{\alpha_\rho^2(1-\sigma_p^2)^2\zeta N + ((1-\sigma_p^2)^2 + \sigma_p^4)(s\sqrt{N\tau(1-\tau)} + N\tau) + \sigma_p^4}}.$$

Next we divide both the numerator and denominator by $\sqrt{N}$ and neglect terms that do not grow with N:

$$w(s) = \frac{\sqrt{N}(\tau - \alpha_\rho(1-\sigma_p^2)\zeta)}{\sqrt{\alpha_\rho^2(1-\sigma_p^2)^2\zeta + \tau((1+\sigma_p^2)^2 + \sigma_p^4)}}. \tag{2.47}$$

As $w(s)$ is now independent of s, averaging over the binomial distribution will have no affect and thus we can write the total outage probability of the system as:

$$p_e \;\approx\; Q\left(\frac{\sqrt{N}(\alpha_\rho(1-\sigma_p^2)\zeta-\tau)}{\sqrt{\alpha_\rho^2(1-\sigma_p^2)^2\zeta+\tau((1+\sigma_p^2)^2+\sigma_p^4)}}\right). \tag{2.48}$$

Similar to the perfect CSI case, we find the achievable rate for a given error probability of ϵ given by:

$$\rho^{\mathrm{MRC}} \approx$$
$$\log_2\left(1 \;+\; \frac{1}{\frac{\tau}{\zeta}\frac{1}{(1-\sigma_p^2)}+\frac{Q^{-1}(\epsilon)\sqrt{\alpha_\rho^2(1-\sigma_p^2)^2\zeta+\tau((1+\sigma_p^2)^2+\sigma_p^4)}}{\zeta(1+\sigma_p^2)\sqrt{N}}}\right),$$

which in the limit leads to:

$$\rho^{\mathrm{MRC}} \;=\; \log_2\left(1 \;+\; \frac{\zeta}{\tau}(1-\sigma_p^2)\right). \tag{2.49}$$

2.4.2 Zero-Forcing

We first start by rewriting the system model given in (2.2) in a matrix-vector product form given by:

$$\mathbf{y}_n = \mathbf{H}\mathbf{x}_n \;+\; \mathbf{w}_n, \tag{2.50}$$

where $\mathbf{H} = [\varepsilon_1\mathbf{h}_1, \ldots, \varepsilon_N\mathbf{h}_N]$ and $\mathbf{x}_n = [x_{1,n}, \ldots, x_{N,n}]^{\mathsf{T}}$. Conditioned on k out of the N total users being active we can write ZF receiver as:

$$\mathbf{W}_{\mathrm{ZF}}^{\mathsf{H}} = \frac{1}{\sqrt{P}}(\mathbf{H}^{\mathsf{H}}\mathbf{H})^{-1}\mathbf{H}^{\mathsf{H}}, \tag{2.51}$$

where now $\mathbf{H}$ is only composed of the channels of the k active transmitters. Applying this linear receiver to $\mathbf{y}_n$ we have:

$$\mathbf{W}_{\mathrm{ZF}}^{\mathsf{H}}\mathbf{y}_n = \mathbf{s}_n \;+\; \mathbf{v}_n, \tag{2.52}$$

where now $\mathbf{s}_n \sim \mathcal{CN}(\mathbf{0}_k, \mathbf{I}_k)$ and $\mathbf{v}_n$ is coloured noise with $\mathbb{E}[\mathbf{v}_n\mathbf{v}_n^{\mathsf{H}}|\mathbf{H}] = \beta(\mathbf{H}^{\mathsf{H}}\mathbf{H})^{-1}$. In this case, the i^{th} user will see a scalar channel and the maximum achievable rate over this channel will be given by $\log_2(1+\mathrm{SNR}_i^{\mathrm{ZF}})$ where $\mathrm{SNR}_i^{\mathrm{ZF}}$ is given by:

$$\mathrm{SNR}_i^{\mathrm{ZF}} = \frac{\mathbb{E}[\mathbf{s}_n\mathbf{s}_n^{\mathsf{H}}]_{i,i}}{\mathbb{E}[\mathbf{v}_n\mathbf{v}_n^{\mathsf{H}}|\mathbf{H}]_{i,i}} = \frac{1}{\beta(\mathbf{H}^{\mathsf{H}}\mathbf{H})^{-1}_{i,i}}. \tag{2.53}$$

$\mathrm{SNR}_i^{\mathrm{ZF}}$ is found to follow a Chi-Squared distribution with $2(M-k+1)$ degrees of freedom (DOF). For the case that no other users are active besides user i, $\mathrm{SNR}_i^{\mathrm{ZF}}$ follows a Chi-Squared distribution with $2M$ DOF [3]. Therefore, averaging over all of the users we can write the error probability as:

$$\begin{aligned} p_e \;&=\; (1-\tau)^{N-1}\int_0^{2^\rho-1} f_{\chi^2_{2M}}(\eta)d\eta \\ &+\sum_{k=1}^{N-1}\binom{N-1}{k}\tau^k(1-\tau)^{N-1-k}\int_0^{2^\rho-1} f_{\chi^2_{2(M-k+1)}}(\eta)d\eta, \end{aligned} \tag{2.54}$$

from which the AoI simply follows from (2.8).

To analyze our system asymptotically under ZF we write our system model as:

$$\mathbf{y}_n = \sqrt{P(1-\sigma_p^2)}\widehat{\mathbf{H}}\mathbf{s}_n \;-\; \sqrt{P}\boldsymbol{\mathcal{E}}\mathbf{s}_n \;+\; \mathbf{w}_n. \tag{2.55}$$

Conditioning on k out of the N users being active the ZF filter can be written as:

$$\mathbf{W}_{\mathrm{ZF}}^{\mathsf{H}} = \frac{1}{\sqrt{P(1-\sigma_p^2)}}(\widehat{\mathbf{H}}^{\mathsf{H}}\widehat{\mathbf{H}})^{-1}\widehat{\mathbf{H}}^{\mathsf{H}}, \tag{2.56}$$

where now $\widehat{\mathbf{H}}$ is only composed of the channels of the k active transmitters. Applying this linear receiver to $\mathbf{y}_n$ we have:

$$\mathbf{W}_{\mathrm{ZF}}^{\mathsf{H}}\mathbf{y}_n = \mathbf{s}_n \;+\; \mathbf{v}_n, \tag{2.57}$$

where now $\mathbf{s}_n \sim \mathcal{CN}(\mathbf{0}_k, \mathbf{I}_k)$ and $\mathbf{v}_n$ is coloured noise with the estimation error term, i.e:

$$\mathbf{v}_n \;=\; -\sqrt{P}\mathbf{W}_{\mathrm{ZF}}^{\mathsf{H}}\boldsymbol{\mathcal{E}}\mathbf{s}_n \;+\; \mathbf{W}_{\mathrm{ZF}}^{\mathsf{H}}\mathbf{w}_n. \tag{2.58}$$

In this case, the i^{th} user will see a scalar channel and the maximum achievable rate over this channel will be given by $\log_2(1+\mathrm{SNR}_i^{\mathrm{ZF}})$ where $\mathrm{SNR}_i^{\mathrm{ZF}}$ is given by:

$$\mathrm{SNR}_i^{\mathrm{ZF}} = \frac{\mathbb{E}[\mathbf{s}_n\mathbf{s}_n^{\mathsf{H}}]_{i,i}}{\mathbb{E}[\mathbf{v}_n\mathbf{v}_n^{\mathsf{H}}]_{i,i}} = \frac{1}{\mathbb{E}[\mathbf{v}_n\mathbf{v}_n^{\mathsf{H}}]_{i,i}}. \tag{2.59}$$

It is easy to show that:

$$\mathbb{E}[\mathbf{v}_n\mathbf{v}_n^{\mathsf{H}}] \;=\; \left(\frac{k\sigma_p^2+\beta}{1-\sigma_p^2}\right)(\widehat{\mathbf{H}}^{\mathsf{H}}\widehat{\mathbf{H}})^{-1}. \tag{2.60}$$

Therefore, we can now write the conditional outage probability as:

$$p_{e|k} \;=\; \Pr\left\{\frac{1}{\left(\frac{k\sigma_p^2+\beta}{1-\sigma_p^2}\right)(\widehat{\mathbf{H}}^{\mathsf{H}}\widehat{\mathbf{H}})_{i,i}^{-1}} \le \frac{1}{\alpha_\rho}\right\} \tag{2.61}$$

For the asymptotic analysis we let M and N grow large while holding their ratio, $\zeta = M/N$, constant. In the case of ZF we additionally have the condition that $\zeta \geq 1$. We can see the first term in (2.54) goes to 0 as N grows large and we focus on the second term. We note that the RV:

$$Z = \frac{\chi^2_{2(M-k+1)} - (M-k+1)/\left(\frac{k\sigma_p^2+\beta}{1-\sigma_p^2}\right)}{\sqrt{M-k+1}/\left(\frac{k\sigma_p^2+\beta}{1-\sigma_p^2}\right)}, \tag{2.62}$$

tend to a normal distributions by the central limit theorem as the number of DOF grow large. Therefore we can rewrite the second integral in (2.54) as:

$$\int_0^{2^\rho-1} f_{\chi^2_{2(M-k+1)}}(\eta)d\eta \;\rightarrow\; \int_{-\sqrt{M-k+1}}^{\lambda_{M,k}} f_Z(z)dz, \tag{2.63}$$

where:

$$\lambda_{M,k} \;=\; \frac{k\sigma_p^2+\beta}{\alpha_\rho(1-\sigma_p^2)\sqrt{M-k+1}} - \sqrt{M-k+1}.$$

We can write the integral in (2.63) as a difference of two Q-functions given by the upper and lower bounds of the integral, i.e:

$$\int_{-\sqrt{M-k+1}}^{\lambda_{M,k}} f_Z(z)dz = Q\left(-\sqrt{M-k+1}\right) - Q(\lambda_{M,k}). \tag{2.64}$$

As we let M grow large for a fixed k the term on the left goes to 1. Making the substitution $M = \zeta N$, approximating $N-1$ by N, and approximating the binomial distribution using the CLT through $k = s\sqrt{(N-1)\tau(1-\tau)} + (N-1)\tau$, we can write the total probability error as:

$$p_{e,i} \;=\; 1 \;-\; \frac{1}{\sqrt{2\pi}} \int_{-\infty}^{\infty} Q(w(s)) e^{-\frac{s^2}{2}} ds, \tag{2.65}$$

where $w(s)$ is given by:

$$w(s) = \frac{\left(\frac{((2^{\rho}-1)\beta)}{1-\sigma_p^2} - 1\right) - (s\sqrt{N\tau(1-\tau)} + N\tau)\left(\frac{(2^{\rho}-1)\sigma_p^2}{(1-\sigma_p^2)} + 1\right) - \zeta N}{\sqrt{\zeta N - (s\sqrt{N\tau(1-\tau)} + N\tau) + 1}}. \tag{2.66}$$

Dividing the numerator and denominator of $w(s)$ by $\sqrt{N}$ and neglecting terms that do not grow with N we get:

$$w(s) = \frac{\sqrt{N}\left(\tau\left(\frac{(2^{\rho}-1)\sigma_p^2}{(1-\sigma_p^2)} + 1\right) - \zeta\right)}{\sqrt{\zeta - \tau}}. \tag{2.67}$$

Finally, since this term does not not depend on s we take it out of the integral and write the asymptotic packet error probability as:

$$p_{e,i} = Q\left(\frac{\sqrt{N}\left(\zeta - \tau\left(\frac{(2^{\rho}-1)\sigma_p^2}{(1-\sigma_p^2)} + 1\right)\right)}{\sqrt{\zeta - \tau}}\right). \tag{2.68}$$

Similarly we find the achievable rate for a given error probability of ϵ:

$$\rho^{\mathrm{ZF}} \approx \log_2\left(1 \;+ \frac{1-\sigma_p^2}{\sigma_p^2}\left(\frac{\zeta}{\tau} - 1 - \frac{Q^{-1}(\epsilon)\sqrt{\zeta-\tau}}{\tau\sqrt{N}}\right)\;\right), \tag{2.69}$$

which in the limit leads to:

$$\rho^{\mathrm{ZF}} \;=\; \log_2\left(1 \;+ \frac{1-\sigma_p^2}{\sigma_p^2}\left(\frac{\zeta}{\tau} - 1\right)\;\right). \tag{2.70}$$

2.5 Numerical Results and Discussion

We now illustrate the results found in the previous sections and further compare recent URA schemes against our bound.

2.5.1 Trade-Off Between AoI and Spectral Efficiency

In order to determine the direct relationship between the spectral efficiency and the AoI, we start by re-writing (2.28) as a function of the spectral efficiency for a given probability of error, $p_e = \epsilon$. In this case, the AoI reduces simply to:

$$\Delta(\zeta, N, \rho, \tau) \;=\; \frac{1}{\tau_\epsilon(1-\epsilon)} \;+\; \mathcal{O}\left(\frac{1}{\sqrt{N}}\right), \tag{2.71}$$

where τ_ϵ is found by solving for τ in the Q-function in (2.28) and is given by

$$\tau_\epsilon = \alpha_\rho \zeta + \frac{Q^{-1}(\epsilon)^2}{2N} - \sqrt{\left(\alpha_\rho\zeta + \frac{Q^{-1}(\epsilon)^2}{2N}\right)^2 + \alpha_\rho^2\left(\frac{Q^{-1}(\epsilon)^2\zeta}{N} - \zeta^2\right)}. \tag{2.72}$$

The identity in (2.72) is valid for $\rho \geq \rho_{\min}(\epsilon)$ where $\rho_{\min}(\epsilon)$ is given in (2.31) evaluated at $\tau = 1$ (this is seen when solving for τ from the Q-function and observing where the solution is valid). In Fig. 2.2, we plot (2.71), ignoring the error terms, for $p_e = 10^{-5}$, $\zeta = 0.3$, and $N = \{100, 500, 1000\}$. We also plot the case of infinite number of users with $p_e = 0$ whose curve is obtained by taking $N \to \infty$ in (2.72), i.e.:

$$\lim_{N\to\infty} \tau_\epsilon \;=\; \alpha_\rho \zeta. \tag{2.73}$$

Each spectral efficiency on the $N = \infty$ curve is the age-limited capacity for a given set of τ and ζ. In both the finite- and infinite-number-of-users scenarios, the AoI is minimized by setting τ to 1, as seen in (2.71). In the finite case, however, the minimum AoI is limited by the probability of error and is given by:

$$\Delta_\epsilon \;=\; \frac{1}{1-\epsilon} \;+\; \mathcal{O}\left(\frac{1}{\sqrt{N}}\right). \tag{2.74}$$

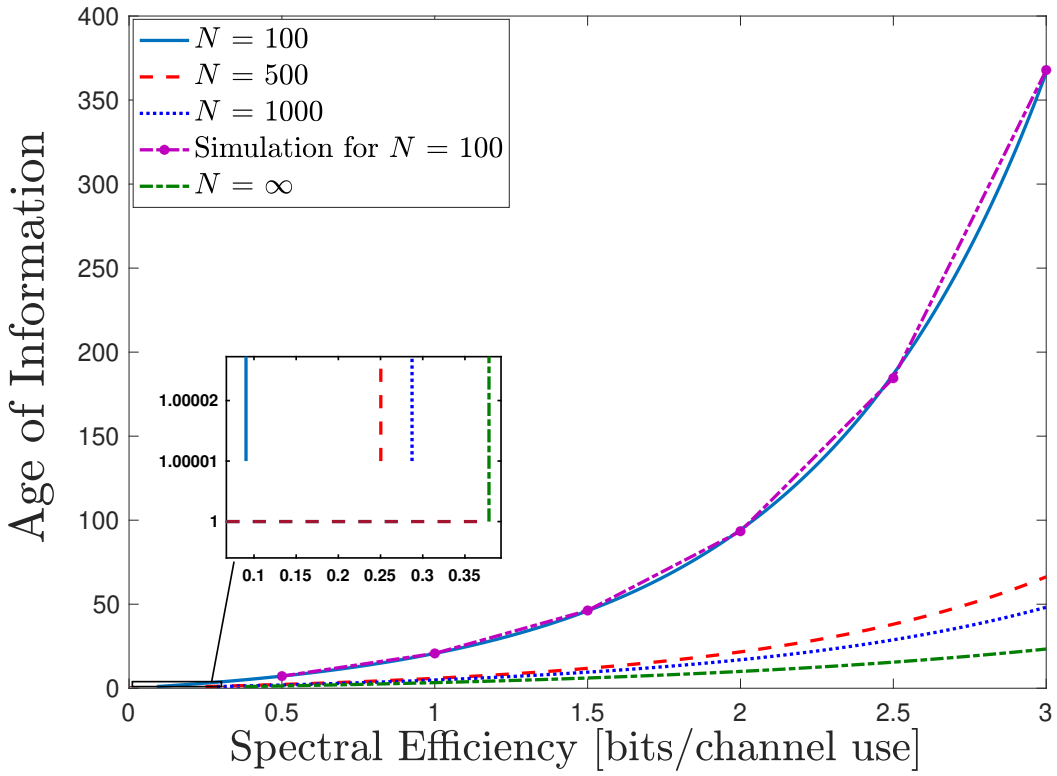

Figure 2.2: AoI vs Spectral Efficiency at $p_e = 10^{-5}$ and $\zeta = 0.3$. In the simulation, for $N = 100$ we set the number of slots to be 10^5.

On the other hand, in the infinite-number-of-users regime the probability of error is driven to zero and the AoI takes the minimum value possible, $\Delta = 1$. This is clearly seen in the zoomed portion of Fig. 2.2. We also add a simulation for $N = 100$. In our simulation we choose a large number of time slots, 10^5, and simulate the network AoI. Indeed, we can see from Fig. 2.2 that the error term in our approximations is small.

2.5.2 Performance under Imperfect CSI

We compare the achievable rates for MRC and ZF for a given MSE in channel estimation in Fig. 2.3. Indeed as expected the ZF receiver performs better given that the channel

estimate is good. However, the MRC receiver is more robust and is not as sensitive to imperfect channel estimates. Additionally, the constraint $\zeta \leq 1$ for ZF heavily limits its use in mMTC where the total number of users is much larger than the number of BS antennas. Similar results follow for both AoI and Outage performance.

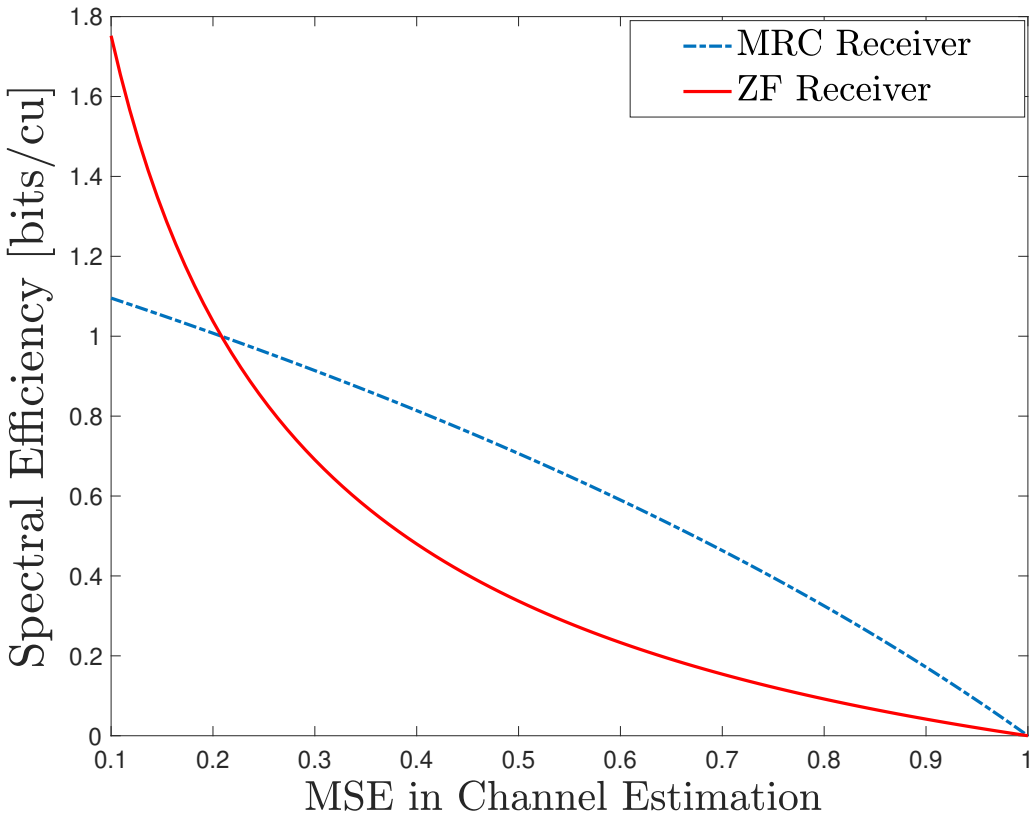

Figure 2.3: Achievable rate against Channel Estimation Error, here we use $\zeta = 1.2$, and $\tau = 0.95$.

2.5.3 Application to Unsourced Random Access (URA)

The URA paradigm, initially analyzed in [11], in which the base station is tasked with providing multiple access to a large number of uncoordinated users, has attracted con-

siderable attention. In [11], the random coding achievability bound was derived and compared against popular multiple-access schemes. A number of algorithmic solutions for URA were proposed in [60–63]. However, all of the above theoretical and algorithmic works focused on the case of a single receive antenna at the BS. To date, the only two algorithmic solutions for the URA paradigm that have so far investigated the use of the massive MIMO technology are [16, 64] whose performances have not been gauged against any achievability bound. We will refer to these two massive MIMO-based URA schemes in [16, 64] as "clustering-based" and "covariance-based", respectively.

In Fig. 2.4, we use computer simulations to compare both schemes to the new achievability bound established in **Theorem 1** as well as to the exact expression established in (2.16). For both the schemes, we fix the bandwidth to $W = 10$ MHz and the noise variance to $\sigma_w^2 = 10^{-19.9} \times W$ [Watts] and then calculate the required transmit power that yields the SNR, $\beta^{-1} = 30$ dB. For the clustering-based URA scheme, we use a Gaussian prior for HyGAMP-based compressed sensing (CS) and communicate $B = 102$ information bits per user/packet over $L = 6$ slots. For the covariance-based scheme, we fix the number of information bits per user/packet to $B = 104$ bits which are communicated over $L = 17$ slots. The parity bit allocation for the outer tree code is set to $p = [0, 8, 8, \ldots, 14]$. We also use $J = 14$ coded bits per slot which leads to the total rate of the outer code $R_{\text{out}} = 0.437$. For both the schemes, we simulate 3 data points with $K_a = [50, 75, 100]$ active users and $M = [30, 45, 60]$ antennas at the base station in which case the achievable spectral efficiency in (2.37) is given by $\log_2\left(1 + \frac{M}{K_a}\right)$. Note that even though the achievable spectral efficiency does not depend on the total number of users, as is the case in [11], the AoI does. In fact, as the total number of users increases, the AoI grows unbounded for any fixed number of active users.

In the plots of Fig. 2.4, apart from the gap between the newly established bound and the existing algorithmic solutions, it is seen that the achievable spectral efficiency of both schemes decreases as the number of active users increases. Actually, it should be possible

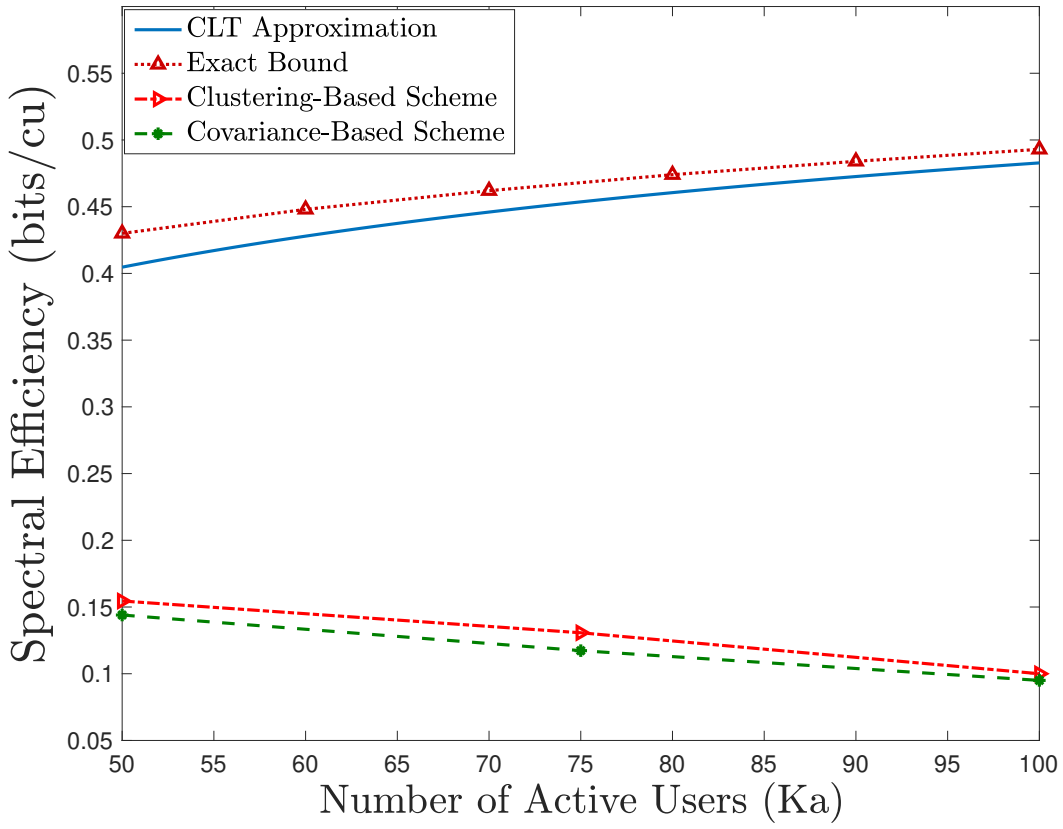

Figure 2.4: Performance of two recent URA schemes against the newly established achievability bound in (2.31) with $p_e = 10^{-2}$.

to rigorously prove this limitation for any CS-based decoding scheme. Roughly speaking, as the number of active users grows, increasing the per-user spectral efficiency requires one to decrease the blocklength thereby rendering the CS-based support recovery task more challenging. In fact, the fundamental limitation of support recovery requires (see Chapter 7 of [65]) the blocklength $L = \mathcal{O}(K_a \log(\frac{2^{B/L}}{K_a}))$ to scale a little faster than the number of active users with a single antenna at the BS. On the contrary, in [15, 64], it was shown that the covariance-based URA scheme with a large-scale antenna array at the BS can recover the support perfectly as long as $K_a \log^2\left(\frac{2^{B/L}}{K_a}\right) = \mathcal{O}(L^2)$ and

$\frac{K_a}{M} = o(1)$. However, in this case, the achievable spectral efficiency goes to infinity and the achievable performance with respect to **Theorem 1** has to be investigated carefully. In particular, a sharper characterization of the $\frac{K_a}{M} = o(1)$ term is required.

Chapter 3

Channel Estimation with Tightly-Coupled Arrays

3.1 System Model

Multiport network analysis is a tool that we will utilize to characterize the properties of the antennas inside a circuit model. A generic multiport communication system (Fig. 3.1) consists of N_t transmit generator voltages, described by $\boldsymbol{v}_G$, that induce N_r voltages at the receiver across the loads, which are described by $\boldsymbol{v}_L$. This model can be written as:

$$\boldsymbol{v}_L(f) = \sqrt{\rho}\boldsymbol{\mathcal{H}}_{\mathit{eff}}(f)\boldsymbol{v}_G(f) + \boldsymbol{n}(f), \tag{3.1}$$

where ρ is the large-scale parameter and $\boldsymbol{n}(f)$ jointly represents the extrinsic and intrinsic noise sources at the receiver. We define $\boldsymbol{\mathcal{H}}_{\mathit{eff}}(f)$ as the "effective channel" as it characterizes the antennas in use in addition to the propagation medium. We refer to the standard MIMO channel in the literature [3] as the "propagation channel" and denote it by $\boldsymbol{\mathcal{H}}(f)$ which is determined based the embedded far-field patterns of the array elements under reference terminations as well as the propagation medium.

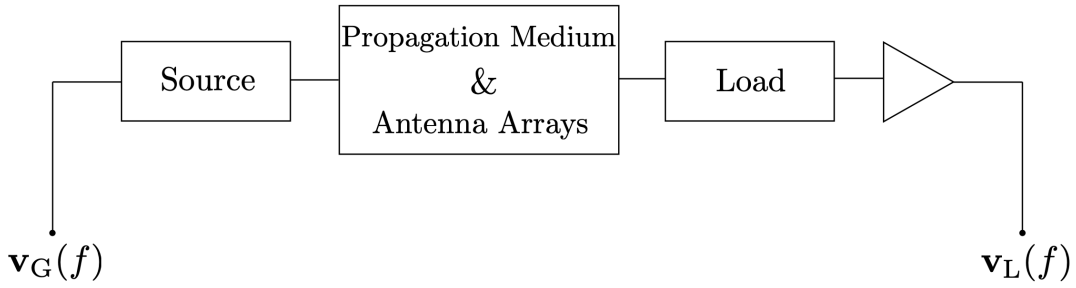

Figure 3.1: Generic Multi-port Communication System

3.1.1 Impedance Description

The first multiport network, seen as a "source" multiport, relates the transmit generator voltages, $\boldsymbol{v}_G(f)$ to the voltages that will be induced on the N_t transmit antennas, $\boldsymbol{v}_T(f)$. This can be thought of as a feeding network for the transmit antennas and will incorporate the source impedances of the transmit voltages. This multiport can be represented by a single output impedance matrix $\mathbf{Z}_{\mathrm{S}}(f)$. The middle multiport network represents the propagation medium and antenna arrays and is described through the impedance matrix, $\mathbf{Z}_{\mathrm{MIMO}}(f)$ given by:

$$\begin{bmatrix} \boldsymbol{v}_T(f) \\ \boldsymbol{v}_R(f) \end{bmatrix} = \underbrace{\begin{bmatrix} \mathbf{Z}_{\mathrm{T}}(f) & \mathbf{Z}_{\mathrm{TR}}(f) \\ \mathbf{Z}_{\mathrm{RT}}(f) & \mathbf{Z}_{\mathrm{R}}(f) \end{bmatrix}}_{\mathbf{Z}_{\mathrm{MIMO}}(f)} \begin{bmatrix} \boldsymbol{i}_T(f) \\ \boldsymbol{i}_R(f) \end{bmatrix}. \tag{3.2}$$

Here the transmit antenna impedance matrix is given by $\mathbf{Z}_{\mathrm{T}}(f)$, the receive antenna impedance matrix is given by $\mathbf{Z}_{\mathrm{R}}(f)$, and the propagation medium will be modeled through the use of $\mathbf{Z}_{\mathrm{RT}}(f)$. By the unilateral approximation [47] we set $\mathbf{Z}_{\mathrm{TR}}(f) = \mathbf{0}$. The interface between the receive antennas and the low-noise amplifiers (LNA) is represented by load matrix $\mathbf{Z}_{\mathrm{L}}(f)$. This $\mathbf{Z}_{\mathrm{L}}(f)$ is the input impedance looking at the load side and represents a "load" multiport. We model the extrinsic noise collected at the receive antennas through the vector $\boldsymbol{v}_{\mathrm{EN}}(f)$ and the intrinsic amplifier noise is modeled through $\boldsymbol{v}_{\mathrm{IN}}(f)$. At last, we assume a single-source LNA with a gain of β. Finally, through basic

circuit analysis, it is simple to show that

$$\boldsymbol{\mathcal{H}}_{\mathit{eff}}(f) = \beta \mathbf{Z}_{\mathrm{L}}(f)[\mathbf{Z}_{\mathrm{R}}(f) + \mathbf{Z}_{\mathrm{L}}(f)]^{-1}\mathbf{Z}_{\mathrm{RT}}(f)[\mathbf{Z}_{\mathrm{T}}(f) + \mathbf{Z}_{\mathrm{S}}(f)]^{-1}, \tag{3.3}$$

and

$$\boldsymbol{n}(f) = \boldsymbol{v}_{\mathrm{IN}}(f) + \beta \mathbf{Z}_{\mathrm{L}}(f)[\mathbf{Z}_{\mathrm{R}}(f) + \mathbf{Z}_{\mathrm{L}}(f)]^{-1}\boldsymbol{v}_{\mathrm{EN}}(f). \tag{3.4}$$

We can write the mutual impedance, $\mathbf{Z}_{\mathrm{RT}}(f)$, that models the propagation channel as follows:

$$\mathbf{Z}_{\mathrm{RT}}(f) \;=\; \left[\mathrm{diag}\left(\sqrt{\Re\{\mathbf{Z}_{\mathrm{R}}(f)\}}\right)\boldsymbol{\mathcal{H}}_{\mathrm{OC}}(f)\,\mathrm{diag}\left(\sqrt{\Re\{\mathbf{Z}_{\mathrm{T}}(f)\}}\right)\right], \tag{3.5}$$

where $\boldsymbol{\mathcal{H}}_{\mathrm{OC}}(f)$ is the propagation channel calculated based on open-circuit embedded pattern ($\neq \boldsymbol{\mathcal{H}}(f)$). To compute the noise correlation matrix it is assumed that the noise voltage sources associated with different amplifiers are independent:

$$\mathbb{E}[\boldsymbol{v}_{\mathrm{IN}}(f)\,\boldsymbol{v}_{\mathrm{IN}}(f)^{\mathsf{H}}] = 4\beta^2\, k_b\, T\ (N_f - 1)R_{in}\mathbf{I}, \tag{3.6}$$

where $(.)^{\mathsf{H}}$ denotes the conjugate-transpose of a matrix, T is the noise temperature in Kelvin and R_{in} is the input impedance of the N_r LNAs. The extrinsic noise correlation matrix, assuming the antenna array is in thermodynamic equilibrium with the environment is given by,

$$\mathbb{E}[\boldsymbol{v}_{\mathrm{EN}}(f)\boldsymbol{v}_{\mathrm{EN}}(f)^{\mathsf{H}}] = 4k_bT\Re\{\mathbf{Z}_{\mathrm{R}}(f)\}. \tag{3.7}$$

With the above, the correlation of the total noise vector in (3.1), $\boldsymbol{R}_{\boldsymbol{n}}(f) \triangleq \mathbb{E}[\boldsymbol{n}(f)\boldsymbol{n}(f)^{\mathsf{H}}]$, can be determined as a sum of extrinsic and intrinsic noise correlations:

$$\begin{aligned}\boldsymbol{R}_{\boldsymbol{n}}(f) = \big[4k_bT\beta^2\mathbf{Z}_L(f)[\mathbf{Z}_R(f) + \mathbf{Z}_L(f)]^{-1}\Re\{\mathbf{Z}_{\mathrm{R}}(f)\}[\mathbf{Z}_R(f) + \mathbf{Z}_L(f)]^{-\mathsf{H}}\mathbf{Z}_L(f)^{\mathsf{H}}\big] \\ + 4k_bT\beta^2(N_f - 1)R_{in}\mathbf{I}.\end{aligned} \tag{3.8}$$

3.1.2 Scattering Description

In the scattering description, incident and reflected power waves at ports are related through scattering parameters. As the scattering parameters are measured using a load termination these are most useful for antenna analysis. The effective channel in the scattering description is given by [66]:

$$\begin{aligned}\boldsymbol{\mathcal{H}}_{\mathit{eff}}(f) = \frac{\beta}{4}\big[\mathbf{I}+\mathbf{S}_{\mathrm{L}}(f)\big]\big[\mathbf{I}-\mathbf{S}_{\mathrm{R}}(f)\mathbf{S}_{\mathrm{L}}(f)\big]^{-1} \\ \times\ \mathbf{S}_{\mathrm{RT}}(f)\big[\mathbf{I}-\mathbf{S}_{\mathrm{S}}(f)\mathbf{S}_{\mathrm{T}}(f)\big]^{-1}\big[\mathbf{I}-\mathbf{S}_{\mathrm{S}}(f)\big],\end{aligned} \tag{3.9}$$

where $\mathbf{S}_{\mathrm{RT}}(f)$ is given by:

$$\mathbf{S}_{\mathrm{RT}}(f) = \sqrt{\mathbf{I}-\mathrm{diag}(\mathbf{S}_{\mathrm{R}}(f)^{\mathsf{H}}\mathbf{S}_{\mathrm{R}}(f))}\,\boldsymbol{\mathcal{H}}(f)\sqrt{\mathbf{I}-\mathrm{diag}(\mathbf{S}_{\mathrm{T}}(f)^{\mathsf{H}}\mathbf{S}_{\mathrm{T}}(f))}. \tag{3.10}$$

Additionally, the corresponding noise correlation matrix is given by:

$$\begin{aligned}\boldsymbol{R}_{\boldsymbol{n}}(f) = \Big[k_b T\beta^2 Z_0[\mathbf{I}+\mathbf{S}_{\mathrm{L}}(f)][\mathbf{I}-\mathbf{S}_{\mathrm{R}}(f)\mathbf{S}_{\mathrm{L}}(f)]^{-1}[\mathbf{I}-\mathbf{S}_{\mathrm{R}}(f)^{\mathsf{H}}\mathbf{S}_{\mathrm{R}}(f)][\mathbf{I}-\mathbf{S}_{\mathrm{R}}(f)\mathbf{S}_{\mathrm{L}}(f)]^{-\mathsf{H}} \\ \times[\mathbf{I}+\mathbf{S}_{\mathrm{L}}(f)]^{\mathsf{H}}\Big] + 4\beta^2 k_{\mathrm{b}} T(N_f-1)R_{in}\mathbf{I}.\end{aligned} \tag{3.11}$$

For the remainder of this chapter we will exclusively use the scattering representation in (3.9) and (3.11) and assume that source and load terminations are designed such that $\mathbf{S}_{\mathrm{S}} = \mathbf{0}$ and $\mathbf{S}_{\mathrm{L}} = \mathbf{0}$.

3.2 Single-Carrier System

When the bandwidth B is much smaller than the carrier frequency f_c, and the channel is constant within the coherence block, the system model can be written in discrete time as:

$$\mathbf{y} \;=\; \sqrt{\rho}\,\mathbf{H}_{\mathit{eff}}\mathbf{x} \;+\; \mathbf{n}, \tag{3.12}$$

where $\mathbf{y}$, $\mathbf{x}$, and $\mathbf{n}$ are discrete time samples of $\boldsymbol{v}_L$, $\boldsymbol{v}_G$ and $\boldsymbol{n}$ respectively. $\mathbf{H}_{\mathit{eff}}$ is the discrete-time version of the channel in (3.1) at the carrier frequency[1] f_c. In this case, $\mathbf{n} \sim \mathcal{CN}(\mathbf{0}, \mathbf{R}_{\mathrm{n}})$ where $\mathbf{R}_{\mathrm{n}}$ is obtained from (3.11) as:

$$\mathbf{R}_{\mathbf{n}} = B\boldsymbol{R}_{\boldsymbol{n}}(f_c). \tag{3.13}$$

The channel, $\mathbf{H}_{\mathit{eff}}$, can be decomposed as the product of three matrices as:

$$\mathbf{H}_{\mathit{eff}} \triangleq \mathbf{Q}\,\mathbf{H}\,\mathbf{F}, \tag{3.14}$$

where,

$$\begin{aligned} \mathbf{F} &\triangleq \sqrt{\mathbf{I} - \mathrm{diag}(\mathbf{S}_{\mathrm{T}}^{\mathsf{H}}\mathbf{S}_{\mathrm{T}})}, \\ \mathbf{Q} &\triangleq \frac{\beta}{4}\sqrt{\mathbf{I} - \mathrm{diag}(\mathbf{S}_{\mathrm{R}}^{\mathsf{H}}\mathbf{S}_{\mathrm{R}})}. \end{aligned} \tag{3.15}$$

In a rich scattering environment the propagation channel $\mathbf{H}$ can itself be written as a product of three matrices [3]:

$$\mathbf{H} = {\mathbf{R}_{\mathrm{R}}}^{1/2}\mathbf{H}_{\mathrm{w}}{\mathbf{R}_{\mathrm{T}}}^{1/2}, \tag{3.16}$$

wherein the entries of $\mathbf{H}_{\mathrm{w}}$ are modeled by i.i.d complex Gaussian random variables and

$$\begin{aligned} \mathbf{R}_{\mathrm{R}}^{1/2} &\triangleq (\mathbf{I} - \mathrm{diag}(\mathbf{S}_{\mathrm{R}}^{\mathsf{H}}\mathbf{S}_{\mathrm{R}}))^{-1/2}(\mathbf{I} - \mathbf{S}_{\mathrm{R}}^{\mathsf{H}}\mathbf{S}_{\mathrm{R}})^{1/2}, \\ \mathbf{R}_{\mathrm{T}}^{1/2} &\triangleq (\mathbf{I} - \mathbf{S}_{\mathrm{T}}^{\mathsf{H}}\mathbf{S}_{\mathrm{T}})^{1/2}(\mathbf{I} - \mathrm{diag}(\mathbf{S}_{\mathrm{T}}^{\mathsf{H}}\mathbf{S}_{\mathrm{T}}))^{-1/2}. \end{aligned} \tag{3.17}$$

The transmit and receive spatial correlation matrices are obtained from the field identity which results from power conservation,

$$(\mathbf{I} - \mathbf{S}^{\mathsf{H}}\mathbf{S})_{m,n} = \int_{4\pi} \mathbf{E}_m^{\mathsf{H}}(\theta,\phi)\mathbf{E}_n(\theta,\phi)d\Omega \tag{3.18}$$

where $\mathbf{E}(\theta,\phi)$ is the embedded far-field pattern of the array, either transmit or receive, with the corresponding phasing of the elements. Further, it can be shown that the correlation matrix of the vectorized channel, vec($\mathbf{H}$), is given by:

$$\mathbf{R}_{\mathbf{H}} = (\mathbf{R}_{\mathrm{T}}^{\mathsf{T}/2}\mathbf{R}_{\mathrm{T}}^{1/2^*}) \otimes ({\mathbf{R}_{\mathrm{R}}}^{1/2}{\mathbf{R}_{\mathrm{R}}}^{\mathsf{H}/2}). \tag{3.19}$$

[1]For the single-carrier case, the channel and network parameters will be evaluated at frequency f_c and we no longer write them as functions of frequency for compactness.

Additionally, since the vectorized effective channel, $\text{vec}(\mathbf{H}_{\mathit{eff}})$, can be written as:

$$\text{vec}(\mathbf{H}_{\mathit{eff}}) \;=\; \mathbf{T}\,\text{vec}(\mathbf{H}), \tag{3.20}$$

where $\mathbf{T} \;\triangleq\; (\mathbf{F}^{\mathsf{T}} \otimes \mathbf{Q})$. We can write the correlation matrix of the vectorized effective channel as:

$$\mathbf{R}_{\mathbf{H}_{\mathit{eff}}} = \mathbf{T}\,\mathbf{R}_{\mathbf{H}}\,\mathbf{T}^{\mathsf{H}}. \tag{3.21}$$

3.2.1 Classical Channel Estimation

Assume that N_p pilot signals, $\mathbf{x}(t) \in \mathbb{C}^{N_t}$, $t = 1, \cdots, N_p$ are sent by the transmit array. The associated space-time matrix, $\mathbf{Y} \in \mathbb{C}^{N_r \times N_p}$, of receive signals is given by:

$$\mathbf{Y} \;=\; \sqrt{\rho}\,\mathbf{H}_{\mathit{eff}}\mathbf{X} \;+\; \mathbf{N}, \tag{3.22}$$

where $\mathbf{X} = [\mathbf{x}(1), \ldots, \mathbf{x}(N_p)]$ and $\mathbf{N} = [\mathbf{n}(1), \ldots, \mathbf{n}(N_p)] \in \mathbb{C}^{N_r \times N_p}$ is the additive noise matrix. The noise vectors, $\mathbf{n}(t),\ t = 1, \ldots, N_p$, are mutually independent and $\mathbf{n}(t) \sim \mathcal{CN}(\mathbf{0}, \mathbf{R}_{\mathbf{n}})\ \forall t$. By vectorizing (3.22) it follows that:

$$\widetilde{\mathbf{y}} = \sqrt{\rho}\,\mathbf{A}\,\text{vec}(\mathbf{H}_{\mathit{eff}}) + \widetilde{\mathbf{n}}, \tag{3.23}$$

where $\widetilde{\mathbf{y}} \triangleq \text{vec}(\mathbf{Y})$, $\widetilde{\mathbf{n}} \triangleq \text{vec}(\mathbf{N})$, and $\mathbf{A} \triangleq (\mathbf{X}^{\mathsf{T}} \otimes \mathbf{I})$. From the model in (3.23) we can estimate $\text{vec}(\mathbf{H}_{\mathit{eff}})$ using the LMMSE estimator:

$$\text{vec}(\widehat{\mathbf{H}}_{\mathit{eff}}) \;=\; \mathbf{W}_{\text{AB}}^{\mathsf{H}}\,\widetilde{\mathbf{y}}, \tag{3.24}$$

where:

$$\mathbf{W}_{\text{AB}} = \sqrt{\rho}\big(\widetilde{\mathbf{R}}_{\widetilde{\mathbf{n}}} + \rho\,\mathbf{A}\widetilde{\mathbf{R}}_{\mathbf{H}_{\mathit{eff}}}\mathbf{A}^{\mathsf{H}}\big)^{-1}\mathbf{A}\widetilde{\mathbf{R}}_{\mathbf{H}_{\mathit{eff}}}. \tag{3.25}$$

While the model in (3.23) better characterizes the physics of communication, standard communication models ignore the channel and noise correlations stemming from mutual coupling of the transmit and receive antennas. This amounts to, wrongly, assuming

$\widetilde{\mathbf{R}}_{\tilde{\mathbf{n}}} = c_1\mathbf{I}$ and $\widetilde{\mathbf{R}}_{\mathbf{H}_{\mathit{eff}}} = c_2\mathbf{I}$ for two constants c_1 and c_2. We will call the LMMSE estimator that does not take the mutual coupling into account the "Antenna Blind" (AB) estimator and denote it by $\mathbf{W}_{\mathrm{AB}}$. The constants c_1 is taken to be the noise power scaling factor in the perfectly matched case, i.e., the constant in (3.11) when $\mathbf{S}_{\mathrm{R}} = \mathbf{0}$. The constant c_2 is the scale in the channel power given by the trace of the correlation matrix of $\mathbf{H}_{\mathit{eff}}$ given by $\mathrm{tr}(\mathbf{R}_{\mathbf{H}_{\mathit{eff}}})/(N_r N_t)$. These values are easily and accurately measured at the receiver.

A useful metric to assess the performance of this estimator is the mean-squared error (MSE) matrix defined as:

$$\mathbf{E}_{\mathit{eff}}^{\mathrm{AB}} \triangleq \mathbb{E}\{(\mathrm{vec}(\mathbf{H}_{\mathit{eff}}) - \mathrm{vec}(\widehat{\mathbf{H}}_{\mathit{eff}}))(\mathrm{vec}(\mathbf{H}_{\mathit{eff}} - \mathrm{vec}(\widehat{\mathbf{H}}_{\mathit{eff}}))^{\mathsf{H}}\}. \tag{3.26}$$

This equals the covariance of the estimation error vector and fully describes the accuracy of the estimator. It can be shown that for the AB estimator, this is given by:

$$\begin{aligned}\mathbf{E}_{\mathit{eff}}^{\mathrm{AB}} \;=\; & \mathbf{R}_{\mathbf{H}_{\mathit{eff}}} \;-\; \rho\mathbf{R}_{\mathbf{H}_{\mathit{eff}}}\mathbf{A}^{\mathsf{H}}\big(\widetilde{\mathbf{R}}_{\tilde{\mathbf{n}}} + \rho\,\mathbf{A}\widetilde{\mathbf{R}}_{\mathbf{H}_{\mathit{eff}}}\mathbf{A}^{\mathsf{H}}\big)^{-1}\mathbf{A}\widetilde{\mathbf{R}}_{\mathbf{H}_{\mathit{eff}}} \\ & -\; \rho\widetilde{\mathbf{R}}_{\mathbf{H}_{\mathit{eff}}}^{\mathsf{H}}\mathbf{A}^{\mathsf{H}}\big(\widetilde{\mathbf{R}}_{\tilde{\mathbf{n}}}^{\mathsf{H}} + \rho\,\mathbf{A}\widetilde{\mathbf{R}}_{\mathbf{H}_{\mathit{eff}}}^{\mathsf{H}}\mathbf{A}^{\mathsf{H}}\big)^{-1}\mathbf{A}\mathbf{R}_{\mathbf{H}_{\mathit{eff}}}^{\mathsf{H}} \;+\; \rho\widetilde{\mathbf{R}}_{\mathbf{H}_{\mathit{eff}}}^{\mathsf{H}}\mathbf{A}^{\mathsf{H}}\big(\widetilde{\mathbf{R}}_{\tilde{\mathbf{n}}}^{\mathsf{H}} + \rho\,\mathbf{A}\widetilde{\mathbf{R}}_{\mathbf{H}_{\mathit{eff}}}^{\mathsf{H}}\mathbf{A}^{\mathsf{H}}\big)^{-1} \\ & \qquad * \big(\mathbf{R}_{\tilde{\mathbf{n}}} + \rho\,\mathbf{A}\mathbf{R}_{\mathbf{H}_{\mathit{eff}}}\mathbf{A}^{\mathsf{H}}\big)\big(\widetilde{\mathbf{R}}_{\tilde{\mathbf{n}}} + \rho\,\mathbf{A}\widetilde{\mathbf{R}}_{\mathbf{H}_{\mathit{eff}}}\mathbf{A}^{\mathsf{H}}\big)^{-1}\mathbf{A}\widetilde{\mathbf{R}}_{\mathbf{H}_{\mathit{eff}}}\end{aligned} \tag{3.27}$$

3.2.2 Antenna Aware Channel Estimation

We start by rewriting (3.22) in terms of the expansion in (3.14):

$$\mathbf{Y} \;=\; \sqrt{\rho}\,\mathbf{Q}\,\mathbf{H}\,\mathbf{F}\mathbf{X} \;+\; \mathbf{N}, \tag{3.28}$$

where $\mathbf{N}$ and $\mathbf{X}$ are the same as in (3.22) and $\mathbf{H}$ is given in (3.16). At the receiver, we whiten the noise by using the Cholesky decomposition, $\mathbf{R}_{\mathbf{n}} = \mathbf{L}\mathbf{L}^{\mathsf{H}}$, by multiplying the received signal by $\mathbf{L}^{-1}$, that is:

$$\mathbf{Y}' \;=\; \sqrt{\rho}\,(\mathbf{L}^{-1}\mathbf{Q})\,\mathbf{H}\,(\mathbf{F}\mathbf{X}) \;+\; \mathbf{N}', \tag{3.29}$$

where $\mathbf{Y}' \triangleq \mathbf{L}^{-1}\mathbf{Y}$ and $\mathbf{N}' \triangleq \mathbf{L}^{-1}\mathbf{N}$. Now the columns, $\{\mathbf{n}'(t)\}_{t=1}^{N_p}$, of $\mathbf{N}'$ are mutually independent and $\mathbf{n}'(t) \sim \mathcal{CN}(\mathbf{0}, \mathbf{I})\ \forall t$. We now apply the vec(.) operator to obtain:

$$\widetilde{\mathbf{y}}' = \sqrt{\rho}\mathbf{A}'\text{vec}(\mathbf{H}) + \widetilde{\mathbf{n}}', \tag{3.30}$$

where $\widetilde{\mathbf{y}}' \triangleq \text{vec}(\mathbf{Y}')$, $\widetilde{\mathbf{n}}' \triangleq \text{vec}(\mathbf{N}')$ and

$$\mathbf{A}' \ \triangleq \ (\mathbf{F}\mathbf{X})^{\mathsf{T}} \otimes (\mathbf{L}^{-1}\mathbf{Q}).$$

We can now use LMMSE estimation to reconstruct vec($\mathbf{H}$) from (3.30). By doing so we have incorporated the mutual coupling effects in estimation and will call this estimator the "Antenna Aware" (AA) estimator given by:

$$\mathbf{W}_{\text{AA}} = \sqrt{\rho}(\mathbf{R}_{\widetilde{\mathbf{n}}'} + \rho\mathbf{A}'\mathbf{R}_{\mathbf{H}}\mathbf{A}'^{\mathsf{H}})^{-1}\mathbf{A}'\mathbf{R}_{\mathbf{H}}, \tag{3.31}$$

where now we have $\mathbf{R}_{\widetilde{\mathbf{n}}'} = \mathbf{I}$ and $\mathbf{R}_{\mathbf{H}}$ is given in (3.19). As the AA estimator estimates vec($\mathbf{H}$), we first write the MSE matrix of vec($\mathbf{H}$) as:

$$\mathbf{E}^{\text{AA}} = \mathbf{R}_{\mathbf{H}} - \rho\mathbf{R}_{\mathbf{H}}\mathbf{A}'^{\mathsf{H}}(\mathbf{R}_{\widetilde{\mathbf{n}}'} + \rho\mathbf{A}'\mathbf{R}_{\mathbf{H}}\mathbf{A}'^{\mathsf{H}})^{-1}\mathbf{A}'\mathbf{R}_{\mathbf{H}}. \tag{3.32}$$

Finally, using the relation in (3.20) we can write the MSE matrix of vec($\mathbf{H}_{\mathit{eff}}$) as:

$$\mathbf{E}_{\mathit{eff}}^{\text{AA}} = \mathbf{T}\,\mathbf{E}^{\text{AA}}\,\mathbf{T}^{\mathsf{H}}. \tag{3.33}$$

3.3 Multicarrier Systems

In OFDM-based transmission, assuming the appropriate length of the cyclic prefix has been chosen, a given subcarrier will experience a frequency flat channel in the frequency domain. That is, the receiver observation $\mathsf{y} \in \mathbb{C}^{N_r}$ of the symbol $\mathsf{x} \in \mathbb{C}^{N_t}$ at subcarrier $k \in \{0, \ldots, K-1\}$ can be written as:

$$\mathsf{y}[k] \ = \ \sqrt{\rho}\,\mathsf{H}_{\mathit{eff}}[k]\,\mathsf{x}[k] \ + \ \mathsf{n}[k], \tag{3.34}$$

where $\mathbf{n}[k]$ is the noise at the receiver. This relationship is also the same as taking a discrete-frequency sample of (3.1) where the k^{th} subcarrier is sampled at frequency f_k. Similar to the single-carrier case, $\mathbf{n}[k] \sim \mathcal{CN}(\mathbf{0}, \mathbf{R}_{\mathrm{n}}[k])$ where $\mathbf{R}_{\mathrm{n}}[k]$ is obtained from (3.11) as:

$$\mathbf{R}_{\mathrm{n}}[k] \;=\; (B/K)\boldsymbol{R_n}(f_k). \tag{3.35}$$

The channel at the k^{th} subcarrier, can be written as:

$$\mathbf{H}_{\mathit{eff}}[k] \;\triangleq\; \mathbf{Q}[k]\,\mathbf{H}[k]\,\mathbf{F}[k] \tag{3.36}$$

where now[2]

$$\begin{aligned} \mathbf{F}[k] &\triangleq \Big(\mathbf{I} - \mathbf{S}_{\mathrm{T}}(f_k)^{\mathsf{H}}\mathbf{S}_{\mathrm{T}}(f_k)\Big)^{-1}, \\ \mathbf{Q}[k] &\triangleq \frac{\beta}{4}\Big(\mathbf{I} - \mathbf{S}_{\mathrm{R}}(f_k)^{\mathsf{H}}\mathbf{S}_{\mathrm{R}}(f_k)\Big)^{-1}. \end{aligned} \tag{3.37}$$

Based on measurements of the PDP (performed independently of the antennas in use) an effective number of taps L can be determined. These taps are due to the frequency selectivity of the propagation medium and as such, we can determine $\mathbf{H}[k]$ from L time-domain taps $\{\mathbf{H}[\ell]\}_{\ell=0}^{L-1}$ using Discrete-Fourier Transform (DFT), i.e.,

$$\mathbf{H}[k] \;=\; \sum_{\ell=0}^{L-1} \mathbf{H}[\ell]\, e^{-j\,\frac{2\pi}{K}\ell k} \qquad k = 0, \ldots, K-1. \tag{3.38}$$

As the distribution of the PDP will not alter our results significantly, for simplicity we assume a uniform PDP, where the entries of $\mathbf{H}[\ell]$ are i.i.d complex Gaussian random variables and the $\{\mathbf{H}[\ell]\}_{\ell=0}^{L-1}$ are independent of one another. Indeed this is well justified in a rich-scattering model where a large number of paths contribute to each tap such that the power across delay should not vary drastically.

[2]For compactness, we combine the terms from the correlation across the antennas and the part from the multiport network.

3.3.1 Classical OFDM Channel Estimation

Channel estimation can be performed in the frequency domain by inserting a pilot sequence over the K subcarriers and using OFDM-based transmission. Additionally, if we assume that the channel is time-invariant we can also use pilots at L_t instances in time. That is, for $k \in \{0, \ldots, K-1\}$ and $t \in \{0, \ldots, L_t - 1\}$ the received signal at subcarrier k and time t can be written as:

$$\mathbf{y}[k,t] \;=\; \sqrt{\rho}\,\mathbf{H}_{\mathit{eff}}[k]\,\mathbf{x}[k,t] \;+\; \mathbf{n}[k,t]. \tag{3.39}$$

Note here that the noise is uncorrelated in frequency and time and correlated in space according to (3.35). In the standard approach, the DFT relationship (3.38) would be applied on $\mathbf{H}_{\mathit{eff}}[k]$ using L taps such that the system model can be expressed as:

$$\mathbf{y}[k,t] \;=\; \sqrt{\rho}\,\mathbf{H}_{\mathit{eff}}[k]\,\mathbf{x}[k,t] \;+\; \mathbf{n}[k,t] \tag{3.40}$$

$$\approx\; \sqrt{\rho}\left(\sum_{\ell=0}^{L-1}\mathbf{H}_{\mathit{eff}}[\ell]\,e^{-j\,\frac{2\pi}{K}\ell k}\right)\mathbf{x}[k,t] \;+\; \mathbf{n}[k,t]. \tag{3.41}$$

If we had neglected the coupling in which $\mathbf{F}[k]$ and $\mathbf{Q}[k]$ would be identity matrices then there would be no approximation in going from (3.40) to (3.41). However, as seen in (3.36) multiplying by $\mathbf{F}[k]$ and $\mathbf{Q}[k]$ in the frequency domain would cause spreading in time requiring a larger number of taps to accurately model the channel. The standard LMMSE estimator would take the relationship in (3.41) as exact and its estimator would be derived under this assumption. Simplifying further we define:

$$\overline{\mathbf{H}}_{\mathit{eff}} \;\triangleq\; \big[\mathbf{H}_{\mathit{eff}}[0] \;\cdots\; \mathbf{H}_{\mathit{eff}}[L-1]\big], \tag{3.42}$$

and

$$\mathbf{u}[k] \;\triangleq\; \left[1\; e^{-j\frac{2\pi}{K}k} \;\cdots\; e^{-j\frac{2\pi}{K}k(L-1)}\right]^{\mathsf{T}}, \tag{3.43}$$

(3.41) becomes:

$$\mathbf{y}[k,t] \;\approx\; \sqrt{\rho}\,\overline{\mathbf{H}}_{\mathit{eff}}\,(\mathbf{u}[k] \otimes \mathbf{x}[k,t]) \;+\; \mathbf{n}[k,t]. \tag{3.44}$$

By applying vec$(\cdot)$ to both sides of (3.44) and using the identity vec$(\mathbf{ABC}) = \left(\mathbf{C}^\top \otimes \mathbf{A}\right)$ vec$(\mathbf{B})$, we obtain:

$$\mathbf{y}[k,t] \;\approx\; \left(\mathbf{u}[k]^\top \otimes \mathbf{x}[k,t]^\top \otimes \mathbf{I}\right) \mathrm{vec}\left(\overline{\mathbf{H}}_{\mathit{eff}}\right) \;+\; \mathbf{n}[k,t]. \tag{3.45}$$

Stacking the observations $\mathbf{y}[k,t]$ first over the K subcarriers and then over the L_t time-domain points we get:

$$\overline{\mathbf{y}} \;\approx\; \sqrt{\rho}\,\mathbf{B}\,\mathrm{vec}\left(\overline{\mathbf{H}}_{\mathit{eff}}\right) \;+\; \overline{\mathbf{n}}, \tag{3.46}$$

where

$$\overline{\mathbf{y}} \;\triangleq\; \left[\mathbf{y}[0,0],\ldots,\mathbf{y}[K-1,L_t-1]\right]^{\mathsf{T}}, \tag{3.47}$$

$$\overline{\mathbf{n}} \;\triangleq\; \left[\mathbf{n}[0,0],\ldots,\mathbf{n}[K-1,L_t-1]\right]^{\mathsf{T}}, \tag{3.48}$$

and the matrix $\mathbf{B}$ is defined as:

$$\mathbf{B} \;\triangleq\; \begin{bmatrix} \mathbf{u}\,[0]^\top \otimes \mathbf{x}\,[0,0]^\top \otimes \mathbf{I} \\ \mathbf{u}\,[1]^\top \otimes \mathbf{x}\,[1,0]^\top \otimes \mathbf{I} \\ \vdots \\ \mathbf{u}\,[K-1]^\top \otimes \mathbf{x}\,[K-1,L_t-1]^\top \otimes \mathbf{I} \end{bmatrix}. \tag{3.49}$$

The LMMSE channel estimate of (3.46) is given by:

$$\mathrm{vec}\left(\widehat{\overline{\mathbf{H}}_{\mathit{eff}}}\right) \;=\; \mathbf{W}_{\mathrm{AB}}^{\mathsf{H}}\;\overline{\mathbf{y}}, \tag{3.50}$$

where

$$\mathbf{W}_{\mathrm{AB}} \;=\; \sqrt{\rho}\,(\widetilde{\mathbf{R}}_{\overline{n}} + \rho\mathbf{B}\widetilde{\mathbf{R}}_{\boldsymbol{H}_{\mathit{eff}}}\mathbf{B}^{\mathsf{H}})^{-1}\mathbf{B}\widetilde{\mathbf{R}}_{\boldsymbol{H}_{\mathit{eff}}}, \tag{3.51}$$

where, similar to the single-carrier case, $\widetilde{\mathbf{R}}_{\overline{n}} = c_3\mathbf{I}$ and $\widetilde{\mathbf{R}}_{\boldsymbol{H}_{\mathit{eff}}} = c_4\mathbf{I}$ are the (incorrectly mismatched) correlations of $\overline{\mathbf{n}}$ and vec$\left(\overline{\mathbf{H}}_{\mathit{eff}}\right)$ respectively. The true noise correlation matrix $\mathbf{R}_{\overline{n}}$ can be found by first concatenating the noise correlation matrices (3.35) of the K subcarriers in a block diagonal matrix $\mathbf{R}_{\mathrm{K}}$, i.e.,

$$\mathbf{R}_{\mathrm{K}} \;=\; \mathrm{blockdiag}(\mathbf{R}_{\mathrm{n}}[0],\mathbf{R}_{\mathrm{n}}[1],\ldots,\mathbf{R}_{\mathrm{n}}[K-1]). \tag{3.52}$$

Since we use the K subcarriers in L_t instances of time we can express the total noise correlation matrix by repeating $\mathbf{R}_{\mathrm{K}}$ in a block diagonal matrix:

$$\mathbf{R}_{\overline{n}} \;=\; \text{blockdiag}\underbrace{\left(\mathbf{R}_{\mathrm{K}}, \mathbf{R}_{\mathrm{K}}, \ldots, \mathbf{R}_{\mathrm{K}}\right)}_{L_t \text{ repetitions}}. \tag{3.53}$$

Again, similar to the single-carrier case we can take c_3 as the noise power scale factor with perfectly matched antennas at all subcarriers frequencies, i.e., the constant in (3.11) when $\mathbf{S}_{\mathrm{R}}(f_k) = \mathbf{0}$. The constant c_4 is chosen such that $\mathrm{tr}(\widetilde{\mathbf{R}}_{\boldsymbol{H}_{\mathit{eff}}})$ is equal the channel power. It is most convenient to find the channel power of $\mathrm{vec}\Big(\overline{\mathbf{H}}_{\mathit{eff}}\Big)$ in the frequency domain. We first start by defining:

$$\begin{aligned} \overline{\mathbf{H}}_{\mathit{eff}} &\triangleq \big[\mathbf{H}_{\mathit{eff}}[0] \;\cdots\; \mathbf{H}_{\mathit{eff}}[K-1]\big], \\ \overline{\mathbf{H}} &\triangleq \big[\mathbf{H}[0] \;\cdots\; \mathbf{H}[L-1]\big], \end{aligned} \tag{3.54}$$

in which the vectorized versions are linearly related by:

$$\mathrm{vec}\Big(\overline{\mathbf{H}}_{\mathit{eff}}\Big) \;=\; \mathbf{C}_1 \,\mathrm{vec}\Big(\overline{\mathbf{H}}\Big), \tag{3.55}$$

where

$$\mathbf{C}_1 \;\triangleq\; \mathbf{D}\,\underbrace{\mathbf{P}_{\mathrm{K}}\left(\mathbf{I}_{N_t} \otimes \left(\boldsymbol{\mathcal{F}}^{\mathsf{H}} \otimes \mathbf{I}_{N_r}\right)\right)\mathbf{P}_{\mathrm{L}}}_{\triangleq\, \mathbf{C}_2}. \tag{3.56}$$

Here $\boldsymbol{\mathcal{F}}$ is a partial DFT matrix of size $L \times K$ with element (m, n) given by:

$$\boldsymbol{\mathcal{F}}_{mn} \;\triangleq\; e^{j\frac{2\pi}{K}(m-1)(n-1)}.$$

$\mathbf{P}_{\mathrm{L}}$ is a block diagonal permutation matrix that groups the taps next to each other to convert them to the frequency domain. $\mathbf{P}_{\mathrm{K}}$ is another block diagonal permutation matrix that now groups the frequency components together. Finally $\mathbf{D}$ is used to get the effective channel in the frequency domain defined by:

$$\mathbf{D} \;\triangleq\; \text{blockdiag}\big(\mathbf{F}^{\mathsf{T}}[0] \otimes \mathbf{Q}[0], \ldots, \mathbf{F}^{\mathsf{T}}[K-1] \otimes \mathbf{Q}[K-1]\big). \tag{3.57}$$

As we assume a uniform PDP, the components of $\mathrm{vec}(\overline{\mathbf{H}})$ are i.i.d Gaussian random variables with unit variance and in light of (3.55) we have:

$$\mathbf{R}_{\mathbf{H}_{\mathit{eff}}} \;=\; \mathbf{C}_1\mathbf{C}_1^{\mathsf{H}}. \tag{3.58}$$

Due to Parseval's theorem the power computed from (3.58) is the same as the power in time and therefore $c_4 = \mathrm{tr}(\mathbf{R}_{\mathbf{H}_{\mathit{eff}}})/(N_rN_tL)$. Using the Parseval theorem again we find the MSE matrix in the frequency domain based on $\mathrm{vec}\big(\overline{\mathbf{H}}_{\mathit{eff}}\big)$. To do this we write the true model in which $\overline{\mathbf{y}}$ is generated by as:

$$\overline{\mathbf{y}} \;=\; \sqrt{\rho}\,\mathbf{B}'\,\mathrm{vec}\big(\overline{\mathbf{H}}_{\mathit{eff}}\big) \;+\; \overline{\mathbf{n}}, \tag{3.59}$$

and the matrix $\mathbf{B}'$ is defined as:

$$\mathbf{B}' \;\triangleq\; \begin{bmatrix} \mathbf{x}\,[0,0]^{\top}\otimes\mathbf{I} \\ \mathbf{x}\,[1,0]^{\top}\otimes\mathbf{I} \\ \vdots \\ \mathbf{x}\,[K-1,L_t-1]^{\top}\otimes\mathbf{I} \end{bmatrix}, \tag{3.60}$$

stacking over the subcarriers first and then the time slots just like $\mathbf{B}$. Additionally to convert the time-domain estimate in (3.50) to the frequency domain we must multiply by $\mathbf{C}_2$. Indeed in this case we do not need to multiply by $\mathbf{D}$ as the AB estimator estimates the effective channel in time and already includes the antenna correlations. After some calculations, the MSE matrix is given by:

$$\begin{aligned}\mathbf{E}_{\mathit{eff}}^{\mathrm{AB}} \;=\; \mathbf{R}_{\mathbf{H}_{\mathit{eff}}} \;-\; \rho\mathbf{R}_{\mathbf{H}_{\mathit{eff}}}\mathbf{B}'^{\mathsf{H}}\big(\widetilde{\mathbf{R}}_{\tilde{\mathbf{n}}}+\rho\,\mathbf{B}\widetilde{\mathbf{R}}_{\mathbf{H}_{\mathit{eff}}}\mathbf{B}^{\mathsf{H}}\big)^{-1}\mathbf{B}\widetilde{\mathbf{R}}_{\mathbf{H}_{\mathit{eff}}}\mathbf{C}_2^{\mathsf{H}} \\ -\;\rho\mathbf{C}_2\,\widetilde{\mathbf{R}}_{\mathbf{H}_{\mathit{eff}}}^{\mathsf{H}}\mathbf{B}^{\mathsf{H}}\big(\widetilde{\mathbf{R}}_{\tilde{\mathbf{n}}}^{\mathsf{H}}+\rho\,\mathbf{B}\widetilde{\mathbf{R}}_{\mathbf{H}_{\mathit{eff}}}^{\mathsf{H}}\mathbf{B}^{\mathsf{H}}\big)^{-1}\mathbf{B}'\mathbf{R}_{\mathbf{H}_{\mathit{eff}}}^{\mathsf{H}} \;+\; \rho\,\mathbf{C}_2\,\widetilde{\mathbf{R}}_{\mathbf{H}_{\mathit{eff}}}^{\mathsf{H}}\mathbf{B}^{\mathsf{H}}\big(\widetilde{\mathbf{R}}_{\tilde{\mathbf{n}}}^{\mathsf{H}}+\rho\,\mathbf{B}\widetilde{\mathbf{R}}_{\mathbf{H}_{\mathit{eff}}}^{\mathsf{H}}\mathbf{B}^{\mathsf{H}}\big)^{-1} \\ *\big(\mathbf{R}_{\tilde{\mathbf{n}}}+\rho\,\mathbf{B}'\mathbf{R}_{\mathbf{H}_{\mathit{eff}}}\mathbf{B}'^{\mathsf{H}}\big)\big(\widetilde{\mathbf{R}}_{\tilde{\mathbf{n}}}+\rho\,\mathbf{B}\widetilde{\mathbf{R}}_{\mathbf{H}_{\mathit{eff}}}\mathbf{B}^{\mathsf{H}}\big)^{-1}\mathbf{B}\widetilde{\mathbf{R}}_{\mathbf{H}_{\mathit{eff}}}\mathbf{C}_2^{\mathsf{H}}.\end{aligned} \tag{3.61}$$

3.3.2 Antenna Aware OFDM Channel Estimation

To extend the antenna aware estimator for the OFDM system we start by writing the OFDM system with the decomposed channel, i.e.,

$$\mathbf{y}[k,t] \;=\; \sqrt{\rho}\,\mathbf{Q}[k]\,\mathbf{H}[k]\,\mathbf{F}[k]\,\mathbf{x}[k,t] + \mathbf{n}[k,t], \tag{3.62}$$

Additionally, the covariance matrix for subcarrier k can be decomposed in its cholesky decomposition, $\mathbf{R}_{\mathrm{n}}[k] \triangleq \mathbf{L}[k]\mathbf{L}[k]^{\mathsf{H}}$ wherein the cholesky factors are now a function of k. Applying $\mathbf{L}^{-1}[k]$ to the received signal $\mathbf{y}[k,t]$ we get:

$$\begin{aligned}\mathbf{y}'[k,t] \;&\triangleq\; \mathbf{L}^{-1}[k]\,\mathbf{y}[k,t] &(3.63)\\ &=\; \sqrt{\rho}\,\mathbf{L}^{-1}[k]\,\mathbf{Q}[k]\,\mathbf{H}[k]\,\mathbf{F}[k]\,\mathbf{x}[k,t] \;+\; \mathbf{n}'[k,t], &(3.64)\end{aligned}$$

where now $\mathbf{n}'[k,t] \sim \mathcal{CN}(\mathbf{0},\mathbf{I})$. By defining $\mathbf{P}[k] \triangleq \mathbf{L}^{-1}[k]\mathbf{Q}[k]$, and following similar steps as (3.40)–(3.46) we get:

$$\overline{\mathbf{y}}' \;=\; \sqrt{\rho}\,\mathbf{M}\,\mathrm{vec}\Big(\overline{\overline{\mathbf{H}}}\Big) \;+\; \overline{\mathbf{n}}'. \tag{3.65}$$

Here $\overline{\mathbf{y}}'$ and $\overline{\mathbf{n}}'$ are defined similar to (3.47) and (3.48) by stacking $\mathbf{y}'[k,t]$ and $\mathbf{n}'[k,t]$ first over the subcarriers and then over time slots. $\mathrm{vec}\Big(\overline{\overline{\mathbf{H}}}\Big)$ is the vectorized channel in the time domain, similar to the channel in (3.46), but now without the $\mathbf{Q}[k]$ and $\mathbf{F}[k]$ factors. The matrix $\mathbf{M}$ is defined as:

$$\mathbf{M} \;\triangleq\; \begin{bmatrix} \mathbf{u}\,[0]^{\mathsf{T}} \otimes (\mathbf{F}[0]\,\mathbf{x}\,[0,0])^{\mathsf{T}} \otimes \mathbf{P}[0] \\ \mathbf{u}\,[1]^{\mathsf{T}} \otimes (\mathbf{F}[1]\,\mathbf{x}\,[1,0])^{\mathsf{T}} \otimes \mathbf{P}[1] \\ \vdots \\ \mathbf{u}\,[K-1]^{\mathsf{T}} \otimes (\mathbf{F}[K-1]\,\mathbf{x}\,[K-1,L_t-1])^{\mathsf{T}} \otimes \mathbf{P}[K-1] \end{bmatrix}. \tag{3.66}$$

Finally, we obtain the OFDM version of the LMMSE Antenna Aware estimator:

$$\mathrm{vec}\left(\widehat{\overline{\mathbf{H}}}\right) = \mathbf{W}_{\mathrm{AA}}^{\mathsf{H}}\;\overline{\mathbf{y}}', \tag{3.67}$$

where

$$\mathbf{W}_{\mathrm{AA}} \;=\; \sqrt{\rho}\,(\mathbf{R}_{\overline{\mathbf{n}}'} \;+\; \rho\,\mathbf{M}\,\mathbf{R}_{\overline{\mathbf{H}}}\,\mathbf{M}^{\mathsf{H}})^{-1}\,\mathbf{M}\,\mathbf{R}_{\overline{\mathbf{H}}}, \tag{3.68}$$

where $\mathbf{R}_{\overline{\mathbf{H}}}$ and $\mathbf{R}_{\overline{\mathbf{n}}'}$ denote the correlation matrices of $\mathrm{vec}\left(\overline{\mathbf{H}}\right)$ and $\overline{\mathbf{n}}'$ respectively. Due to the noise whitening process, $\mathbf{R}_{\overline{\mathbf{n}}'} = \mathbf{I}$ and since channels are i.i.d $\mathbf{R}_{\overline{\mathbf{H}}} = \mathbf{I}$. Similar to the single-carrier case, we first write the MSE matrix of $\mathrm{vec}\left(\overline{\mathbf{H}}\right)$ as:

$$\mathbf{E}^{\mathrm{AA}} \;=\; \mathbf{R}_{\overline{\mathbf{H}}} \;-\; \rho\,\mathbf{R}_{\overline{\mathbf{H}}}\mathbf{M}^{\mathsf{H}}(\mathbf{R}_{\overline{\mathbf{n}}'} \;+\; \rho\mathbf{M}\,\mathbf{R}_{\overline{\mathbf{H}}}\,\mathbf{M}^{\mathsf{H}})^{-1}\mathbf{M}\,\mathbf{R}_{\overline{\mathbf{H}}}. \tag{3.69}$$

Using the relation in (3.55) we can write the MSE matrix of $\mathrm{vec}\left(\overline{\mathbf{H}}_{\mathit{eff}}\right)$ as:

$$\mathbf{E}^{\mathrm{AA}}_{\mathit{eff}} \;=\; \mathbf{C}_1\,\mathbf{E}^{\mathrm{AA}}\,\mathbf{C}_1^{\mathsf{H}}. \tag{3.70}$$

3.4 Simulation Results

We first illustrate the broadband properties of the connected array of slot antennas by plotting its SNR over a bandwidth of 4.5 [GHz]. We will use the slot antennas at the transmitter and receiver sides in all simulations scenarios. We demonstrate the advantages of using the antenna aware estimation algorithms first for the single-carrier case and then in OFDM systems. For the large-scale parameter we use the extended Friis model:

$$\rho = \left(\frac{c}{4\pi f d_{\mathrm{ref}}}\right)^2 \left(\frac{d_{\mathrm{ref}}}{d}\right)^{\alpha}, \tag{3.71}$$

where d_{ref} is the reference pathloss distance, chosen as 1 [m], and α is the pathloss exponent. We use i.i.d BPSK pilot signals in all simulations and unless stated otherwise we take $d = 100$ [m] and use a pathloss exponent of $\alpha = 2$ in all simulations. We assess the performance of the estimators using the normalized mean-square error (NMSE) as a performance metric:

$$\mathrm{NMSE}(\widehat{\mathbf{x}}) \;=\; \frac{\mathbb{E}\{\|\mathbf{x}-\widehat{\mathbf{x}}\|^2\}}{\mathbb{E}\{\|\mathbf{x}\|^2\}}, \tag{3.72}$$

where $\mathbf{x}$ is the theoretical value and $\widehat{\mathbf{x}}$ is the estimated value. We also measure the gains in spectral efficiency when using the AA estimator over the AB one by lower bounding the achievable rate taking the channel estimation error into account. Finally, we demonstrate the equivalence between the impedance and scattering descriptions using an example of an array of dipoles.

3.4.1 Connected Array of Slot Antennas

The connected array of slot antennas [5] are promising for next-generation wireless systems due to their wide bandwidth, large scan angles, and scalability. An image of the designed antenna array using HFSS [67] is shown in Fig. 3.2. The frequency band under investigation is [0.5, 5] GHz where the antenna ports are separated by half-wavelength $\lambda_h/2$ at 5 [GHz], the highest frequency of operation. The width of the slots is chosen to be $w = \lambda_h/60$. With 16 antenna elements, the total length of the slot is $2\lambda_h$ where the metallic plate is taken as a square perfect electric conductor (PEC) of dimensions $(2\lambda_h + \lambda_h/4) \times (2\lambda_h + \lambda_h/4)$. The thickness of the plate is $t = w$. We also utilize a design with the connected array backed by a metallic plate of the same dimensions as the original plate placed at $\lambda_h/2$ below the antenna. Defining the empirical single-carrier signal-to-noise ratio (SNR) as:

$$\text{SNR} \triangleq \frac{\mathbb{E}\{\|\sqrt{\rho}\,\mathbf{H}_{\mathit{eff}}\mathbf{x}\|^2\}}{\mathbb{E}\{\|\mathbf{n}\|^2\}}, \tag{3.73}$$

we demonstrate the broadband properties of the arrays in use in Fig. 3.3 where we plot the SNR against carrier frequency with and without the backed-plane (BP) using 1000 Monte-Carlo (MC) simulations. Using the scattering parameters extracted from HFSS, $\mathbf{H}_{\mathit{eff}}$ and $\mathbf{n}$ are found from the model in (3.12). We use a bandwidth of 5 [MHz] with a BPSK symbol power of 1 [W] at each frequency. Indeed we see that these arrays have an SNR above 5 [dB] almost over the entire frequency range of interest. This is unlike narrowband antennas which will be resonant over a small band of frequencies. At low

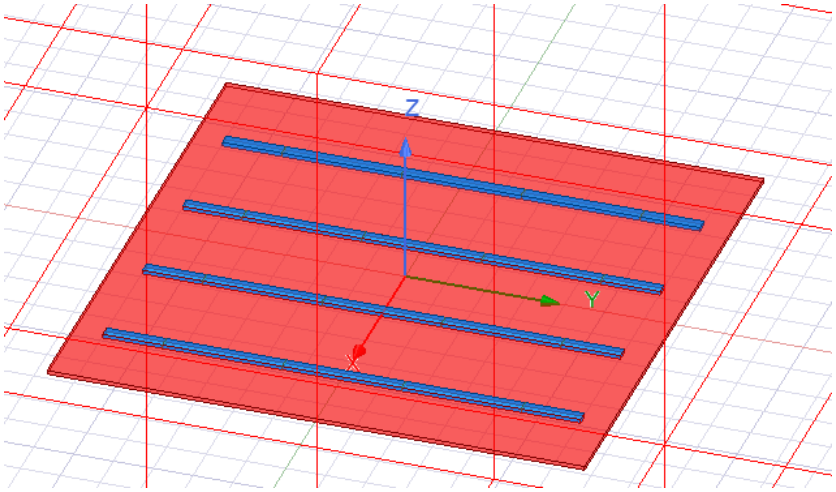

Figure 3.2: Connected array of slot antennas with 16 antenna elements

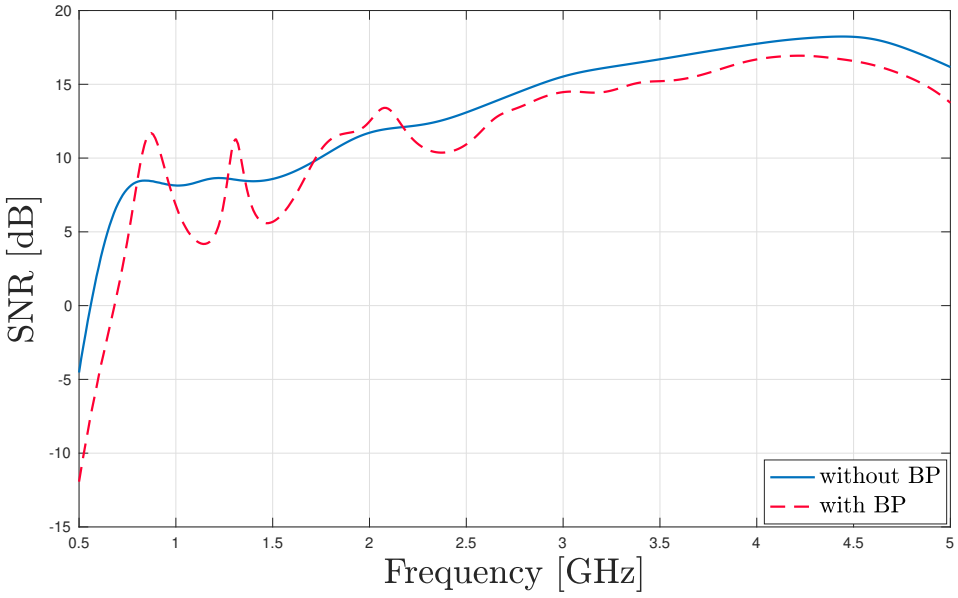

Figure 3.3: Empirical SNR against carrier frequency for the array with and without the backed-plane. Total Symbol Power is 1 [W] with a bandwidth of 5 [MHz] for each frequency point.

frequencies, we see a large degradation of SNR due to an inability to collect power because of the array's small physical area. We also note the enhanced frequency selectivity of the array with the backed plane due to the constructive/destructive reflection.

3.4.2 Single-Carrier System

We can compute the theoretical NMSE for the AB estimators using the MSE matrix (3.27) and the covariance of the channel (3.21):

$$\text{NMSE}_{\text{AB}} = \frac{\text{tr}(\mathbf{E}_{\mathit{eff}}^{\text{AB}})}{\text{tr}(\mathbf{R}_{\mathbf{H}_{\mathit{eff}}})}. \tag{3.74}$$

NMSE_{AA} for the AA estimator is derived similarly using (3.33) and (3.21). We plot the NMSE against pilot power in Fig. 3.4 for the AB and AA estimators using the connected array without the backed plane (similar results follow for the array with the BP). In this

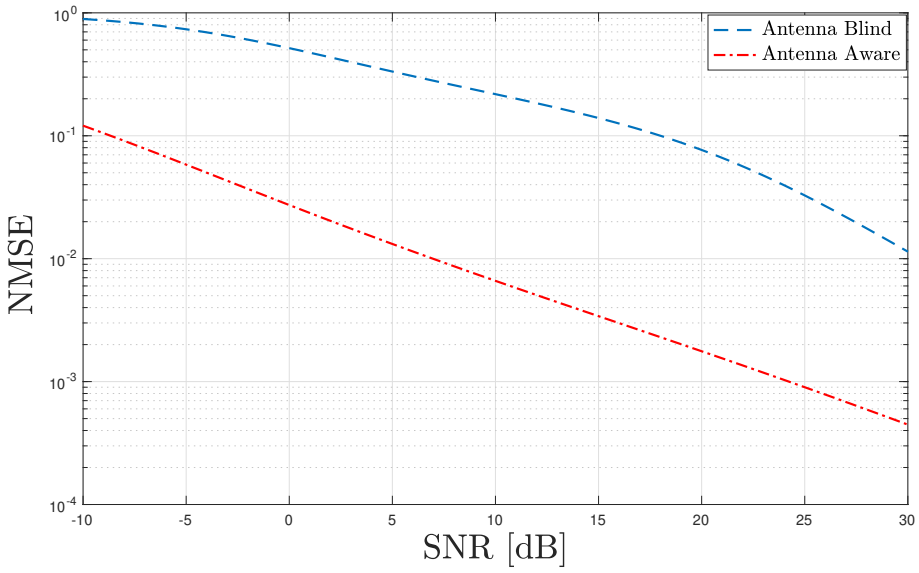

Figure 3.4: NMSE against pilot power at carrier frequency of 1 [GHz] with a bandwidth of 5 [MHz].

plot we run 1000 MC to compute the SNR and use $L_t = 20$ time-slots to estimate the

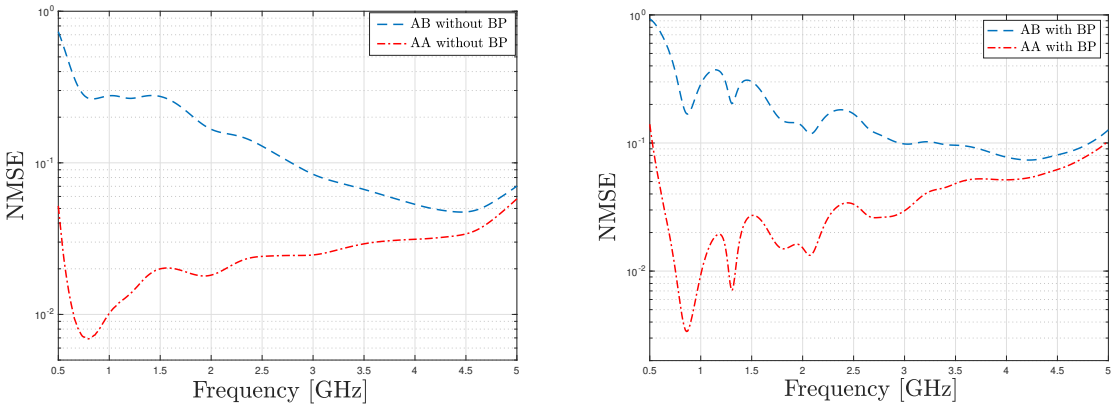

(a) Array without the BP

(b) Array with BP

Figure 3.5: NMSE against carrier frequency where total power used in estimation for each frequency is 1 [W] with a bandwidth of 5 [MHz].

channel. This is done at a carrier frequency of 1 [GHz] with a bandwidth of 5 [MHz]. We see more than 20 [dB] improvement in the NMSE for the AA estimator as compared to the AB estimator. At high SNR we see the gains start to decrease as the increase in pilot power overcomes the mismatched covariance assumptions. We next plot the NMSE against carrier frequency for the array with and without the BP in Fig. 3.5. In these plots, we use a bandwidth of 5 [MHz] and total pilot power of 1 [W]. We see that as the carrier frequency increases the gain of the AA estimator decreases. This is because the fixed spacing of the array elements, $\lambda_h/2$, starts to become a significant fraction of the carrier wavelength, λ_c, as the carrier frequency increases, and thus the coupling between antennas becomes negligible. We also see that our AA estimator brings in most gains in the frequency range of 0.6-1 [GHz] where the array is well matched and the mutual coupling is significant.

Next, we study the impact of channel estimation on the achievable rate (a key figure-of-merit in communication systems). To do this, we denote the estimated effective channel using the AB and AA estimators by $\widehat{\mathbf{H}}_{\mathit{eff}}^{\mathrm{AB}}$ and $\widehat{\mathbf{H}}_{\mathit{eff}}^{\mathrm{AA}}$ respectively. We assume

that the channel estimate is available at both the transmitter and receiver, this can occur in a time-division-duplex (TDD) system with a reciprocal channel. As our goal is solely to investigate the impact of channel estimation we assume that after estimation both the AA and AB methods are aware of the full model in (3.12). Without loss of generality, we first whiten the noise by multiplying (3.12) by $\mathbf{L}^{-1}$ (recall $\mathbf{R_n} = \mathbf{L}\mathbf{L}^{\mathsf{H}}$). For the purposes of precoding and processing at the receiver we define the singular-value decomposition (SVD) of the product of $\mathbf{L}^{-1}$ and the estimated channels by:

$$\begin{aligned} \mathbf{L}^{-1}\widehat{\mathbf{H}}_{\mathit{eff}}^{\mathrm{AB}} &\triangleq \mathbf{U}^{\mathrm{AB}}\mathbf{\Sigma}^{\mathrm{AB}}(\mathbf{V}^{\mathrm{AB}})^{\mathsf{H}}, \\ \mathbf{L}^{-1}\widehat{\mathbf{H}}_{\mathit{eff}}^{\mathrm{AA}} &\triangleq \mathbf{U}^{\mathrm{AA}}\mathbf{\Sigma}^{\mathrm{AA}}(\mathbf{V}^{\mathrm{AA}})^{\mathsf{H}}. \end{aligned} \tag{3.75}$$

For the AB system[3] we use $\mathbf{V}^{\mathrm{AB}}$ to precode the transmit signal according to:

$$\mathbf{x} = \sqrt{\frac{P_T}{N_t}}\mathbf{V}^{\mathrm{AB}} \begin{bmatrix} (\mathbf{P}_{\mathrm{AB}})^{1/2} \\ \mathbf{0} \end{bmatrix} \mathbf{s}, \tag{3.76}$$

in which P_T is the transmit power and $\mathbf{s} \in \mathbb{C}^{N_s \times 1}$ is the information bearing signal whose components contain N_s independently coded data streams. The matrix $(\mathbf{P}_{\mathrm{AB}})^{1/2}$ is a diagonal matrix containing the square root of the set of optimal powers allocated across the N_s data streams based on the singular values from $\mathbf{\Sigma}^{\mathrm{AB}}$. These are found using the water-filling policy under a per-symbol average power constraint, i.e., $\mathrm{tr}(\mathbf{P}) = N_t$. In addition to multiplying the received signal by $\mathbf{L}^{-1}$ we also pre-process it by multiplying by $(\mathbf{U}^{\mathrm{AB}})^{\mathsf{H}}$. If the estimates $\mathbf{U}^{\mathrm{AB}}$ and $\mathbf{V}^{\mathrm{AB}}$ were perfect, this process would yield a bank of parallel subchannels with capacity given by:

$$C(\mathbf{H}_{\mathit{eff}}) = \sum_{j=0}^{N_{\min}-1} \log_2(1 + \mathrm{SNR}_j), \tag{3.77}$$

where $\mathrm{SNR}_j = \frac{\rho P_T \sigma_j^2 P_j^*}{N_t}$, σ_j is the j^{th} singular value of $\mathbf{L}^{-1}\mathbf{H}_{\mathit{eff}}$, and P_j^* is the power allocated to the j^{th} stream. Channel estimation errors, however, introduce inter-stream

[3]The same process is done for the AA system

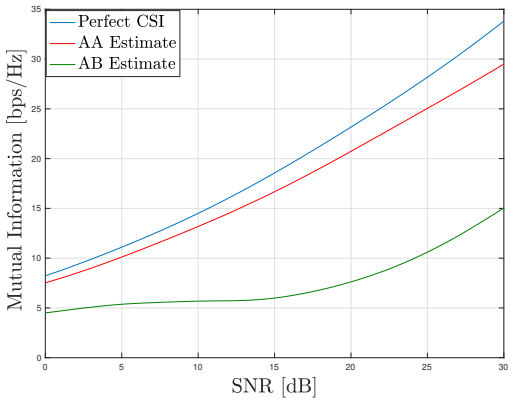

Figure 3.6: Achievable rate at $f_c = 1$ [GHz].

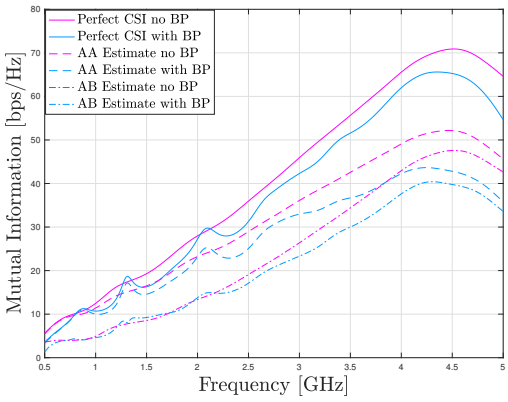

Figure 3.7: Rate against frequency.

interference which is independent of the background noise. By treating such interference as one more additive noise term while still decoding the streams separately, the mutual information between $\mathbf{s}$ and $\mathbf{y}$ (scaled accordingly to get units of bits/s/Hz) of this system given $\mathbf{H}_{\mathit{eff}}$ is lower bounded by [3]:

$$I(\widehat{\mathbf{H}}_{\mathit{eff}}^{\mathrm{AB}}|\mathbf{H}_{\mathit{eff}}) \triangleq \sum_{j=0}^{N_{\min}-1} \log_2(1+\mathrm{SINR}_j^{\mathrm{AB}}), \tag{3.78}$$

where

$$\mathrm{SINR}_{\mathrm{j}}^{\mathrm{AB}} = \frac{\frac{\rho P_T}{N_t} P_j^{\mathrm{AB}^*} |(\mathbf{u}_j^{\mathrm{AB}})^{\mathsf{H}}(\mathbf{L}^{-1}\mathbf{H}_{\mathit{eff}})\mathbf{v}_j^{\mathrm{AB}}|^2}{1 \;+\; \frac{\rho P_T}{N_t} \sum_{l\neq j} P_l^{\mathrm{AB}^*} |(\mathbf{u}_j^{\mathrm{AB}})^{\mathsf{H}}(\mathbf{L}^{-1}\mathbf{H}_{\mathit{eff}})\mathbf{v}_l^{\mathrm{AB}}|^2}, \tag{3.79}$$

and $P_l^{\mathrm{AB}^*}$ is the power allocated to the l^{th} stream using the waterfilling algorithm based on the singular values from $\mathbf{\Sigma}^{\mathrm{AB}}$ in (3.75). In Fig. 3.6 we plot the average achievable rate against SNR without the backed-plane (results are similar with the BP). This was done at $f_c = 1$ [GHz], a bandwidth of 5 [MHz] and with 1000 MC simulations. At moderate to high SNR, when the noise effects are not dominant we see a gain of about $10-15$ [bpcu]. Next in Fig. 3.7 we plot the achievable rate against the carrier frequency with and without the backed plate. Again, we see the that the array with the backed plane is more frequency selective and has performance degradation compared to the one

without the backed plate. The largest gains for both arrays are found around 2 [GHz] where there is significant mutual coupling. At larger frequencies we do not see much gains using the antenna aware estimator as the mutual coupling becomes insignificant. We also see that the gap to the perfect CSI case increases. This is due to the fact that the SNR (see Fig. 3.3) becomes large at higher frequencies and the decrease in interference in the denominator of (3.79) is negligible compared to the increase in SNR given by the numerator of (3.79).

3.4.3 OFDM System

The OFDM AB (3.51) and AA (3.68) estimators will provide an estimate of the given L-tap MIMO channels in time given by (3.50) and (3.67) respectively. The theoretical NMSE for the AB and AA estimators can be found using (3.61), (3.70), and (3.58):

$$\begin{aligned} \mathrm{NMSE}_{\mathrm{AB}} &= \frac{\mathrm{tr}(\mathbf{E}_{\mathit{eff}}^{\mathrm{AB}})}{\mathrm{tr}(\mathbf{R}_{\mathbf{H}_{\mathit{eff}}})}, \\ \mathrm{NMSE}_{\mathrm{AA}} &= \frac{\mathrm{tr}(\mathbf{E}_{\mathit{eff}}^{\mathrm{AA}})}{\mathrm{tr}(\mathbf{R}_{\mathbf{H}_{\mathit{eff}}})}. \end{aligned} \tag{3.80}$$

The large scale parameter (3.71) depends on the frequency of operation and in broadband OFDM systems this can vary significantly with the subcarrier frequency. As this can be estimated easily at the receiver we add the frequency dependence in the pilot symbols so that we can use one common large-scale parameter as in (3.51) and (3.68). In Fig. 3.8 we plot the the NMSE against the pilot power parameterized by the number of channel taps using 10 monte-carlo for each data point and 10 time-domain pilots. This is done over the frequency band from [1 GHz, 1.8 GHz] with a total bandwidth of 800 [MHz] with 64 subcarriers. At low SNR, for the AB estimator, we see that the NMSE increases as the number of taps increase. Note here at 10 [dBm] of power the NMSE for the 8-tap channel is higher than the 2-tap channel, and decreasing the power more we will see a bigger gap between the two. This low SNR behaviour is due to

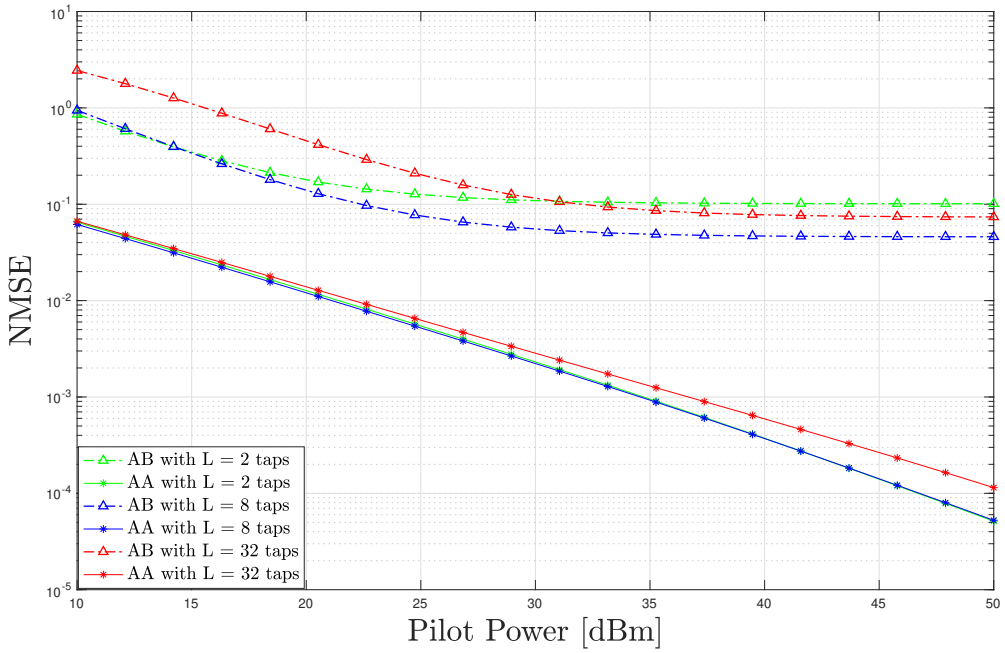

Figure 3.8: NMSE against pilot power in OFDM Estimation using total bandwidth of 708 [MHz]

the fact that the model mismatch effects become negligible as the noise is dominant. Therefore, for a given power, it is easier to estimate a smaller number of variables. At high SNR however, the model mismatch effects become dominant. Indeed, we see that the 2 tap channel has the highest NMSE followed by the 32 and 8 taps channel. Again, if we increase the pilot power more we will see that the 32-tap channel will have the lowest NMSE. Here this is due to the fact that increasing the assumed number of taps more accurately captures the frequency selectivity introduced by the antennas, i.e., the model is more correctly matched. For the AA estimator, we see that the NMSE for 2 and 8 tap channels are almost the same over all SNRs and that the 32 tap channel is also the same except at high SNR, where the matrix conditioning in the estimator (3.68) gets worse with more taps leading to noise enhancement effects. This is further

demonstrated in Fig. 3.9 where we plot the NMSE against the number of channel taps (L). This is done at high SNR (pilot power 50 [dBm]) where we can see the full effects of the model mismatch. As confirmed in Fig. 3.3 the array with the backed plane is more frequency selective and hence should introduce more taps than the array in free space. Due to this, in Fig. 3.9, we see the gains using the AA estimator over the AB estimator are greater for the backed array with the highest gains at a low number of taps consistent with intuition.

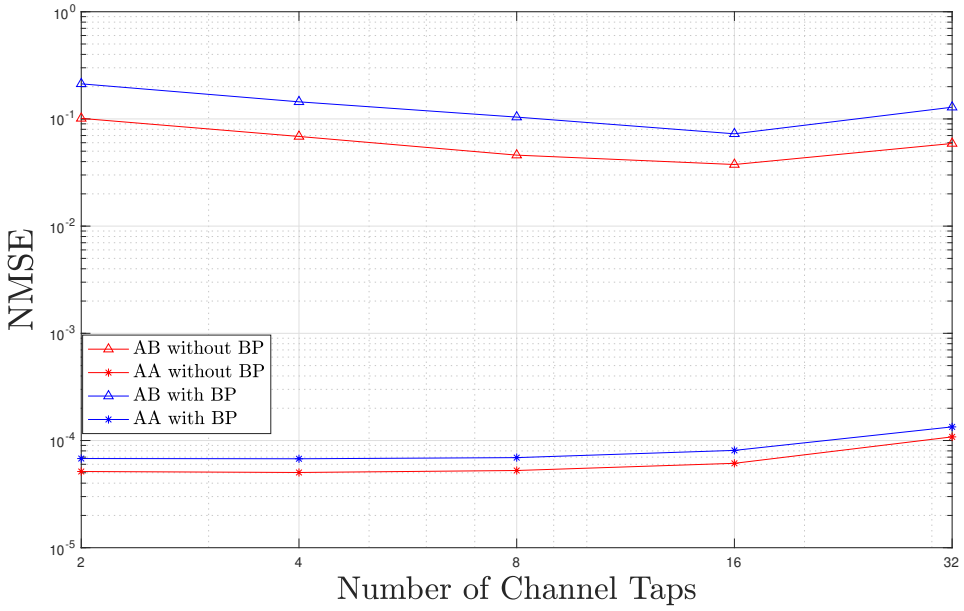

Figure 3.9: NMSE against number of taps at high SNR with and without the BP

Similar to the single-carrier case we can assess the AA and AB estimators using the achievable rate performance criteria. Due to the properties of OFDM transmission, a frequency selective channel can be converted to a bank of K parallel subchannels given by:

$$\mathbf{y}[k] \;=\; \sqrt{\rho}\mathbf{H}_{\mathit{eff}}[k]\,\mathbf{x}[k] + \mathbf{n}[k]. \tag{3.81}$$

One approach to obtain the achievable rate is to allocate power uniformly over the subcarriers and then apply the waterfilling algorithm over space. However, when using broadband arrays this approach will be sub-optimal due to the enhanced frequency selectivity of the arrays. Therefore, to optimize the mutual information, we jointly allocate power over space and frequency. This is first done by whitening the noise for each subcarrier in (3.81) and taking the SVD, i.e.,

$$\mathbf{L}^{-1}[k]\mathbf{H}_{\mathit{eff}}[k] \triangleq \mathbf{U}[k]\,\mathbf{\Sigma}[k]\,\mathbf{V}^{\mathsf{H}}[k]. \tag{3.82}$$

Next the product $\mathbf{L}^{-1}[k]\mathbf{H}_{\mathit{eff}}[k]$ can be concatenated in a block-diagonal matrix over the K subcarriers. The SVD of this newly constructed block diagonal matrix is a block-diagonal matrix of the $\mathbf{U}[k]$'s multiplied by a block-diagonal matrix of the $\mathbf{\Sigma}[k]$'s multiplied by a block-diagonal matrix of the $\mathbf{V}[k]$'s. Now based on this block-diagonal matrix of the $\mathbf{\Sigma}[k]$'s we can perform power allocation under a per-symbol power constraint over all subcarriers equal to $K\,N_t$. We precode based off the blocks of the block diagonal $\mathbf{V}[k]$'s and process the received signal by blocks of the block diagonal $\mathbf{U}[k]$'s. If this process was done based on imperfect CSI then we can lower bound the mutual information by treating the interference as Gaussian noise. To get the achievable rate in bpcu we must sum over the number of subcarriers and normalize by the number of subcarriers as they are transmitted serially. The lower bound of the mutual information for the AB estimator, in bpcu, is given by:

$$I(\{\widehat{\mathbf{H}}^{\mathrm{AB}}_{\mathit{eff}}\}_{k=0}^{K-1}|\{\mathbf{H}_{\mathit{eff}}\}_{k=0}^{K-1}) \triangleq \frac{1}{K}\sum_{k=0}^{K-1}\sum_{j=0}^{N_{\min}-1}\log_2(1+\mathrm{SINR}^{\mathrm{AB}}_{kj}), \tag{3.83}$$

where

$$\mathrm{SINR}^{\mathrm{AB}}_{\mathrm{kj}} = \frac{\frac{\rho_k P_T}{N_t} P^{\mathrm{AB}}_{kj}|(\mathbf{u}^{\mathrm{AB}}_{kj})^{\mathsf{H}}(\mathbf{L}^{-1}\mathbf{H}_{\mathit{eff}})\mathbf{v}^{\mathrm{AB}}_{kj}|^2}{1 \;+\; \frac{\rho_k P_T}{N_t}\sum_{l\neq j} P^{\mathrm{AB}}_{kl}|(\mathbf{u}^{\mathrm{AB}}_{kj})^{\mathsf{H}}(\mathbf{L}^{-1}\mathbf{H}_{\mathit{eff}})\mathbf{v}^{\mathrm{AB}}_{kl}|^2}. \tag{3.84}$$

In Fig. 3.10(a) we plot the achievable rate against power using the backed-plane array with 64 subcarriers from $1-1.5$ [GHz] and 2 channel taps. We see that achievable rate

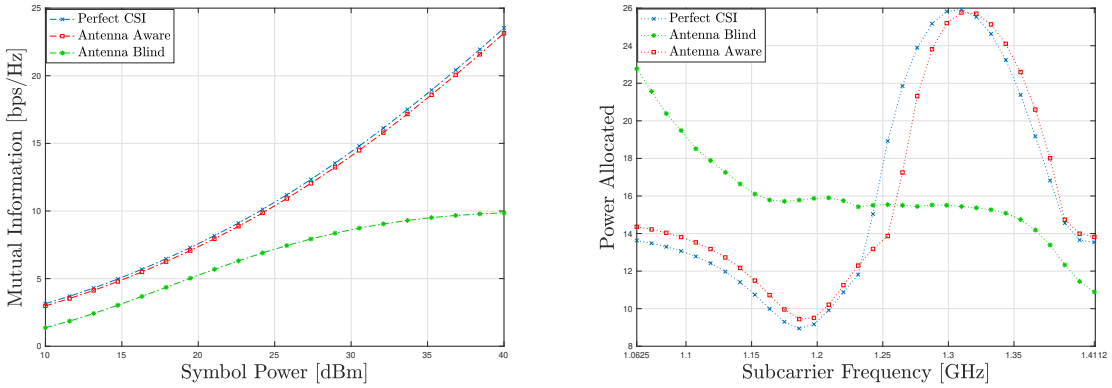

(a) Achievable Rate against Power

(b) Power Allocation over Subcarriers

Figure 3.10: Achievable rate plot and power allocation plot using the backed-plane array with 64 subcarriers over the frequency band $1 - 1.5$ [GHz] with 2 channel taps.

obtained using the AA channel estimate is very close to perfect CSI as the estimation error is very small. We also see that at higher SNR the gap between the AB achievable rate and the perfect CSI grow. This is due to the model mismatch effects that become prominent at higher SNR as explained previously. In Fig. 3.10(b) we plot the total power allocated for each subcarrier against the subcarrier frequency using a symbol power of 10 [dBm]. Indeed, the power's allocated for the perfect CSI case and the AA case follow the SNR plot of the backed-plane array over the band $1 - 1.5$ [GHz] seen in Fig. 3.3 demonstrating the utility in our approach. Furthermore, we see the effect that an inaccurate channel estimate can have as the powers allocated for the AB estimator have no resemblance to the SNR in Fig. 3.3.

3.4.4 Scattering/Impedance Channel Equivalence

In this section, we will numerically demonstrate the equivalence between the MIMO channel description in (3.3) using impedance parameters and the description in (3.9)

using scattering parameters. To our best knowledge, the simple circuit-based channel model using scattering description in (3.9) did not yet appear in the literature. Most works on wireless network modeling with S-parameters either use a hybrid Impedance/Scattering description [48], or utilize a field based approach with infinite expansion for the radiation pattern [68]. The scattering description in (3.9) is simple since only finitely many basis functions are needed to represent the field, yet it is not hybrid and does not use the open/short circuit patterns which are much more difficult to measure in practice. To show the equivalence we simulate an array of two half-wavelength dipole antennas at 1[GHz] both for the transmitter and the receiver. The antennas are assumed to have parallel configuration with half-wavelength spacing. The simple HFSS set-up is shown in Fig.3.11. The considered propagation channel is

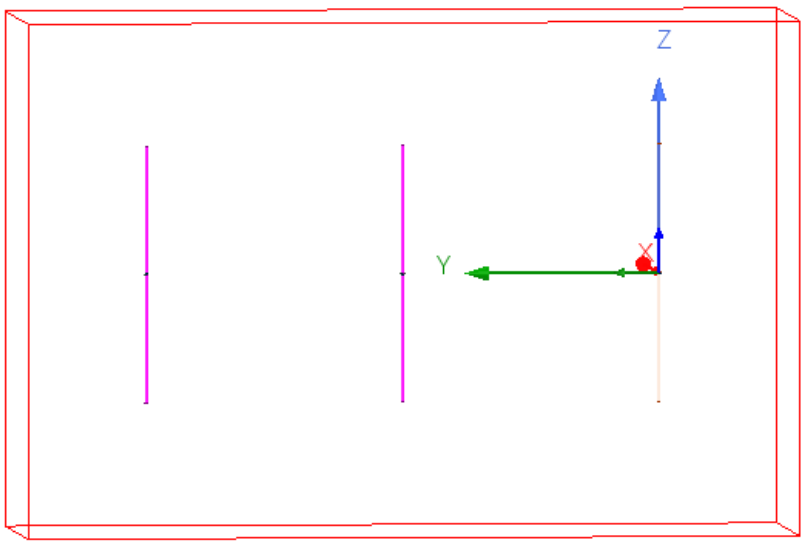

Figure 3.11: Array of two dipole antennas

Line-of-sight (LoS) link with the Friis pathloss which is given by,

$$\boldsymbol{\mathcal{H}}_{\mathrm{OC/Term}}(f) = \frac{c}{4\pi f d} G_{\mathrm{OC/Term}} \mathbf{1}\mathbf{1}^{\mathsf{T}}, \tag{3.85}$$

where $G_{\mathrm{OC/Term}}$ stands for either an open circuit or a terminated gain, and $\boldsymbol{\mathcal{H}}_{\mathrm{OC/Term}}(f)$

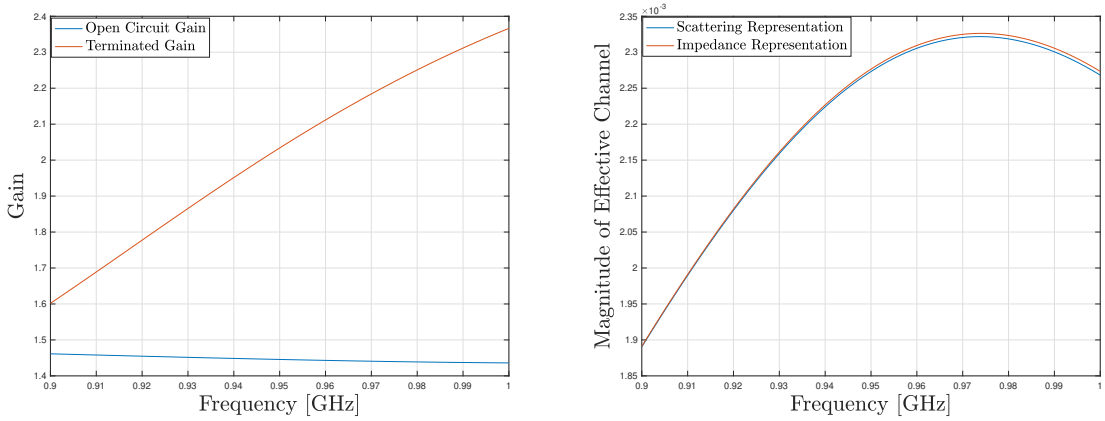

(a) Open Circuit/Terminated Gain

(b) Effective channel magnitude

Figure 3.12: Open circuit/Terminated antenna gains as well as effective channels

stands for the propagation channel from the impedance/scattering description. As can be seen in Fig.3.12, the terminated and open circuit embedded gains are very different, yet the description in (3.9) captures this difference theoretically (since $\boldsymbol{\mathcal{H}}_{\text{eff}}(f)$ is the same) effectively converting terminated gain into an open circuit gain.

Chapter 4

Conclusion and Future Directions

4.1 Concluding Remarks

Here we reiterate the main contributions of this thesis. In the first work we have established achievability and converse results in the K_a-user GMAC with a large-scale antenna array at the BS. We have defined the age-limited capacity as the maximum spectral efficiency achievable such that the AoI is finite in asymptotic system limits. In this case, we have shown that in order to minimize the system AoI all devices must be active in every transmission period. This is also the case in finite system sizes in which the AoI is, however, limited by the probability of error. We have used our bound to compare the two recent massive MIMO URA algorithms, thereby revealing a huge gap between their performance and the overall spectral efficiency that can be potentially achieved in practice.

In the second work, we developed a novel LMMSE channel estimator for single- and multi-carrier systems that takes advantage of the mutual coupling in the transmit/receice antenna arrays. We model the mutual coupling through multiport networks and express the single-user MIMO communication channel in terms of the impedance

and scattering parameters of the antenna arrays. In frequency-flat single-carrier systems, we show that neglecting the coupling in the arrays leads to an inaccurate characterization of the channel and noise correlations. In frequency-selective multi-carrier channels, we show this same effect and also demonstrate that the coupling in the arrays will increase the number of channel taps. Standard LMMSE estimators developed under these inaccurate models become sub-optimal and hence we develop an LMMSE estimator that calibrates the coupling and optimally estimates the channel. It is shown that appropriately accounting for mutual coupling through the developed physically consistent model leads to remarkable improvements in terms of channel estimation performance. We have demonstrated the gains in our algorithm in a rich-scattering environment using a connected array of slot antennas both at the transmitter and receiver sides.

4.2 Future Directions

4.2.1 User-Scheduled Access Scheme

In future work, considering the overloaded system [12], $\zeta/\tau < 1$, it is desirable to do some scheduling in order to control the inter-user interference. One approach could be to subdivide each slot into J scheduling intervals. Then the asymptotic joint optimization of the spectral efficiency as well as the AoI could be performed over the number of scheduling intervals.

4.2.2 Improving the Channel Estimation Algorithm

For the estimation algorithm, it would be useful to explore the design of the pilot sequences to match the antenna rather than choosing orthogonal pilots as is done conventionally. Other avenues could be to explore the channel-sparsity as well as the

estimation of the AoA/AoD.

4.2.3 Physically-Consistent Modelling of Multi-User Systems

Finally, it would be useful to merge the physically-consistent modelling of the antenna arrays and take it into account in a multi-user setting. Here we can more accurately model the physics of propagation and the impairments due to coupling and analyze the trade-offs between the achievable rate and AoI in the system

Appendix A

Derivation of the AoI

Recall from (2.5) the definition of AoI. The latter is a limit of a time-average of the age sample function as the time horizon grows large. Instead of computing the integral in (2.5) directly, we can express it as a function of the inter-update times, as shown pictorially in Fig. A.1.

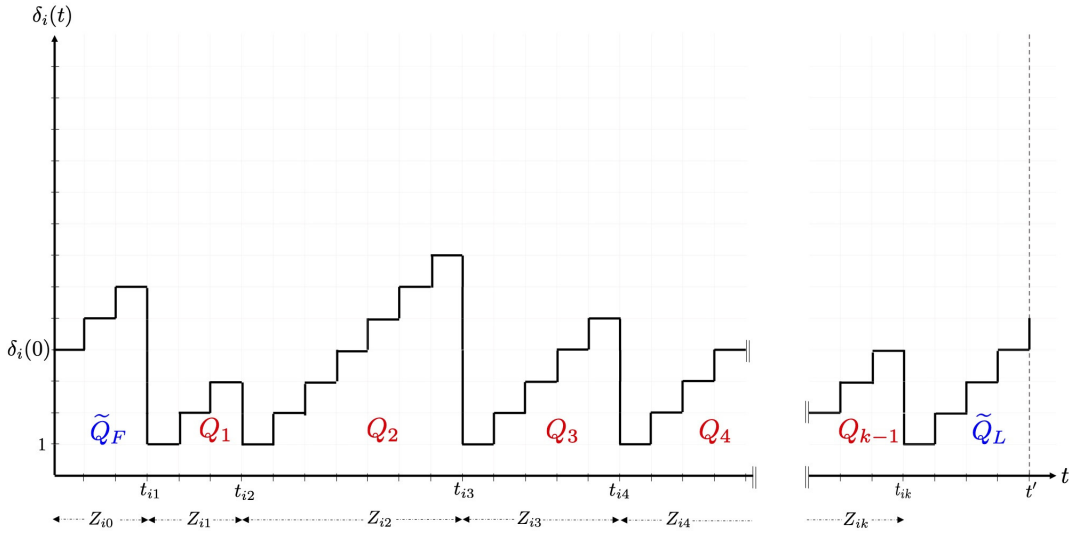

Figure A.1: Decomposition of a sample function of the AoI.

The area below the sample function shown in Fig. A.1 consists of a rectangular base

of width t' and unit height, jagged triangular structures, and boundary pieces (both above the base rectangle). We denote the area of the triangular pieces by Q_l and the first and last boundary pieces by $\widetilde{Q}_F$ and $\widetilde{Q}_L$, respectively. Now (2.5) can be re-written as:

$$\int_0^{t'} \delta_i(t)dt \;=\; t' + \widetilde{Q}_F + \widetilde{Q}_L + \sum_{k=1}^{N(t')-1} Q_k, \tag{A.1}$$

where $N(t')$ denotes the number of arrivals by time t'. The Q_l's can be written in terms of the inter-update intervals as:

$$Q_l = \frac{Z_{il}(Z_{il}-1)}{2}. \tag{A.2}$$

Dividing the right-hand side of (A.1) by t' and taking the limit (as t' goes to $+\infty$) we have:

$$\Delta_i = \lim_{t'\to\infty} \left(1 + \frac{\widetilde{Q}_F + \widetilde{Q}_L}{t'} + \sum_{k=1}^{N(t')-1} \frac{Z_{ik}(Z_{ik}-1)}{2t'}\right). \tag{A.3}$$

The first term can be taken out of the limit and the second term goes to 0 WP1. We re-write the last term in (A.3) as follows:

$$\lim_{t'\to\infty} \left(\frac{N(t')}{2t'} - \frac{1}{2t'}\right) \sum_{k=1}^{N(t')-1} \frac{Z_{ik}(Z_{ik}-1)}{N(t')-1}. \tag{A.4}$$

As the Bernoulli process is a renewal process, we have $\frac{N(t')}{2t'} \to \frac{1}{2\mathbb{E}[Z_i]}$ WP1 [69]. Also, from the strong law of large numbers (SLLN) the sum in the limit converges to $\mathbb{E}[Z_i^2] - \mathbb{E}[Z_i]$ WP1. Therefore, we have:

$$\Delta_i \;=\; \frac{\mathbb{E}[Z_i^2]}{2\mathbb{E}[Z_i]} + \frac{1}{2}. \tag{A.5}$$

Appendix B

Proofs of the Various Approximations

Lemma 1. *The inverse CDF of the sum of random variables,* $\sum_{m=1}^{2M} S_m + \sum_{l=1}^{2k} V_l$*, converges uniformly to the standard normal inverse CDF, where the convergence rate is bounded above by* $\mathcal{O}\left(\frac{1}{\sqrt{M+k}}\right)$*,*

$$\Pr\left\{\sum_{m=1}^{2M} S_m + \sum_{l=1}^{2k} V_l \geq \beta\right\} \;=\; Q(w(k)) + \mathcal{O}\left(\frac{1}{\sqrt{M+k}}\right), \tag{B.1}$$

in which $w(k) = \frac{\beta - \alpha_\rho M + k}{\sqrt{\alpha_\rho^2 M + k}}$*.*

Proof. Let B_{2M+2k} be the following normalized RV:

$$B_{2M+2k} \;\triangleq\; \frac{1}{\sqrt{\alpha_\rho^2 M \;+\; k}}\left[\sum_{m=1}^{2M} S_m + \sum_{l=1}^{2k} V_l \;-\; (M\alpha_\rho - k)\right],$$

whose inverse CDF is denoted as $F_{2M+2k}(x)$. From the Berry-Essen inequality for non identically distributed random variables, the difference between $F_{2M+2k}(x)$ and the standard normal inverse CDF is bounded uniformly, i.e.

$$\sup_{x\in\Re} |F_{2M+2k}(x) - Q(x)| \leq K\phi_1(2M+2k)\phi_2(2M+2k), \tag{B.2}$$

where K is a constant, and

$$\phi_1(2M+2k) = \left(\sum_{m=1}^{2M}\mathbb{E}[|S_m-\mathbb{E}[S_m]|^2]+\sum_{m=1}^{2k}\mathbb{E}[|V_l-\mathbb{E}[V_l]|^2]\right)^{-\frac{3}{2}}, \tag{B.3}$$

$$\phi_2(2M+2k) = \left(\sum_{m=1}^{2M}\mathbb{E}[|S_m-\mathbb{E}[S_m]|^3]+\sum_{l=1}^{2k}\mathbb{E}[|V_l-\mathbb{E}[V_l]|^3]\right). \tag{B.4}$$

Since $S_m \sim \Gamma(\frac{1}{2},\alpha_\rho)$ and $V_l \sim \Gamma(\frac{1}{2},1)$, it can be verified by computing the fourth central moment that the second- and third-order central moments are finite. Let $\mathbb{E}[|S_m-\mathbb{E}[S_m]|^3] = \frac{C_1}{2} > 0$, $\mathbb{E}[|V_l-\mathbb{E}[V_l]|^3] = \frac{C_2}{2} > 0$, $\mathbb{E}[|S_m-\mathbb{E}[S_m]|^2] = \frac{C_3}{2} > 0$, and $\mathbb{E}[|V_l-\mathbb{E}[V_l]|^2] = \frac{C_4}{2} > 0$. Using these notations, we rewrite (B.2) as follows:

$$|F_{2M+2k}(x)-Q(x)| \leq \frac{C_1M+C_2k}{(C_3M+C_4k)^{\frac{3}{2}}} \quad \forall x. \tag{B.5}$$

Since $C_1M+C_2k < \max\{C_1,C_2\}(M+k)$ and $C_3M+C_4k > \min\{C_3,C_4\}(M+k)$ we obtain:

$$|F_{2M+2k}(x)-Q(x)| \leq \frac{\max\{C_1,C_2\}(M+k)}{\min\{C_3,C_4\}(M+k)^{\frac{3}{2}}} = \frac{C}{\sqrt{M+k}} \quad \forall x, \tag{B.6}$$

where $C = \frac{\max\{C_1,C_2\}}{\min\{C_3,C_4\}}$. This implies:

$$F_{2M+2k}(x)-Q(x) \;=\; \mathcal{O}\left(\frac{1}{\sqrt{M+k}}\right) \quad \forall x.$$

This can be used to show that:

$$\Pr\left\{\sum_{m=1}^{2M}S_m+\sum_{l=1}^{2k}V_l \geq \beta\right\} = F_{2M+2k}(w(k)) \;=\; Q(w(k))+\mathcal{O}\left(\frac{1}{\sqrt{M+k}}\right). \tag{B.7}$$

□

Lemma 2. *The probability of error in (2.17) is given by,*

$$p_e \;=\; 1 \;-\; \frac{1}{\sqrt{2\pi}} \int_{-\infty}^{\infty} e^{-\frac{s^2}{2}} Q(w(s)) ds \;+\; \mathcal{O}\left(\frac{1}{\sqrt{N}}\right). \tag{B.8}$$

Proof. We begin by noting that the expression in (2.17) is the expected value of (2.18) with respect to a Binomial distribution with parameters $N-1$ and τ. Here, we show that this expected value can be instead taken with respect to a Gaussian distribution with $\mathcal{O}\left(\frac{1}{\sqrt{N}}\right)$ error term. To start with, since the Binomial distribution does not admit a density function it is more convenient to use Stieltjes integrals over a compact interval before going to infinity. First, we show that $\mathcal{O}\left(\frac{1}{\sqrt{M+k}}\right) = \mathcal{O}\left(\frac{1}{\sqrt{N}}\right)$ by noticing that:

$$\left|\mathcal{O}\left(\frac{1}{\sqrt{M+k}}\right)\right| < \frac{C}{\sqrt{M+k}} = \frac{C}{\sqrt{N(\zeta+\delta)}} = \frac{\widetilde{C}(\delta)}{\sqrt{N}}, \tag{B.9}$$

where $0 < \delta = \frac{k}{N} < 1$. We also write the error resulting from integrating with respect to different CDFs as follows:

$$\left| \int_{-x}^{x} \left(Q(w(k)) + \mathcal{O}\left(\frac{1}{\sqrt{N}}\right)\right) dF(k) \;- \int_{-x}^{x} \left(Q(w(k)) + \mathcal{O}\left(\frac{1}{\sqrt{N}}\right)\right) d\widetilde{F}(k)\right|, \tag{B.10}$$

where $F(k)$ is the CDF of a Binomial RV with mean $(N-1)\tau$ and variance $(N-1)\tau(1-\tau)$ and $\widetilde{F}(k)$ is the CDF of the approximating Gaussian distribution with the same mean and variance. Since both $F(k)$ and $\widetilde{F}(k)$ are non-decreasing on any compact interval $[-x, x]$, the difference $F(k) - \widetilde{F}(k)$ is of bounded variation, and hence the Stieltjes integral with respect to $F(k) - \widetilde{F}(k)$ is defined for any continuous function. Since $Q(w(k))$ is continuous at $w(k)$, we can re-write (B.10) as follows:

$$\left| \int_{-x}^{x} \left(Q(w(k)) + \mathcal{O}\left(\frac{1}{\sqrt{N}}\right)\right) d\left(F(k) - \widetilde{F}(k)\right)\right|. \tag{B.11}$$

Furthermore, since $Q(w(k))$ is of bounded variation on $[-x, x]$, the integral in (B.11) can be integrated by parts to yield:

$$\left| \int_{-x}^{x} \left(Q(w(k)) + \mathcal{O}\left(\frac{1}{\sqrt{N}}\right)\right) d\left(F(k) - \widetilde{F}(k)\right)\right| \;= \; |M_1(x) - M_2(x) - M_3(x)|, \tag{B.12}$$

with

$$M_1(x) = \left(Q(x) + \mathcal{O}\left(\frac{1}{\sqrt{N}}\right)\right)\left(F(x) - \widetilde{F}(-x)\right) \tag{B.13}$$

$$M_2(x) = \left(Q(-x) + \mathcal{O}\left(\frac{1}{\sqrt{N}}\right)\right)\left(F(-x) - \widetilde{F}(-x)\right) \tag{B.14}$$

$$M_3(x) = \int_{-x}^{x}\left(F(k) - \widetilde{F}(k)\right) dQ(w(k)). \tag{B.15}$$

Now, by the triangle inequality, it follows from (B.12) that:

$$\left|\int_{-x}^{x}\left(Q(w(k)) + \mathcal{O}\left(\frac{1}{\sqrt{N}}\right)\right) d\left(F(k) - \widetilde{F}(k)\right)\right| \quad \leq$$
$$|M_1(x)| + |M_2(x)| + |M_3(x)|. \tag{B.16}$$

Then, since $0 < Q(x) < 1$, (B.16) can be further bounded by:

$$K_1\left|F(x) - \widetilde{F}(x)\right| + K_2\left|\widetilde{F}(-x) - F(-x)\right| \; +$$
$$\sup_{k\in[-x,x]}\left|F(k) - \widetilde{F}(k)\right| V_{-x}^{x}(Q), \tag{B.17}$$

where $V_{-x}^{x}(Q) < \infty$ is the total variation of the Q-function over $[-x, x]$. Recall, also that $F(x)$ represents the CDF of a large sum of $N-1$ binary random variables. Consequently, upon appropriate normalization and by applying the Berry-Essen inequality for i.i.d random variables we see that (B.17) is less than:

$$\frac{A_1}{\sqrt{N}} + \frac{A_2}{\sqrt{N}} + \frac{A_3}{\sqrt{N}} \;=\; \mathcal{O}\left(\frac{1}{\sqrt{N}}\right), \tag{B.18}$$

for some positive constants A_1, A_2 and A_3. Now, coming back to (B.10) we see that:

$$\int_{-x}^{x}\left(Q(w(k)) + \mathcal{O}\left(\frac{1}{\sqrt{N}}\right)\right) dF(k) \;=$$
$$\int_{-x}^{x}\left(Q(w(k)) + \mathcal{O}\left(\frac{1}{\sqrt{N}}\right)\right) d\widetilde{F}(k) + \mathcal{O}\left(\frac{1}{\sqrt{N}}\right), \tag{B.19}$$

where the $\mathcal{O}(\frac{1}{\sqrt{N}})$ on the left- and right-hand sides can be safely dropped since both CDFs are bounded, thereby yielding:

$$\int_{-x}^{x} Q(w(k)) dF(k) \;=\; \int_{-x}^{x} Q(w(k)) d\widetilde{F}(k) + \mathcal{O}\left(\frac{1}{\sqrt{N}}\right). \tag{B.20}$$

The right-hand side integral in (B.20) is with respect to a Gaussian CDF and can now be explicitly written in terms of a density by making the substitution $s = \frac{k-(N-1)\tau}{\sqrt{(N-1)\tau(1-\tau)}}$

$$\int_{-x}^{x} Q(w(k))d\widetilde{F}(k) \;=\; \frac{1}{\sqrt{2\pi}}\int_{-x'}^{x'} Q(w(s))e^{-\frac{s^2}{2}}ds. \tag{B.21}$$

Since the approximation is uniform in x and the integrals are convergent, we can go to the limit in (B.20) and obtain:

$$\int_{-\infty}^{\infty} Q(w(k))dF(k) \;= \\ \frac{1}{\sqrt{2\pi}}\int_{-\infty}^{\infty} Q(w(s))e^{-\frac{s^2}{2}}ds + \mathcal{O}\left(\frac{1}{\sqrt{N}}\right). \tag{B.22}$$

By further noticing that the left-hand side of (B.19) is nothing but the expression of $1-p_e$, we finally obtain:

$$p_e \;=\; 1 - \frac{1}{\sqrt{2\pi}}\int_{-\infty}^{\infty} Q(w(s))e^{-\frac{s^2}{2}}ds + \mathcal{O}\left(\frac{1}{\sqrt{N}}\right). \tag{B.23}$$

□

Lemma 3. *$w(s)$ in (2.21) can be approximated as follows,*

$$w(s) \;=\; \frac{\beta - \alpha_\rho M + s\sqrt{N\tau(1-\tau)} + N\tau}{\sqrt{\alpha_\rho^2 M + s\sqrt{N\tau(1-\tau)} + N\tau}} \;+\; \mathcal{O}\left(\frac{1}{\sqrt{N}}\right). \tag{B.24}$$

Proof. We denote the first term in (B.24) by $w_a(s)$ and start by re-writing (2.21) as:

$$w(s) \;=\; \frac{\beta - \alpha_\rho M + s\sqrt{N\tau(1-\tau)} + N\tau}{\sqrt{\alpha_\rho^2 M + s\sqrt{(N-1)\tau(1-\tau)} + (N-1)\tau}} \\ + \;\frac{s\sqrt{\tau(1-\tau)}(\sqrt{N-1}-\sqrt{N}) - \tau}{\sqrt{\alpha_\rho^2 M + s\sqrt{(N-1)\tau(1-\tau)} + (N-1)\tau}}. \tag{B.25}$$

Dividing and multiplying the first term in (B.25) by the denominator of the first term in (B.24) yields:

$$w(s) = w_a(s)\frac{\sqrt{\alpha_\rho^2 M + s\sqrt{N\tau(1-\tau)} + N\tau}}{\sqrt{\alpha_\rho^2 M + s\sqrt{(N-1)\tau(1-\tau)} + (N-1)\tau}} \\ + \;\frac{s\sqrt{\tau(1-\tau)}(\sqrt{N-1}-\sqrt{N}) - \tau}{\sqrt{\alpha_\rho^2 M + s\sqrt{(N-1)\tau(1-\tau)} + (N-1)\tau}}. \tag{B.26}$$

Recall that M grows proportionally to N with proportionality coefficient ζ (i.e. $M = \zeta N$). Therefore, after multiplying and dividing the second term in (B.26) by $\frac{1}{\sqrt{N}}$, one can see it is $\mathcal{O}\left(\frac{1}{\sqrt{N}}\right)$. Using this fact and simplifying the first term, (B.26) can be written as:

$$w(s) \;=\; \tag{B.27}$$
$$w_a(s)\left(1+\frac{s\sqrt{\tau(1-\tau)}(\sqrt{N}-\sqrt{N-1})+\tau}{\alpha_\rho^2\zeta N+s\sqrt{(N-1)\tau(1-\tau)}+(N-1)\tau}\right)^{\frac{1}{2}}+\mathcal{O}\left(\frac{1}{\sqrt{N}}\right).$$

Taking a first order Taylor expansion of the coefficient of $w_a(s)$ in (B.27) we obtain the desired result. □

Lemma 4. *By neglecting the terms $\frac{\beta}{\sqrt{N}}$ and $\frac{s}{\sqrt{N}}\sqrt{\tau(1-\tau)}$ in (2.23) we obtain:*

$$w(s) \;=\; \frac{\sqrt{N}(\tau-\alpha_\rho\zeta)+s\sqrt{\tau(1-\tau)}}{\sqrt{\alpha_\rho^2\zeta+\tau}}+\mathcal{O}\left(\frac{1}{\sqrt{N}}\right). \tag{B.28}$$

Proof. We denote the first term in (B.28) by $w_a'(s)$. Factoring out $\frac{\beta}{\sqrt{N}}$ from the first term in (2.23) and resorting to some simplifications, (2.23) is re-written as follows:

$$w(s) \;=\; \frac{\sqrt{N}(\tau-\alpha_\rho\zeta)+s\sqrt{\tau(1-\tau)}}{\sqrt{\alpha_\rho^2\zeta+\frac{s}{\sqrt{N}}\sqrt{\tau(1-\tau)}+\tau}}+\mathcal{O}\left(\frac{1}{\sqrt{N}}\right). \tag{B.29}$$

Then, multiplying and dividing the first term in (B.29) by $\sqrt{\alpha_\rho^2\zeta+\tau}$ leads to:

$$w(s) \;=\; w_a'(s)\frac{\sqrt{\alpha_\rho^2\zeta+\tau}}{\sqrt{\alpha_\rho^2\zeta+\frac{s}{\sqrt{N}}\sqrt{\tau(1-\tau)}+\tau}}+\mathcal{O}\left(\frac{1}{\sqrt{N}}\right), \tag{B.30}$$

which is equivalent to:

$$w(s) \;=\; w_a'(s)\left(1+\frac{s\sqrt{\tau(1-\tau)}}{(\alpha_\rho^2\zeta+\tau)\sqrt{N}}\right)^{-\frac{1}{2}}+\mathcal{O}\left(\frac{1}{\sqrt{N}}\right). \tag{B.31}$$

Taking a first order Taylor expansion of the coefficient of $w_a'(s)$ in (B.31) we obtain the desired result. □

Lemma 5. *By ignoring the term $s\sqrt{\tau(1-\tau)}$ in (2.24), we obtain:*

$$w \;=\; \frac{\sqrt{N}(\tau-\alpha_\rho\zeta)}{\sqrt{\alpha_\rho^2\zeta+\tau}}+\mathcal{O}(1), \tag{B.32}$$

Proof. Since the term $\frac{s\sqrt{\tau(1-\tau)}}{\sqrt{\alpha_\rho^2\zeta+\tau}}$ is independent of N we make a constant error in neglecting it from (2.24). □

Lemma 6. *Taking $Q(w(s))$ outside of the integral in (2.20) leads to*

$$p_e \;=\; 1 - Q(w) \;+\; \mathcal{O}\left(\frac{1}{\sqrt{N}}\right). \tag{B.33}$$

Proof. We first rewrite $w(s)$, given in (2.24), as follows:

$$w(s) \;=\; \frac{\sqrt{N}(\tau-\alpha_\rho\zeta)}{\sqrt{\alpha_\rho^2\zeta+\tau}} + s\sqrt{\frac{\tau(1-\tau)}{\alpha_\rho^2\zeta+\tau}} + \mathcal{O}\left(\frac{1}{\sqrt{N}}\right), \tag{B.34}$$

and denote the first term by w. We denote the error probability in (2.20) by p_t and the one in (2.26) by p_a. The absolute error between p_t and p_a is then given by:

$$\begin{aligned} &|p_t - p_a| \;= \\ &\left|\frac{1}{\sqrt{2\pi}}\left(\int_{-\infty}^{\infty}\big(Q(w)-Q(w(s))\big)e^{-\frac{s^2}{2}}ds\right) + \mathcal{O}\left(\frac{1}{\sqrt{N}}\right)\right|. \end{aligned} \tag{B.35}$$

Using the definition of the Q-function in (2.19) we can rewrite (B.35) as follows:

$$\begin{aligned} &|p_t - p_a| \;= \\ &\left|\frac{1}{2\pi}\left(\int_{-\infty}^{\infty}\left(\int_{w}^{w(s)} e^{\frac{t'^2}{2}}dt'\right)e^{-\frac{s^2}{2}}ds\right) + \mathcal{O}\left(\frac{1}{\sqrt{N}}\right)\right|. \end{aligned} \tag{B.36}$$

Since $e^{-\frac{t^2}{2}} \leq 1\ \forall t$ we can replace the inner integrand function by 1 thereby leading to:

$$\begin{aligned} |p_t - p_a| &\leq \left|\frac{1}{2\pi}\int_{-\infty}^{\infty}(w(s)-w)e^{-\frac{s^2}{2}}ds + \mathcal{O}\left(\frac{1}{\sqrt{N}}\right)\right|. \\ &= \left|\frac{1}{2\pi}\int_{-\infty}^{\infty}\left(s\sqrt{\frac{\tau(1-\tau)}{\alpha_\rho^2\zeta+\tau}} + \mathcal{O}\left(\frac{1}{\sqrt{N}}\right)\right)e^{-\frac{s^2}{2}}ds \right. \\ &\qquad \left. + \mathcal{O}\left(\frac{1}{\sqrt{N}}\right)\right|. \\ &= \left|\frac{1}{\sqrt{2\pi}}\sqrt{\frac{\tau(1-\tau)}{\alpha_\rho^2\zeta+\tau}}\int_{-\infty}^{\infty}\frac{s}{\sqrt{2\pi}}e^{-\frac{s^2}{2}}ds \right. \\ &\qquad \left. + \mathcal{O}\left(\frac{1}{\sqrt{N}}\right)\right|. \end{aligned} \tag{B.37}$$

The remaining integral in (B.37) is nothing but the expected value of a zero-mean Gaussian RV and therefore we have:

$$|p_t - p_a| \leq \frac{K}{\sqrt{N}}, \tag{B.38}$$

for some positive constant K. Since the absolute error is $\mathcal{O}\left(\frac{1}{\sqrt{N}}\right)$ we obtain the desired result. □

Lemma 7. *The $\mathcal{O}\left(\frac{1}{\sqrt{N}}\right)$ term in (2.27) can be taken out of the denominator in the AoI expression and the AoI expression becomes*

$$\Delta(\zeta, N, \rho, \tau) \;=\; \frac{1}{\tau\left(1 - Q\left(\frac{\sqrt{N}(\alpha_\rho\zeta - \tau)}{\sqrt{\alpha_\rho^2\zeta + \tau}}\right)\right)} + \mathcal{O}\left(\frac{1}{\sqrt{N}}\right). \tag{B.39}$$

Proof. We denote the first term in (B.39) by Δ_a and define Δ_t as:

$$\Delta_t \;\triangleq\; \frac{1}{\tau\left(1 - Q\left(\frac{\sqrt{N}(\alpha_\rho\zeta - \tau)}{\sqrt{\alpha_\rho^2\zeta + \tau}}\right) + \mathcal{O}\left(\frac{1}{\sqrt{N}}\right)\right)}. \tag{B.40}$$

The absolute error between Δ_t and Δ_a is given by,

$$|\Delta_t - \Delta_a| \;=\; \left| \frac{1}{\tau\left(1 - Q\left(\frac{\sqrt{N}(\alpha_\rho\zeta - \tau)}{\sqrt{\alpha_\rho^2\zeta + \tau}}\right) + \mathcal{O}\left(\frac{1}{\sqrt{N}}\right)\right)} - \frac{1}{\tau\left(1 - Q\left(\frac{\sqrt{N}(\alpha_\rho\zeta - \tau)}{\sqrt{\alpha_\rho^2\zeta + \tau}}\right)\right)} \right|.$$

Combining the two terms and resorting to some simplifications we obtain:

$$|\Delta_t - \Delta_a| = \mathcal{O}\left(\frac{1}{\sqrt{N}}\right). \tag{B.41}$$

The fact that the absolute error between Δ_t and Δ_a is $\mathcal{O}\left(\frac{1}{\sqrt{N}}\right)$ implies the desired result in (B.39). □

Appendix C

Finding the Spectral Efficiency from the Packet Error Probability

From (2.27), we see that the condition $p_e < \epsilon$ leads to:

$$Q\left(\frac{\sqrt{N}(\alpha_\rho\zeta - \tau)}{\sqrt{\alpha_\rho^2\zeta + \tau}}\right) \;<\; \epsilon_1, \tag{C.1}$$

where $\epsilon_1 = \epsilon + \mathcal{O}\left(\frac{1}{\sqrt{N}}\right)$. Inverting the Q-function and re-arranging the terms yields:

$$\zeta\left(\zeta - \frac{Q^{-1}(\epsilon_1)^2}{N}\right)\alpha_\rho^2 - (2\zeta\tau)\alpha_\rho + \tau\left(\tau - \frac{Q^{-1}(\epsilon_1)^2}{N}\right) \;>\; 0. \tag{C.2}$$

The left-hand side of (C.1) equation is a quadratic form of α_ρ whose zeroes are given by:

$$\alpha_\rho^+ \;=\; \tau\frac{1 + \sqrt{1 - (1 - \frac{Q^{-1}(\epsilon_1)^2}{N\zeta})(1 - \frac{Q^{-1}(\epsilon_1)^2}{N\tau})}}{\zeta - \frac{Q^{-1}(\epsilon_1)^2}{N}}, \tag{C.3}$$

and

$$\alpha_\rho^- \;=\; \tau\frac{1 - \sqrt{1 - (1 - \frac{Q^{-1}(\epsilon_1)^2}{N\zeta})(1 - \frac{Q^{-1}(\epsilon_1)^2}{N\tau})}}{\zeta - \frac{Q^{-1}(\epsilon_1)^2}{N}}, \tag{C.4}$$

Recall that $\alpha_\rho = \frac{1}{2^\rho - 1}$ and since $\rho \geq 0$ then α_ρ is nonnegative.

Case 1: $\zeta > \frac{Q^{-1}(\epsilon_1)^2}{N}$

In the case that $\zeta > \frac{Q^{-1}(\epsilon_1)^2}{N}$, the parabola in (C.2) is convex with real roots and, therefore, the inequality in (C.2) is satisfied whenever $\alpha_\rho < \alpha_\rho^-$ or $\alpha_\rho > \alpha_\rho^+$. Note that α_ρ^+ is always positive and any $\alpha_\rho > \alpha_\rho^+$ is a valid solution. However, if $\tau \leq \frac{Q^{-1}(\epsilon_1)^2}{N}$, α_ρ^- will be non-positive and solutions $\alpha_\rho < \alpha_\rho^-$ are invalid as α_ρ must be non-negative. Yet, even in the case $\tau > \frac{Q^{-1}(\epsilon_1)^2}{N}$, $\alpha_\rho < \alpha_\rho^-$ leads to incorrect solutions for small ϵ_1. Re-writing (C.1), we have:

$$\frac{\sqrt{N}(\alpha_\rho\zeta - \tau)}{\sqrt{\alpha_\rho^2\zeta + \tau}} \;>\; Q^{-1}(\epsilon_1). \tag{C.5}$$

Now if ϵ_1 is small, i.e. smaller than $\frac{1}{2}$, then $Q^{-1}(\epsilon_1) > 0$ and hence the term on the left-hand side of (C.5) should be positive as well. In this case, α_ρ^- should be greater than $\frac{\tau}{\zeta}$ and re-writing α_ρ^- as:

$$\alpha_\rho^- \;=\; \frac{\tau}{\zeta}\left(\frac{1-\sqrt{1-(1-\frac{Q^{-1}(\epsilon_1)^2}{N\zeta})(1-\frac{Q^{-1}(\epsilon_1)^2}{N\tau})}}{1-\frac{Q^{-1}(\epsilon_1)^2}{\zeta N}}\right), \tag{C.6}$$

we see that this is equivalent to the term inside the brackets in (C.6) being greater than 1. In that case, we have:

$$1-\sqrt{1-\left(1-\frac{Q^{-1}(\epsilon_1)^2}{N\zeta}\right)\left(1-\frac{Q^{-1}(\epsilon_1)^2}{N\tau}\right)} \;>\; 1-\frac{Q^{-1}(\epsilon_1)^2}{\zeta N}. \tag{C.7}$$

This implies:

$$\left(\frac{Q^{-1}(\epsilon_1)^2}{N\zeta}\right)^2 > \left(\frac{Q^{-1}(\epsilon_1)^2}{N\zeta}\right)\left(1-\frac{Q^{-1}(\epsilon_1)^2}{N\tau}\right) + \frac{Q^{-1}(\epsilon_1)^2}{N\tau}. \tag{C.8}$$

Dividing both sides of (C.8) by $\left(\frac{Q^{-1}(\epsilon_1)^2}{N\zeta}\right)$ and rearranging the terms, we obtain:

$$\left(\frac{Q^{-1}(\epsilon_1)^2}{N\zeta}\right)\left(1+\frac{\zeta}{\tau}\right) \;>\; \left(1+\frac{\zeta}{\tau}\right), \tag{C.9}$$

from which it follows that:

$$\zeta \;<\; \frac{Q^{-1}(\epsilon_1)^2}{N}. \tag{C.10}$$

As we are assuming $\zeta > \frac{Q^{-1}(\epsilon_1)^2}{N}$ we have a contradiction and thus $\alpha_\rho < \alpha_\rho^-$ is an invalid solution.

Case 2: $\zeta < \frac{Q^{-1}(\epsilon_1)^2}{N}$

In this case, the quadratic form involved in (C.2) is concave. Its zeroes are still given by (C.3) and (C.4) and solutions to (C.2) are $\alpha_\rho^+ < \alpha_\rho < \alpha_\rho^-$. In this case, α_ρ^+ is always negative and only when $\tau > \frac{Q^{-1}(\epsilon_1)^2}{N}$, α_ρ^- is positive. Since α_ρ must always be non-negative, valid solutions to (C.2) are $0 < \alpha_\rho < \alpha_\rho^-$ under the condition that $\tau > \frac{Q^{-1}(\epsilon_1)^2}{N}$. Yet, even we will show that this leads to invalid solutions. If ϵ_1 is small, i.e. less than $\frac{1}{2}$, then $Q^{-1}(\epsilon_1)$ is positive and so $\alpha_\rho\zeta - \tau$ must be greater than 0 or we have a contradiction. Assuming that $\alpha_\rho^-\zeta - \tau$ is positive, it follows that:

$$\alpha_\rho^-\zeta - \tau \; > \; 0, \tag{C.11}$$

which is equivalent to:

$$\frac{\tau}{\zeta}\left(\frac{\sqrt{1+(\frac{Q^{-1}(\epsilon_1)^2}{N\zeta}-1)(1-\frac{Q^{-1}(\epsilon_1)^2}{N\tau})}-1}{\frac{Q^{-1}(\epsilon_1)^2}{N\zeta}-1}\right) \; > \; \frac{\tau}{\zeta}, \tag{C.12}$$

where in (C.12) we multiplied the numerator and denominator of α_ρ^- given in (C.4) by $\frac{1}{\zeta}$. Simplifying (C.12) further leads to:

$$\zeta \; > \; \frac{Q^{-1}(\epsilon_1)^2}{N}. \tag{C.13}$$

As we are assuming that $\zeta < \frac{Q^{-1}(\epsilon_1)^2}{N}$, we arrive at a contradiction. Therefore, if $\zeta < \frac{Q^{-1}(\epsilon_1)^2}{N}$ there are no valid solutions.

Bibliography

[1] A. Ghosh, A. Maeder, M. Baker, and D. Chandramouli, "5g evolution: A view on 5g cellular technology beyond 3gpp release 15," *IEEE access*, vol. 7, pp. 127 639–127 651, 2019.

[2] F. W. Vook, A. Ghosh, E. Diarte, and M. Murphy, "5g new radio: Overview and performance," in *2018 52nd Asilomar conference on signals, systems, and computers*. IEEE, 2018, pp. 1247–1251.

[3] R. W. Heath Jr and A. Lozano, *Foundations of MIMO communication*. Cambridge University Press, 2018.

[4] E. G. Larsson, O. Edfors, F. Tufvesson, and T. L. Marzetta, "Massive mimo for next generation wireless systems," *IEEE communications magazine*, vol. 52, no. 2, pp. 186–195, 2014.

[5] D. Cavallo, "Connected array antennas: Analysis and design," 2011.

[6] E. Dutkiewicz, X. Costa-Perez, I. Z. Kovacs, and M. Mueck, "Massive machine-type communications," *IEEE Network*, vol. 31, no. 6, pp. 6–7, 2017.

[7] Y. Yuan, Z. Yuan, G. Yu, C.-h. Hwang, P.-k. Liao, A. Li, and K. Takeda, "Non-orthogonal transmission technology in lte evolution," *IEEE Communications Magazine*, vol. 54, no. 7, pp. 68–74, 2016.

[8] L. Liu, E. G. Larsson, W. Yu, P. Popovski, C. Stefanovic, and E. De Carvalho, "Sparse signal processing for grant-free massive connectivity: A future paradigm for random access protocols in the internet of things," *IEEE Signal Processing Magazine*, vol. 35, no. 5, pp. 88–99, 2018.

[9] R. Gallager, "A perspective on multiaccess channels," *IEEE Transactions on information Theory*, vol. 31, no. 2, pp. 124–142, 1985.

[10] X. Chen, T.-Y. Chen, and D. Guo, "Capacity of gaussian many-access channels," *IEEE Transactions on Information Theory*, vol. 63, no. 6, pp. 3516–3539, 2017.

[11] Y. Polyanskiy, "A perspective on massive random-access," in *2017 IEEE International Symposium on Information Theory (ISIT)*, 2017, pp. 2523–2527.

[12] L. Liu and W. Yu, "Massive connectivity with massive mimo—part i: Device activity detection and channel estimation," *IEEE Transactions on Signal Processing*, vol. 66, no. 11, pp. 2933–2946, 2018.

[13] ——, "Massive connectivity with massive mimo—part ii: Achievable rate characterization," *IEEE Transactions on Signal Processing*, vol. 66, no. 11, pp. 2947–2959, 2018.

[14] T. L. Marzetta, "Noncooperative cellular wireless with unlimited numbers of base station antennas," *IEEE Transactions on Wireless Communications*, vol. 9, no. 11, pp. 3590–3600, 2010.

[15] A. Fengler, S. Haghighatshoar, P. Jung, and G. Caire, "Non-bayesian activity detection, large-scale fading coefficient estimation, and unsourced random access with a massive mimo receiver," *IEEE Transactions on Information Theory*, vol. 67, no. 5, pp. 2925–2951, 2021.

[16] V. Shyianov, F. Bellili, A. Mezghani, and E. Hossain, "Massive unsourced random access based on uncoupled compressive sensing: Another blessing of massive

mimo," *IEEE Journal on Selected Areas in Communications*, vol. 39, no. 3, pp. 820–834, 2020.

[17] A. Decurninge, I. Land, and M. Guillaud, "Tensor-based modulation for unsourced massive random access," *IEEE Wireless Communications Letters*, vol. 10, no. 3, pp. 552–556, 2020.

[18] J. Che, Z. Zhang, Z. Yang, X. Chen, C. Zhong, and D. W. K. Ng, "Unsourced random massive access with beam-space tree decoding," *IEEE Journal on Selected Areas in Communications*, vol. 40, no. 4, pp. 1146–1161, 2022.

[19] R. Ayachi, M. Akrout, V. Shyianov, F. Bellili, and A. Mezghani, "Massive unsourced random access based on bilinear vector approximate message passing," in *ICASSP 2022-2022 IEEE International Conference on Acoustics, Speech and Signal Processing (ICASSP)*. IEEE, 2022, pp. 5283–5287.

[20] M. Ke, Z. Gao, M. Zhou, D. Zheng, D. W. K. Ng, and H. V. Poor, "Next-generation massive urllc with massive mimo: A unified semi-blind detection framework for sourced and unsourced random access," *arXiv preprint arXiv:2303.04414*, 2023.

[21] G. Durisi, T. Koch, and P. Popovski, "Toward massive, ultrareliable, and low-latency wireless communication with short packets," *Proceedings of the IEEE*, vol. 104, no. 9, pp. 1711–1726, 2016.

[22] P. Popovski, "Ultra-reliable communication in 5g wireless systems," in *1st International Conference on 5G for Ubiquitous Connectivity*. IEEE, 2014, pp. 146–151.

[23] N. A. Johansson, Y.-P. E. Wang, E. Eriksson, and M. Hessler, "Radio access for ultra-reliable and low-latency 5g communications," in *2015 IEEE International Conference on Communication Workshop (ICCW)*. IEEE, 2015, pp. 1184–1189.

[24] O. N. Yilmaz, Y.-P. E. Wang, N. A. Johansson, N. Brahmi, S. A. Ashraf, and J. Sachs, "Analysis of ultra-reliable and low-latency 5g communication for a factory

automation use case," in *2015 IEEE international conference on communication workshop (ICCW)*. IEEE, 2015, pp. 1190–1195.

[25] S. Kaul, R. Yates, and M. Gruteser, "Real-time status: How often should one update?" in *2012 Proceedings IEEE INFOCOM*. IEEE, 2012, pp. 2731–2735.

[26] S. Kaul, M. Gruteser, V. Rai, and J. Kenney, "Minimizing age of information in vehicular networks," in *2011 8th Annual IEEE Communications Society Conference on Sensor, Mesh and Ad Hoc Communications and Networks*, 2011, pp. 350–358.

[27] Z. Jiang, B. Krishnamachari, X. Zheng, S. Zhou, and Z. Niu, "Timely status update in wireless uplinks: Analytical solutions with asymptotic optimality," *IEEE Internet of Things Journal*, vol. 6, no. 2, pp. 3885–3898, 2019.

[28] I. Kadota, A. Sinha, and E. Modiano, "Scheduling algorithms for optimizing age of information in wireless networks with throughput constraints," *IEEE/ACM Transactions on Networking*, vol. 27, no. 4, pp. 1359–1372, 2019.

[29] M. Bastopcu and S. Ulukus, "Partial updates: Losing information for freshness," in *2020 IEEE International Symposium on Information Theory (ISIT)*. IEEE, 2020, pp. 1800–1805.

[30] A. Baknina, S. Ulukus, O. Oze, J. Yang, and A. Yener, "Sening information through status updates," in *2018 IEEE International Symposium on Information Theory (ISIT)*, 2018, pp. 2271–2275.

[31] H. Chen, Q. Wang, Z. Dong, and N. Zhang, "Multiuser scheduling for minimizing age of information in uplink mimo systems," in *2020 IEEE/CIC International Conference on Communications in China (ICCC)*. IEEE, 2020, pp. 1162–1167.

[32] Z. Zhu, B. Yu, and Y. Cai, "Status update performance in uplink massive mu-mimo short-packet communication systems," in *2020 International Conference on*

Wireless Communications and Signal Processing (WCSP). IEEE, 2020, pp. 115–119.

[33] S. Feng and J. Yang, "Precoding and scheduling for aoi minimization in mimo broadcast channels," *IEEE Transactions on Information Theory*, 2022.

[34] B. Yu and Y. Cai, "Age of information in grant-free random access with massive mimo," *IEEE Wireless Communications Letters*, vol. 10, no. 7, pp. 1429–1433, 2021.

[35] P. Popovski, K. F. Trillingsgaard, O. Simeone, and G. Durisi, "5g wireless network slicing for embb, urllc, and mmtc: A communication-theoretic view," *Ieee Access*, vol. 6, pp. 55 765–55 779, 2018.

[36] J. G. Andrews, S. Buzzi, W. Choi, S. V. Hanly, A. Lozano, A. C. Soong, and J. C. Zhang, "What will 5g be?" *IEEE Journal on selected areas in communications*, vol. 32, no. 6, pp. 1065–1082, 2014.

[37] W. Saad, M. Bennis, and M. Chen, "A vision of 6g wireless systems: Applications, trends, technologies, and open research problems," *IEEE network*, vol. 34, no. 3, pp. 134–142, 2019.

[38] C. Saha, J. Y. Siddiqui, and Y. M. Antar, *Multifunctional ultrawideband antennas: trends, techniques and applications*. CRC Press, 2019.

[39] M. Akrout, V. Shyianov, F. Bellili, A. Mezghani, and R. W. Heath, "Super-wideband massive mimo," *arXiv preprint arXiv:2208.01556*, 2022.

[40] C. E. Shannon, "A mathematical theory of communication," *Bell system technical journal*, vol. 27, no. 3, pp. 379–423, 1948.

[41] C. A. Balanis, *Antenna theory: analysis and design*. John wiley & sons, 2016.

[42] J. D. Jackson, "Classical electrodynamics," 1999.

[43] M. Franceschetti, *Wave theory of information*. Cambridge University Press, 2017.

[44] F. K. Gruber and E. A. Marengo, "New aspects of electromagnetic information theory for wireless and antenna systems," *IEEE Transactions on Antennas and Propagation*, vol. 56, no. 11, pp. 3470–3484, 2008.

[45] M. D. Migliore, "On electromagnetics and information theory," *IEEE Transactions on Antennas and Propagation*, vol. 56, no. 10, pp. 3188–3200, 2008.

[46] A. Pizzo, T. L. Marzetta, and L. Sanguinetti, "Degrees of freedom of holographic mimo channels," in *2020 IEEE 21st International Workshop on Signal Processing Advances in Wireless Communications (SPAWC)*. IEEE, 2020, pp. 1–5.

[47] M. T. Ivrlač and J. A. Nossek, "Toward a circuit theory of communication," *IEEE Transactions on Circuits and Systems I: Regular Papers*, vol. 57, no. 7, pp. 1663–1683, 2010.

[48] J. W. Wallace and M. A. Jensen, "Mutual coupling in mimo wireless systems: A rigorous network theory analysis," *IEEE transactions on wireless communications*, vol. 3, no. 4, pp. 1317–1325, 2004.

[49] V. Shyianov, M. Akrout, F. Bellili, A. Mezghani, and R. W. Heath, "Achievable rate with antenna size constraint: Shannon meets chu and bode," *IEEE Transactions on Communications*, 2021.

[50] M. Akrout, V. Shyianov, F. Bellili, A. Mezghani, and R. W. Heath, "Achievable rate of near-field communications based on physically consistent models," *arXiv preprint arXiv:2111.08928*, 2021.

[51] P. S. Taluja and B. L. Hughes, "Information theoretic optimal broadband matching for communication systems," in *2010 IEEE Global Telecommunications Conference GLOBECOM 2010*. IEEE, 2010, pp. 1–6.

[52] S. Saab, A. Mezghani, and R. W. Heath, "Capacity based analysis of a wideband simo system in the presence of mutual coupling," in *2019 IEEE Global Communications Conference (GLOBECOM)*. IEEE, 2019, pp. 1–6.

[53] Y. Wu, J. Bergmans, and S. Attallah, "Effects of antenna correlation and mutual coupling on the carrier frequency offset estimation in mimo systems," in *2010 6th International Conference on Wireless Communications Networking and Mobile Computing (WiCOM)*. IEEE, 2010, pp. 1–4.

[54] H. S. Lui and H. T. Hui, "Mutual coupling compensation for direction-of-arrival estimations using the receiving-mutual-impedance method," *International journal of Antennas and Propagation*, vol. 2010, 2010.

[55] S. Lu, H. T. Hui, M. E. Bialkowski, X. Liu, H. Lui, and N. Shuley, "The effect of antenna mutual coupling on channel estimation of mimo-ofdm systems," in *2007 IEEE Antennas and Propagation Society International Symposium*. IEEE, 2007, pp. 2945–2948.

[56] W. Yang, G. Durisi, T. Koch, and Y. Polyanskiy, "Quasi-static multiple-antenna fading channels at finite blocklength," *IEEE Transactions on Information Theory*, vol. 60, no. 7, pp. 4232–4265, 2014.

[57] R. D. Yates and S. K. Kaul, "Status updates over unreliable multiaccess channels," in *2017 IEEE International Symposium on Information Theory (ISIT)*, 2017, pp. 331–335.

[58] B. Li, R. Li, and A. Eryilmaz, "Throughput-optimal scheduling design with regular service guarantees in wireless networks," *IEEE/ACM Transactions on Networking*, vol. 23, no. 5, pp. 1542–1552, 2014.

[59] A. Shah and A. M. Haimovich, "Performance analysis of maximal ratio combining and comparison with optimum combining for mobile radio communications with

cochannel interference," *IEEE Transactions on Vehicular Technology*, vol. 49, no. 4, pp. 1454–1463, 2000.

[60] V. K. Amalladinne, A. Vem, D. K. Soma, K. R. Narayanan, and J.-F. Chamberland, "A coupled compressive sensing scheme for unsourced multiple access," in *2018 IEEE International Conference on Acoustics, Speech and Signal Processing (ICASSP)*, 2018, pp. 6628–6632.

[61] R. Calderbank and A. Thompson, "Chirrup: a practical algorithm for unsourced multiple access," *Information and Inference: A Journal of the IMA*, vol. 9, no. 4, pp. 875–897, 2020.

[62] A. Pradhan, V. Amalladinne, A. Vem, K. R. Narayanan, and J.-F. Chamberland, "A joint graph based coding scheme for the unsourced random access gaussian channel," in *2019 IEEE Global Communications Conference (GLOBECOM)*. IEEE, 2019, pp. 1–6.

[63] A. K. Pradhan, V. K. Amalladinne, K. R. Narayanan, and J.-F. Chamberland, "Polar coding and random spreading for unsourced multiple access," in *ICC 2020-2020 IEEE International Conference on Communications (ICC)*. IEEE, 2020, pp. 1–6.

[64] A. Fengler, G. Caire, P. Jung, and S. Haghighatshoar, "Massive mimo unsourced random access," *arXiv preprint arXiv:1901.00828*, 2019.

[65] M. J. Wainwright, *High-dimensional statistics: A non-asymptotic viewpoint*. Cambridge University Press, 2019, vol. 48.

[66] N. Jamaly, *Multiport antenna systems for space-time wireless communications*. Chalmers Tekniska Hogskola (Sweden), 2013.

[67] ANSYS, "3D Electromagnetic Field Simulator for RF and Wireless Design," 2021. [Online]. Available: https://www.ansys.com/products/electronics/ansys-hfss

[68] A. Gately, D. Stock, and B.-S. Cheo, "A network description for antenna problems," *Proceedings of the IEEE*, vol. 56, no. 7, pp. 1181–1193, 1968.

[69] R. G. Gallager, *Stochastic Processes: Theory for Applications*. Cambridge University Press, 2013.